



**NTNU – Trondheim**  
Norwegian University of  
Science and Technology

# Petrography and petrophysical well log interpretation for evaluation of sandstone reservoir quality in the Skalle well (Barents Sea)

**Sanaz Javid**

Petroleum Geosciences

Submission date: June 2013

Supervisor: Mai Britt E. Mørk, IGB

Norwegian University of Science and Technology  
Department of Geology and Mineral Resources Engineering



## **Abstract**

39 thin sections and petrophysical log data from the Skalle well in the Hammerfest Basin, in the southwestern part of the Barents Sea, have been studied to interpret lithology, and diagenesis and their effect on the reservoir quality, and to compare reservoir properties of the different reservoir units. Petrophysical log data have been calibrated for reservoir description in cases where core material is not available.

The studied formations are comprised by the Stø, Fuglen, Hekkingen, Knurr, Kolje and the Lower Kolmule Formations. The Knurr and Kolje Formations have been identified and interpreted only by wire line logs, as core material was not available for those intervals.

The Lower Kolmule Formation of sandstones of lithic greywacke composition, and the Stø Formation with sandstones of subarkosic arenite composition are considered as possible reservoir rocks. All the formations are water filled which is reflected by the low resistivity logs responses. The mature sandstones of the Stø Formation show high reservoir quality (high porosity and permeability) compared to the Lower Kolmule Formation. The Hekkingen Formation is a potential source rock for the Lower Kolmule Formation, as well as a seal (cap rock) for the Stø Formation. Cementation, dissolution, compaction, clay mineral authigenesis and stylolitization are the most significant diagenetic processes affecting the reservoir quality. Some other type of processes such as glauconitization and bioturbation are also common in the studied well.

## **Acknowledgements**

I would like to appreciate my supervisor, Dr. Mai Britt E. Mørk, for her time, support and precious comments during the work. I would also like to thank Lundin AS Company, for providing the core images, thin sections and wire line log data. I wish to present my special thanks to Dr. Helge Langeland for his good advices and guidance during this thesis and the special thanks goes to Mohammahhossein Mohammadlou for great advises during work with the Interactive Petrophysics software.

Sanaz Javid

Trondheim 10.06.2013

# Contents

1. Introduction .....	11
1.1 Background and geological frame work of area.....	11
1.2 Objectives of study .....	15
1.3 Previous works.....	15
1.3.1 The Formations .....	16
2. Analytical approach .....	19
2.1 Methods.....	19
2.1.1 Optical Microscopy .....	19
2.1.2 Modal analysis .....	19
2.1.3 Petrophysical log interpretation .....	19
2.2 Sources of Error.....	20
3. Diagenesis.....	21
3.1 The major detrital minerals .....	22
3.2 The Clay minerals.....	22
3.3 The heavy minerals .....	23
3.4 Other types of minerals .....	24
3.5 Common diagenetic process in sandstones .....	24
3.6 Diagenetic processes in the interpreted rock types.....	25
4. Petrography.....	26
4.1 Modal Analysis.....	28
4.2 Formations.....	31
4.2.1 The Lower Kolmule Formation .....	31
4.2.2 The Hekkingen Formation .....	40
4.2.3 The Fuglen Formation .....	43
4.2.4 The Stø Formation.....	44
5. Evaluation of wire line logs .....	48
5.1 Introduction (literature review) .....	48
5.1.1 Mechanical log (Caliper log) .....	49
5.1.2 Natural radiation log (Gamma ray log) .....	50

5.1.3 Electrical log (resistivity logs) .....	53
5.1.4 Acoustic log (sonic log).....	54
5.1.5 Artificial radiation logs.....	55
5.2 Logs interpretation and work flow .....	56
5.3 Lithology from Sidewall Cores and wire line Logs.....	59
5.4 Lithology and fluid types .....	60
5.5 Formations.....	63
5.5.1 The Lower Kolmule Formation interpretation.....	63
5.5.2 The Kolje Formation interpretation.....	66
5.5.3 The Knurr Formation interpretation .....	66
5.5.4 The Hekkingen Formation interpretation .....	67
5.5.5 The Fuglen Formation .....	70
5.5.6 The Stø Formation interpretation .....	70
6. Discussion.....	74
6.1 The Stø Formation .....	76
6.2 The Fuglen Formation.....	77
6.3 The Hekkingen Formation .....	77
6.4 The Knurr and Kolje Formations.....	77
6.5 The lower Kolmule Formation .....	78
6.6 Comments on diagenesis and reservoir quality .....	78
7. Conclusion .....	81
References .....	83

## List of figures

<b>Figure 1.</b> Regional setting and location of the study area (the Hammerfest Basin) (Modified from Barrère et al., 2008). .....	12
<b>Figure 2.</b> The lithostratigraphical scheme. The Stø, Fuglen, Hekkingen and Kolmule Formations are illustrated (Dalland et al., 1988).....	14
<b>Figure 3.</b> According to Nelson, (2013) the major framework composition, arenites are broken down into: Quartzarenite, arkosic arenite, lithic arenite and wackes, and with > 15% matrix break down into: quartzwacke, feldspathic greywacke, lithic greywacke (modified from Dott, 1964). 28	
<b>Figure 4.</b> Quartz-Feldspar-Lithics (QFL) plot of the sandstones of the Lower Kolmule Formation. “Lith” includes mica, heavy minerals, glauconite and the rock fragments. Two Samples (15, 18) show the sublith arenite and samples number 11 and 13 show the lithic greywacke composition due to their clay matrix composition. ....	29
<b>Figure 5.</b> Quartz-Feldspar-Lithics (QFL) plot of the sandstones in the Hekkingen Formation. “Lith” includes mica, heavy minerals, Glauconite and the rock fragments. Only one sample was taken for rock types identification which shows the lithic greywacke composition due to high clay matrix content (more than 15%). .....	30
<b>Figure 6.</b> Quartz-Feldspar-Lithics (QFL) plot of the sandstones in the Stø Formation. “Lith” includes mica, heavy minerals, Glauconite and the rock fragments. There is a variation in the rock types but more samples are concentrated in subarkose classification. Samples 31 and 35 are defined as lithic greywacke. ....	30
<b>Figure 7.</b> The Lower Kolmule Formation. Pyrite (Py) can be seen as a dark grain, detrital quartz grains (Qtz) are white in plane polarized light, Organic matter (OM) as a dark spots within the clay matrix, glauconite (Glc) as a rounded grain with a green color, Qtz C (quartz cement\ quartz overgrowth), dissolved Feldspar(D Fsp), and precipitation of clay minerals (Cly) (depth 1583.10).....	31
<b>Figure 8.</b> The coarse Rock fragment (RF) consists of organic matter and fine-grained clay in the left part of the figure (depth 1589.1).....	33
<b>Figure 9.</b> Polycrystalline quartz rock fragment (RF) indicator of a metamorphic source. A) In cross polars, B) In normal light (depth 1595.40).....	34

<b>Figure 10.</b> Glauconite (Glc), dissolved Feldspar (D Fsp). Porosity (Po) and quartz (Qtz) are shown in this figure. Glauconite is displaying kidney shape in this sample (depth 1583.10).....	35
<b>Figure 11.</b> Combination of illite and chlorite clay minerals, filling the pores. Organic matter (OM) and rock fragments (RF) are illustrated in the figure (depth 1587.1).....	36
<b>Figure 12.</b> Chlorite (Cly) is filling the pores and reduces the porosity. Quartz (Qtz), organic matter (OM) and muscovite (Mus) are shown in this figure. Muscovite shows mechanical compaction (depth 1590.75).....	37
<b>Figure 13.</b> Pyrite (Py) is observed as a single grain in the right side of figure and also as cement in the left side of figure along with organic matter and glauconite (depth 1590.75).....	37
<b>Figure 14.</b> The evidence of dissolved fossil fragment (FF). This sample consists of quartz as a major grain, rock fragments and minor clay matrix (depth 1635.80). ....	38
<b>Figure 15.</b> The glauconitization (Glc) process is observed around the pellets. The presence of organic matter (OM), Clay minerals (cly), rock fragment (RF), feldspar (Fsp) are determined (Depth 1602.05).....	39
<b>Figure 16.</b> The Stylolitization process due to the mineral dissolution and accumulation of clay minerals and organic matter on the stylolite surface (depth 1584.05m). ....	40
<b>Figure 17.</b> The evidence of stylolitization in the Hekkingen Formation is illustrated in core number 5. Only two samples are available from this core, 2002.05m and 2010.65m. ....	41
<b>Figure 18.</b> The depth interval of 2010.65 shows a significant decrease in porosity due to the extensive quartz cementation which creates the unique ribbon-like texture. The clay matrix (Cly) occurs between the quartz (Qtz) grains. ....	42
<b>Figure 19.</b> Quartz overgrowth is observed in the 2002.05m. The quartz contacts show the suture and concave-convex shapes due to compaction. ....	42
<b>Figure 20.</b> The Fuglen Formation consists of dark shale and pyritic mudstone with interbedded white to brownish grey limestone according to core number6.....	43
<b>Figure 21.</b> The muscovite is bended due to mechanical compaction in the Stø Formation (depth 2094.9m).....	45
<b>Figure 22.</b> The fracture is observed due to the compaction and may have been enlarged by breakage of samples during preparation in the Stø Formation (depth 2133.9m). ....	45
<b>Figure 23.</b> The stylolitization process in the Stø Formation. The stylolites are occupied by the illite and chlorite clay matrix along with the organic matter (depth 2099.85m). ....	46



<b>Figure 24.</b> The bioturbation took place in the Stø Formation. Figure A shows the extensive accumulation of organic matter and redistributed particles. Figure B shows a big organic matter particle in the red color accompanied with the detrital grains (depth 2094m). .....	47
<b>Figure 25.</b> Typical caliper responses to various lithologies (Glover, 2012).....	49
<b>Figure 26.</b> Mineral identification from a Thorium – Potassium plot (Schlumberger) .....	52
<b>Figure 27.</b> Corrected concentrations of K, U, and Th (Halliburton).....	52
<b>Figure 28.</b> Typical resistivity log responses (Glover, 2012). .....	54
<b>Figure 29.</b> Pef curve shows a complex of lithologies. Sandstone (SS) shows the lowest Pef value, Dolomite (DOL) In the middle of the track and limestone (LS) with high pef value (White, 2012).....	56
<b>Figure 30.</b> The conventional logs overview from the depth 1583.1m to 2152m (Skalle well 7120/2-3S). There is no evidence of stationary reading. The green shaded areas in the track 1 show the washed out effect, while the yellow shaded areas show the permeable zones. In track 2 the separation between RDEP and RMIC shows the permeable zones. Tack 4 shows the shale (the green shaded areas) and sand (the yellow shaded areas).....	58
<b>Figure 31.</b> Permeable zones are identified from the depth 2126.9 to the depth 2242.3. Presence of mudcake (the yellow shading between caliper log and bit size log), the separation between RDEP and RMIC (the blue shading)and high porosity ( according to acoustic log with low values), low gamma ray and similar porosity reading of density- neutron are indicated the permeable zone. ....	59
<b>Figure 32.</b> The overview of petrophysical logs interpretation from 1576.1 to 2609.75m show 10 formations with different lithologies, fluid types and porosity. ....	62
<b>Figure 33.</b> Scale 1:1200, Permeable zones are defined by the yellow color in track 1 (caliper log shows the lower values than the bit size) and 3 (the separation between RDEP and RMIC). In track 4 the green shaded (neutron and density show high values) shows the shale, while the yellow shaded colour (neutron and density logs show low values) shows the sand lithologies. ..	64
<b>Figure 34.</b> The petrophysical logs interpretation of the Lower Kolmule Formation (1576.73-1750.01m).....	65
<b>Figure 35.</b> The petrophysical logs interpretation of Kolje Formation (1750.01-1989.6 m).....	68
<b>Figure 36.</b> The petrophysical logs interpretation of Knurr Formation (1989.6-1999.5 m).....	69
<b>Figure 37.</b> The petrophysical logs interpretation of Hekkingen Formation (1999.5-2017.9m). ..	69

**Figure 38.** The petrophysical logs interpretation of Fuglen Formation (2017.9-2071m). .....72  
**Figure 39.** The petrophysical logs interpretation of Stø Formation (2071-2220m).....73

## List of tables

<b>Table 1.</b> Petrographic analysis of 39 thin-sections showing the formations, grain size (mm), porosity (%), sorting and roundness. The modal analyses of 14 thin-sections are also presented (see page III for abbreviations).....	27
<b>Table 2.</b> Th/K ratio in clay minerals, shows the highest value for kaolinite and the lowest value for potassium evaporate .....	74
<b>Table 3.</b> Mineral identification using Th/K ratio for the Lower Kolmule, Kolje, Knurr, Hekkingen, Fuglen, and Stø Formations.....	75

## Abbreviations

**Cc:** Calcite cement

**Ch:** Chlorite

**Clst:** Claystone

**Cly:** Clay

**Dp:** Depth

**FF:** fossil fragment

**Fsp:** Feldspar

**Glc:** Glauconite

**Hm:** Heavy minerals

**Ill:** Illite

**KFsp:** K-feldspar

**KFmic:** K-feldspar microcline

**Lith:** Lithology

**Mic:** Mica

**Mus:** Muscovite

**OM:** Organic matter

**Po:** Porosity

**P:** Phosphate

**PIQ:** Polycrystalline quartz

**Py:** Pyrite

**Qtz:** Quartz

**RF:** Rock fragment

**Rw:** Water resistivity

**SN:** Sample Number

**FF:** Fossil fragment

**Qtzc:** Quartz cement

## **1. Introduction**

This master thesis is written at the Department of Geology and Mineral Resources Engineering at NTNU, during the spring of 2013. The thesis is part of the 2 years international master program in Petroleum geology.

This is a thin section study of side-wall cores combined with a petrophysical study of the Skalle well 7120/2-3S in the Barents Sea. The aim is to identify the petrography, mineralogy, texture, porosity and diagenetic process and compare with the petrophysical data to predict reservoir quality.

The Skalle well is situated approximately 25 kilometers north of the Snøhvit Field, in the Hammerfest Basin in the southwestern part of the Barents Sea (Fig. 1).

According to the publication by Spring Energy, the objective of the well was to prove hydrocarbons in the Cretaceous Kolmule and Knurr Formations, as well as the Jurassic Stø/Tubåen and the Triassic Fruholmen/Snadd Formations. The well proved gas in the Kolmule, Knurr and Stø Formations, whereas the Tubåen/Fruholmen/Snadd Formations were water filled. The recoverable reserves proven by the Skalle discovery well is estimated to be between 2.5 and 8 GSm<sup>3</sup> of gas.

This is the first exploration well in production license 438 (NPD factpage). The operation started in 2008 but the well is now being permanently plugged and abandoned.

### **1.1 Background and geological frame work of area**

The Barents Sea (Fig.1) is located between the Norwegian-Russian mainland, the Arctic Ocean margin and the Norwegian-Greenland Sea. The Barents Sea covers a vast shelf area that extends from Novaya Zemlya in the east to the continental slope of the Norwegian-Greenland Sea in the west, and from Svalbard and Franz Josef Land in the north to the coasts of Norway and Russia in the south.

In the Barents Sea, the thick Upper Paleozoic to Tertiary succession forms a continuous shelf area between Svalbard and the Norwegian coast.

The post-Devonian succession which shows an uplift in the northern part of the Barents Sea has several similarities to the upper Paleozoic to Tertiary succession on Svalbard. However, the latest Permian and Early Triassic succession in the western part of the Barents Sea has been uplifted and eroded (Brekke et al., 2001).

The Mesozoic succession in the southern Barents Sea is of special interest as it has proven the potential for generating hydrocarbons.

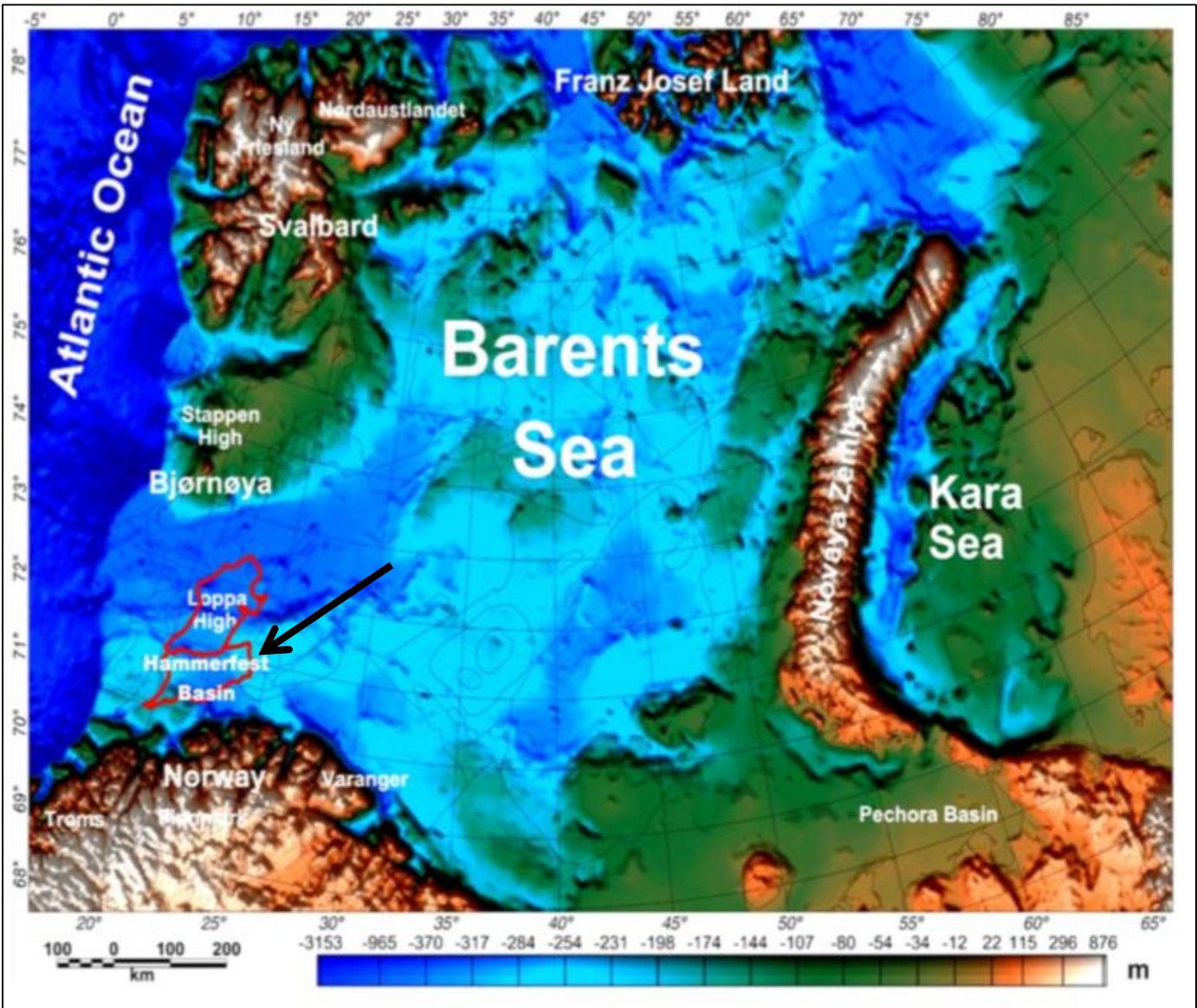


Figure 1. Regional setting and location of the study area (the Hammerfest Basin) (Modified from Barrère et al., 2008).

The Hammerfest Basin, in the south western part of the Barents Sea (Fig.1), is bounded by the Finnmark Platform in the south and the Loppa High and the Bjarmeland Platform in the north (Larssen et al., 2002). The Hammerfest Basin is shallow and has an ENE-WSW striking axis (Rønnevik et al., 1984). This basin began forming during Late Jurassic and is predominately a Cretaceous aged extensional basin (Burley, 1997) and containing Upper Palaeozoic to Cenozoic sediments. The sediments were influenced by minor Mesozoic tectonism (Olaussen et al., 1984).

A total of 29 exploration wells have been drilled in the Hammerfest Basin which like the Skalle well was finished drilled down to the upper Triassic Snadd Formation (Fig. 2).

The major gas discovery in the Snøhvit field and the oil discovery in the Goliat field are both located in the Hammerfest Basin. This basin has a high oil accumulation potential that has encouraged research for further explorations.

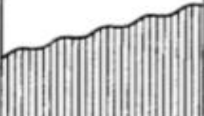





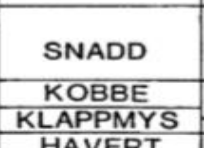
PERIOD		NEO-GENE		PALEOGENE			CRETACEOUS			JURASSIC			TRIASSIC															
EPOCH		MIO	P/P	EOC		OLI	LATE		EARLY		LATE		EARLY		LATE													
AGE				Ypr	Lut	Prb	Rup	Cht																				
		Dan	Tha	San	Cmp	Maa	Alb	Apt	Brm	Hau	Vlg	Rya	Vol	Kim	Oxf	Civ	Bth	Bas	Aal	Toa	Pib	Sin	Het	Rht	Nor	Crn	Lad	Ans
		PROPOSALS HEREIN		INFORMAL UNITS																								
		GROUP	FORMATION	"T-UNIT"	FM	GP																						
		NORDLAND		T7		Egga																						
		SOTBAKKEN		T6-1/3	Loppa Ingey Oksvik	Nordkapp																						
		NY-GRUNNEN		T5		Kvaløy																						
		NORDVEST-BANKEN		T4-4 T4-2/3 T4-1	Torsvåg Tamsey/Anda Slettnes	Senja																						
		TEISTEN-GRUNNEN		T3-2 T3-1	Olderfjord Risfjord	Finnmark																						
		REALGRUNNEN		T2-5 T2-4 T2-3 T2-1/2	Stø Nordmela Dyroy Ytterøy Helgøy	Troms																						
		INGØY-DJUPET		T1-4 T1-3 T1-2 T1-1	Aun Gimsey Andenes Svolvær	Lofoten																						

Figure 2. The lithostratigraphical scheme. The Stø, Fuglen, Hekkingen and Kolmule Formations are illustrated (Dalland et al., 1988).



## **1.2 Objectives of study**

The main purpose of this work is to explain the mineralogy and petrography of this well and document any possible diagenetic processes and their effect on the reservoir quality as well as compare the reservoir properties of the different reservoir units. Another aim is to use the petrography to calibrate the petrophysical log data for the reservoir description. For achieving this goal, 39 thin sections from the Skalle well have been studied and compared with some petrophysical data from this area for getting precise results. The samples are provided from depths 1583.1 to 2152m. The depths compare the Lower Kolmule Formations of Cretaceous age, the Hekkingen, and Fuglen Formations of Late Jurassic age and the Stø Formations of Middle Jurassic age. Core materials are not available for the Kolje and Knurr Formations, so the lithology was interpreted from petrophysical log data.

## **1.3 Previous works**

The Barents Shelf consists of several kilometers thick Paleozoic to Cenozoic sedimentary successions (Worsley et al., 1988, Brekke et al., 2001) and many studies have been done on the geology in particular around the western and southern part of the Barents Sea.

The Cenozoic evolution of the Barents Sea area has been explained by Ryseth et al., (2003) and detailed studies of the Mesozoic succession have been published (Olaussen et al., 1984, Bugge et al., 2002, Walderhaug and Bjørkum, 2003). Mesozoic diagenetic studies are focused on the Jurassic part of the succession as the main discoveries have been made in the Jurassic reservoirs (Walderhaug and Bjørkum, 2003, Suslova et al., 2007). The Middle Jurassic to Lower Cretaceous succession is dominated by dark, commonly organic-rich mudstones, but includes also deltaic and shelf sandstones (Leith et al., 1993, Bøe et al., 2010).

The Middle-Upper Triassic succession consists of the Snadd, Fruholmen and Tubåen Formations (Worsley et al., 1988). The sandstone reservoir rocks show immature lithic-arenite and subarkosic composition in the Triassic ranging to quartz arenites at the Triassic- Jurassic transition (Mørk, 1999).

The incomplete Upper Cretaceous succession suggests events of erosion and uplift in large scale in the Tertiary (Walderhaug and Bjørkum, 2003).

Previous lithology and petrophysical study of the Cretaceous and Jurassic Formations are summarized as the following:

### **1.3.1 The Formations**

#### **1.3.1.1 The Lower Kolmule Formation**

The Kolmule Formation is belonged to the Nordvestbanken Group (Fig.2). This formation has a thickness of 945 m in the type well (7119/12-1) and 530 m in the reference well (7120/12-1) and belongs to the Aptian to Mid-Cenomanian (Cretaceous) (factpages.npd.no).

The Kolmule Formation was deposited in marine environment. This Formation consists of grey to green claystone and shale, in some parts the evidence of silt with minor thin siltstone interbeds is observed. Limestone and dolomite stringers are present in some parts. Traces of glauconite and pyrite occur.

The petrophysical log response in the type well and reference well is the same and both of them show the sharp increase in the neutron and acoustic log trend at the base of the formation. However, the type well shows a slight decrease in the gamma ray, and the reference well shows a gradual increase in gamma ray log response (NPD factpage).

#### **1.3.1.2 The Kolje Formation**

This formation of Early-Cretaceous (Early Aptian) age belongs to the Nordvestbanken Group (Fig. 2). The Kolje Formation has a thickness of 437m in the type well (7119/12-1) and 103m in reference well (7120/12-1) (Dalland et al., 1988).

The Kolje Formation consists of dark shale with limestone and dolomite interbeds, but at the top of this formation thin interbeds of sandstone and siltstone can be observed. The base of this formation is marked by decreasing in gamma ray log, decreasing in acoustic log and increasing density log responses (NPD factpage).

### **1.3.1.3 The Knurr Formation**

The Knurr Formation belongs to the Nordvestbanken Group with Early-Cretaceous (Valanginian to early Barremian age). The formation has a thickness of 56m in the type well (7119/12-1) and 285 in the reference well (7120/12-1) (Dalland et al., 1988).

The Knurr Formation consists of brown claystone at the top of the formation with limestone and dolomite interbeds. At the lower part of this formation the thin sandstones are observed. The base is defined by decreasing gamma ray log and acoustic log responses. The general pattern in most of the well shows an increase in the density log response (NPD factpage).

### **1.3.1.4 The Hekkingen and Fuglen Formations**

These two Formations are belonged to the Teistengrunnen Group (Fig.2) of Late Jurassic age. The Fuglen Formation has a thickness of 28m in the type well (7120/12-1) and 48m in the reference well (7119/12-1), and the Hekkingen Formation has a thickness of 359m in the type well (7120/12-1) and 113m in the reference well (7119/12-1) (Dalland et al., 1988).

The Fuglen Formation consists of pyritic mudstone (dark brown shale) with interbedded white to brownish grey limestone. The Hekkingen Formation consists of the dark grey shale with thin interbeds of limestone, dolomite, siltstone and sandstone. The Hekkingen Formation is the most important source rock in the Norwegian Barents Sea (Pedersen et al., 2013). The transition zone from the Fuglen Formation to the Hekkingen Formation is defined by a transition from the carbonate cemented and pyrite mudstones to poorly consolidated shales which cause a sudden increase in acoustic log and a decrease in bulk density values (NPD factpage).

### **1.3.1.5 The Stø Formation**

This formation of Mid-Jurassic age belongs to the Realgrunnen Group (Fig. 2). It has 77m thickness in the type well (7121/5-1) and 145m in the reference well (7119/12-2) (Dalland et al., 1988).

The Stø Formation dominantly consists of fine- to medium-grained mature sandstones that are classified as quartz arenites and associated with thin shale and siltstone interbeds. Commonly marine micro-fossils, glauconitic grains and authigenic phosphate occur in distinct beds (Olaussen et

al., 1984). This formation is subdivided in three units, S-I to S-III, and the S-II unit is formed during marine transgression and is correlatable over the entire area (Olaussen et al., 1984). The mature sandstones of Stø Formation are deposited on a stable platform and deposition took place under transgressive regime during Middle and Lower Jurassic (Olaussen et al., 1984). Diagenesis of quartz arenites of this formation could be related to the distribution of stylolites, and have been divided in two categories: 1) cases where the spacing between clay rich laminae that evolve within the stylolites is large, up to several meters, and detrital clay is not available. 2) In intervals where minor detrital clay matrix occurs stylolite spacing is less than a centimeter (Walderhaug et al., 2003). Walderhaug et al., (2003) also indicate that there is a correlation between the quartz cementation and distance to nearest stylolites. They explain that there is a decreasing trend in quartz cementation outwards from stylolites due to absence of clay-rich (except chlorite-coating) or micaceous laminae. Density readings in this formation are gradually decreasing upward over the boundary (the Stø and Fuglen boundary) and the gamma ray almost shows a smooth, linear and cylinder-shaped pattern with low readings (NPD factpage).

## **2. Analytical approach**

In order to study the Skalle well for getting some information regarding lithology, porosity, diagenesis, petrography, and reservoir quality some methods are achieved. Different methods will be compared together for getting precise results. The methods can be summarized as following:

### **2.1 Methods**

#### **2.1.1 Optical Microscopy**

From the well 7120/2-3S thirty-nine thin-sections from side-wall cores were provided from Lundin Norway AS from the depth interval 1583.1 to 2152 meters from the Stø (Middle Jurassic), Hekkingen, Fuglen (Late Jurassic) and Lower Kolmule (Cretaceous) Formations. The thin-sections were studied petrographically and mineralogically by using a Nikon polarizing microscope and during this procedure detrital minerals and diagenetic minerals as well as texture, porosity and properties were determined. As the thin sections were unpolished, the quality was, however, not optimal. In some of the provided samples the alkali feldspars were stained and identified as the yellow colour in order to distinguish between K-rich and Na-rich feldspars.

#### **2.1.2 Modal analysis**

The optical point counting method has been used for rock classification and porosity estimation. The Modal analysis was carried out using a Pelcon Point Counter program, the analysis was based on 300 points in each thin section. A step length of 0.2 mm for each sample was used. The modal data was used as a basis for classification and comparison of different rock types in this study and as a basis for interpretation the petrophysical logs.

#### **2.1.3 Petrophysical log interpretation**

The petrophysical data from the well were provided by Lundin Norway AS and used as a supplementary tool to the side-wall thin-sections and cores images. The petrophysical data were interpreted using the Interactive Petrophysics version 4.0 (IP). These conventional logs were used as a

supplementary method for getting some information about lithology, porosity, fluid types and possible diagenetic processes. The conventional logs include; the gamma ray log (GR), neutron porosity log, density log, Acoustic log, resistivity (medium, deep and micro resistivity) logs and pef log. The GR log was used as a base for clay volume calculations. The thorium, potassium and uranium logs were obtained for better clay types and mineralogy interpretation.

## **2.2 Sources of Error**

Due to poor preparation of the thin sections, as they were not polished, it was hard to distinguish between some minerals like quartz and alkali feldspars and between chert and polycrystalline quartz. In most of the samples there were lots of damaged grains and lots of fractures cutting the quartz grains. Therefore the optical images have low resolution difficulty in distinguishing between the grains and with possibilities for misinterpretations.

In the case of heterogeneity of the samples, a selection of only 300 points in each sample can't be representative for the whole sample so the results won't be accurate enough and comparison with the core images and petrophysical logs are needed as they represent smaller volumes than the petrophysical log data.

### 3. Diagenesis

Diagenesis refers to all chemical, physical and biological processes that happen after the sediment deposition and continuing through compaction and litification. In other words diagenesis comprises all processes that convert raw sediments to sedimentary rocks (Syed et al., 2010). These processes can continue at increasing temperature and pressure until onset of metamorphism. Worden and Burley (2003) argued that a temperature transition of 180-250 °C is thought to separate the two regimes, however, Sujkowski (1958) believed that the limit between diagenesis and metamorphism is not precise in the term of pressure and temperature.

There are various factors controlling the diagenetic processes of the sedimentary units in different stages of eogenesis, mesogenesis and telogenesis including the grain size, primary composition, the sedimentation rate, depositional environment and the physical and chemical changes during burial.

Diagenesis can take place from eogenesis at near surface in the depositional regime to burial depths 10km or more. The mesogenesis regime is characterized by increased pressure, temperature and changes in pore water composition. Uplift and exposure of the sediment pile bring sediments in to the telogenetic regime, proceeding at lowered temperature and pressure and by generally oxidizing meteoric pore waters (Boggs, 1992).

According to a survey by Primmer et al., (1997) of the diagenetic history of 100 sandstone reservoirs around the world, there are five common and repetitive diagenetic styles for the sandstones. These main diagenetic styles are: "1) quartz with lesser quantities of neoformed clay (illite and kaolinite) and late diagenetic ferroan carbonate; 2) clay minerals (illite or kaolinite) with lesser quantities of quartz or zeolite and late diagenetic carbonate; 3) early diagenetic grain coating clay minerals cements such as chlorite that inhibits the quartz cementation during burial; 4) early diagenetic carbonate or evaporates cement that reduces the porosity and net pay at very shallow burial depth; and 5) zeolites, which occur over a wide range in burial temperature usually associated with clay minerals such as chlorite or smectite and late-diagenetic, nonferroan carbonate."

The main diagenetic processes that change the reservoir properties and are observed in Hammerfest Basin are mechanical compaction, quartz cementation, carbonate cementation,

kaolinitization, dissolution and illitization. Diagenesis is mainly controlled by depositional environment and porosity distribution can be controlled by post-depositional tectonics (Olaussen et al., 1984). The main detrital and diagenetic minerals can be discussed as the following:

### **3.1 The major detrital minerals**

The principal component grain types in sandstones in general are quartz, feldspar and rock fragments and the matrix of such sediments can be the fine-grained weathering products, such as clay minerals, or it may be secondary cement (Adams et al., 1984). Quartz can form as a single crystal or made up of a number of crystals (polycrystalline). Polycrystalline quartz of sand size, especially if more than five individual crystals are present and with a sutured contact is a better indicator of a metamorphic source (Nelson, 2013). Composite quartz from igneous sources has straighter crystal boundaries (Adams et al. 1984). Feldspar is the second major component in the sandstones. Alkali feldspars are more common compared to plagioclase due to their stability in weathering. Clay minerals and mica can be the products of chemical weathering of the feldspars. Rock fragments are made up of multiple grains that are connected on the grain scale. They may be consisting of chert, polycrystalline quartz or fine-grained materials like shale fragments. With the exception of fragments of polycrystalline quartz, lithic fragments are generally unstable in the sedimentary environment, yet, if present in sandstone they give the best clues to provenance (Nelson, 2013).

### **3.2 The Clay minerals**

Clay minerals are very small particles with layered structure (phyllosilicate) and large specific surface areas. They are the main component of claystones and shales but they are common in sandstones and can affect the reservoir properties. Clay minerals form in different diagenetic environments (eogenesis, mesogenesis) and by weathering of the feldspars. Diagenetic clay minerals can be discrete particles or pore-filling aggregates. They can be recognized in the form of pore-bridging or grain-coating. Glauconite is a type of clay mineral which is rich in potassium ( $K^+$ ) and contains both ferric and ferrous iron, and forms at suboxic conditions in marine environments where the sedimentation rate is low and can be created by the decay of organic matter within the fecal pellets and bioclasts (Banerjee et al., 2011). Fecal pellets are always rich in elements necessary for the formation of glauconite. The term glauconite has been employed in two senses. It has been used most



commonly as a morphological term for sand-sized greenish grains found in sedimentary rocks, but also as a name for a specific mineral species, a hydrated iron-rich micaceous clay mineral (McRae, 1972). Illite is a hydrated phyllosilicate clay mineral which contains K, Al and Si. It can influence on the permeability of the formation and reduce it significantly. In sandstones it can develop and create large volumes of microporosity that binned the water in the host grains and causes high irreducible water saturation in the formation (Almon and Davies, 1981). Mostly it occurs along with the organic matter and pyrite, suggesting that bioturbation, mass flow and soft sediments deformation are likely mechanisms for introducing detrital clay minerals into the fabric of marine sandstones (Worden and Burley, 2003). The illite as an authigenic mineral fills the pores and reduces the porosity.

Chlorites are clay minerals which are classified in two different types according to their chemical composition, Fe chlorite and Mg chlorite. Chlorite is a stable clay mineral that occurs in the early stage of mesogenesis and can be remained in the end of the telegenesis regime. The reservoir quality strongly changes with the proportion of pore-filling vs. pore-lining chlorite. The best in terms of reservoir quality is the coarser-grained sandstones, where chlorite forms a thin pore-lining layer that does not hinder significantly the permeability and preserves porosity.

The chlorite-bearing reservoir sandstones are deposited in specific settings, namely in the transitional environments, where mixing between Fe-rich fresh waters and marine waters occurs (Arduini et al., 2009). Chlorite-coated sandstones are often associated with iron-rich depositional environments like the glaucony and oolitic ironstone facies (Storvoll et al., 2002). The onset of significant chlorite growth is related to shallow or intermediate burial settings. Chlorite coatings preserve the porosity by inhibiting quartz cementation. Porosity preservation has been demonstrated in a number of earlier publications. It is well known that chlorite coatings inhibit quartz cementation so that porosity can be preserved, but in the study by Storvoll et al., (2002) they show that also illite and illite/chlorite coatings can be very effective preventing the quartz cementation and thereby help preserving the primary porosity.

### **3.3 The heavy minerals**

The resistant heavy minerals occur in metamorphic and igneous rock with low concentrations, and being chemically and physically resistant to weathering, and having comparatively

high specific gravity, they tend to accumulate in placer deposits in river channels or along coastal shorelines.

### **3.4 Other types of minerals**

Pyrite and phosphate are diagenetic minerals that can be found in the six case study formations (the Stø, Fuglen, Hekkingen, Knurr, Kolje and Lower Kolmule Formations). In order to form the pyrite, reducing conditions are necessary and a precursor iron monosulfide is requested (Boggs, 1992). Due to the difficulty of direct nucleation of pyrite, direct precipitation of pyrite from the solution is strongly inhibited (Mackenzie, 2004). Pyrite is formed as a crystal form mineral, or filling the pores as cement.

### **3.5 Common diagenetic process in sandstones**

Burley and Kantorowicz (1986) argued that sandstone diagenesis proceeds through several steps, starting with reduction in porosity due to compaction and later with dissolution, cementation, alteration and transformation of mineral phases in more deeply buried sandstone. They also have mentioned that continued solution at depth can develop the secondary porosity within sandstones. Beside these processes, glauconitization and bioturbation can be mentioned as a diagenetic process.

Sandstone reservoir quality is largely determined by diagenetic processes that either reduce or enhance porosity. Mechanical compaction, intergranular pressure solution and cementation reduce the porosity, while framework grain dissolution, and cement dissolution have all been documented as playing significant roles in increasing porosity of various sandstones (Houseknecht, 1987).

Bioturbation is referred to as all transport processes (particle reworking and burrow ventilation) carried out by animals that directly or indirectly affect sediment matrix, and particle reworking occurs through this process (Kristensen et al., 2012).

Glauconitization processes which are common in suboxic conditions are referred as a chemical exchange and precipitation in pores and cracks of the detrital mineral such as quartz and chert. The maturation of glauconite pellets occurs when  $K_2O$  and  $SiO_2$  are increased and the amount of  $Al_2O_3$  is released from the glauconite structure, but the maturation of glauconite infillings is achieved

when Mg is removed. The maturation process is not affected by the total amount of Fe<sub>2</sub>O<sub>3</sub> (Banerjee et al., 2011).

Stylolitization is referred to as the pressure solution features that can occur in the homogenous rocks such as carbonate, sandstone and cherts, approximately parallel to bedding. Stylolite surfaces are sites of insoluble residues (clays, iron oxides and organic matters) accumulation, so stylolites appear dark.

Cementation is common diagenesis processes which reduce the intergranular porosity with no directly related reduction of bulk volume by authigenic minerals precipitation (Houseknecht, 1987). Quartz cementation needs the silica source which can be obtained from the internal or external sources. Among possible internal sources, dissolution of quartz at stylolites interface (Olaussen, 1984) and individual grain contact (Waldschmidt, 1941, and Houseknecht, 1987) are the most common. The dissolution of quartz at stylolites and individual grain contacts can be the result of pressure solution processes where the dissolution is a function of stress on grains contact, or dissolution is favored due to catalytic effects of mica or clay contact. Temperature is an important factor. After dissolution, silica diffusion happens which leads to quartz precipitation as quartz overgrowths on quartz grain surfaces (Walderhaug et al., 2003).

### **3.6 Diagenetic processes in the interpreted rock types**

The major diagenetic processes within the interpreted rocks are the formation of quartz cement, carbonate cement and clay minerals precipitation. Evidence of compaction, chloritization, stylolitization and glauconitization is also detected. The observed compaction is consisting of physical and chemical compactations near the surface, and at deeper depth of burial dominates chemical compaction. The observed diagenetic processes will be discussed in Chapter 4.

## 4. Petrography

A summary of the result from study of 39 thin-sections between depth intervals 1583.1 to 2152 meters is shown in Table. 1. Eighteen thin-sections are from the Lower Kolmule Formation (1583.1m to 1636.95m), two thin-sections are from the Hekkingen Formation (2002.05m and 2010.65m), one thin-section is from the Fuglen Formation (2019.35m) and the rest of the thin-sections are from the Stø Formation (2079.98m to 2152m) (Table.1).

Grain size was determined by measuring the longest axis of several grains per sample and calculating the mean value. Clays and shales are too fine-grained to be studied by petrographic microscope so their grain size and mineralogy can be identified using electron microscopy and X-ray diffraction methods which was not part of the study. Sorting and roundness observation of the grains were defined using the standard that was published by Pettijohn et al., (1973). In this classification the sorting of the grains were divided in four categories; poorly-sorted, moderately-sorted, well-sorted and very well-sorted. This division is used to define the distribution of particle sizes in a rock. Sorting is often measured by calculating the standard deviation of sediment particle diameters. A well-sorted rock is composed of particles of similar size. A poorly-sorted rock consists of particles with a wide range of sizes (Bennington, 1999). Particles become sorted on the basis of density because of the energy of the transporting medium. High energy (high velocity) currents can carry larger fragments. Roundness is shown by the degree to which the sharp edges of a particle have been smoothed. Defining the sorting and roundness characterizes the textural maturity of the sandstone and defines the transport history of the sediment that can be important for predicting the reservoir quality. The high quality reservoir consists of well-rounded coarse-grained sediments (high porosity and permeability) with fewer amounts of clay minerals (high maturity).

The general overview of Table. 1 shows that most of the samples consist of subrounded to subangular grains with well to moderately-sorted texture except in some of the samples such as samples number 8 and 15 from the Kolmule Formation which show the poor-sorted texture due to high clay contents with angular and subrounded to subangular grains, respectively.

Table 1. Petrographic analysis of 39 thin-sections showing the formations, grain size (mm), modal porosity (%), sorting and roundness. The modal analyses of 14 thin-sections are also presented (see page III for abbreviations).

SN	well N.	Depth	Formation	grain size (mm)	porosity (%)	Roundness	Sorting	Modal analysis	Fsp	Lith	Qtz	Mica	Glc	FF	Hm	OM	Py	Pho	Cc	Clv
1	7120/2-3S	1583.1	L.Kolmule	0.27	20	Subrounded to subangular	well -sorted	No												
2	7120/2-3S	1584.05	L.Kolmule	0.28	20	Subrounded to subangular	well -sorted	No												
3	7120/2-3S	1587.1	L.Kolmule	0.25	18	Subrounded to subangular	well to moderately -sorted	No												
4	7120/2-3S	1589.1	L.Kolmule	0.29	10	Subrounded to subangular	moderately-sorted	No												
5	7120/2-3S	1590.75	L.Kolmule	0.21	7	Subrounded to subangular	moderately-sorted	Yes	22	13.4	34.5	0.6	6.7	0	2.4	0	0	2.1	0	7
6	7120/2-3S	1592.05	L.Kolmule	0.24	7	Subrounded to subangular	moderately-sorted	No												
7	7120/2-3S	1593.05	L.Kolmule	0.24	3	subangular to angular	Moderately to poor-sorted	Yes	39	8.3	36.5	0	3	0	0.3	0	0.7	0	0	28.3
8	7120/2-3S	1595.4	L.Kolmule	0.17	2	angular	poor-sorted	No												
9	7120/2-3S	1597.1	L.Kolmule	0.28	15	Subrounded to subangular	moderately-sorted	No												
10	7120/2-3S	1599.15	L.Kolmule	0.18	15	Subrounded to subangular	moderately-sorted	No												
11	7120/2-3S	1600.1	L.Kolmule	0.21	3	subangular to angular	moderately-sorted	Yes	9.7	5.4	38.1	0.9	7.1	0	0.6	0	1.7	0	0	34.1
12	7120/2-3S	1602.05	L.Kolmule	0.2	3	subangular to angular	moderately-sorted	No												
13	7120/2-3S	1628.9	L.Kolmule	0.25	20	subrounded to rounded	well to moderately -sorted	Yes	8.9	6.7	37.4	0	7.1	0	0	0.9	0	0	0	36.2
14	7120/2-3S	1632.75	L.Kolmule	0.11	15	Subrounded to subangular	moderately-sorted	No												
15	7120/2-3S	1634.38	L.Kolmule	0.35	15	Subrounded to subangular	poor-sorted	Yes	7.9	10.3	53.2	0	3	0	0.3	0.9	0	1.2	0	1.5
16	7120/2-3S	1635.8	L.Kolmule	0.23	20	Subrounded to subangular	well -sorted	No												
17	7120/2-3S	1636.6	L.Kolmule	0.19	20	Subrounded to subangular	well to moderately -sorted	No												
18	7120/2-3S	1636.95	L.Kolmule	0.27	1	subangular to angular	Moderately to poor-sorted	Yes	6.6	9.9	48.6	0	2.7	4.4	0	4.5	0	1	7.2	1.4
19	7120/2-3S	2002.05	Hekkingen	0.15	15	Subrounded to subangular	well -sorted	No												
20	7120/2-3S	2010.65	Hekkingen	0.084	0	Subrounded to subangular	moderately-sorted	Yes	6.6	7.6	47.4	0	1	7.6	2.6	6.6	0	0	1.7	18.9
21	7120/2-3S	2019.35	Fuglen	0.175	3	Subrounded to subangular	well to moderately -sorted	No												
22	7120/2-3S	2079.98	Stø	0.115	20	Subrounded to subangular	well -sorted	Yes	6.9	1.2	72.5	1.2	2.4	0	1.3	0	3	2.7	0	8.8
23	7120/2-3S	2080.83	Stø	0.12	15	Subrounded to subangular	well -sorted	No												
24	7120/2-3S	2082.98	Stø	0.13	15	Subrounded to subangular	well -sorted	Yes	18.4	7.2	45.1	0	1.1	0	1.6	0	2.1	3.7	0	4.3
25	7120/2-3S	2083.4	Stø	0.13	15	subangular to angular	well -sorted	No												
26	7120/2-3S	2087.2	Stø	0.125	10	Subrounded to subangular	well -sorted	Yes	15.6	9.4	37.8	0.7	1	0	4	0	5	4.2	0	2.5
27	7120/2-3S	2094.74	Stø	0.08	10	subrounded to rounded	well -sorted	No												
28	7120/2-3S	2094.9	Stø	0.05	5	rounded	well -sorted	Yes	14.5	6.9	39.5	0	2.6	0	3.6	11	4.9	0	0	5.9
29	7120/2-3S	2095.9	Stø	0.03	1	Subrounded to subangular	moderately-sorted	No												
30	7120/2-3S	2097.98	Stø	0.05	5	Subrounded to subangular	well -sorted	No												
31	7120/2-3S	2099.85	Stø	0.05	3	Subrounded to subangular	well -sorted	Yes	4.8	3.7	31.2	6.8	1.7	0	4.8	19	3	1	0	19.4
32	7120/2-3S	2107	Stø	0.1	3	subangular to angular	well -sorted	No												
33	7120/2-3S	2108.93	Stø	0.07	10	subangular to angular	well -sorted	No												
34	7120/2-3S	2115.83	Stø	0.08	10	Subrounded to subangular	well to moderately -sorted	No												
35	7120/2-3S	2117.86	Stø	0.07	15	Subrounded to subangular	well -sorted	Yes	5	1.9	44.3	4.3	1.1	0	7.5	4.4	4.2	0	0	20.6
36	7120/2-3S	2125.88	Stø	0.15	15	Subrounded to subangular	well to moderately -sorted	No												
37	7120/2-3S	2133.9	Stø	0.155	20	subrounded to rounded	well -sorted	No												
38	7120/2-3S	2139.6	Stø	0.136	20	Subrounded to subangular	well -sorted	Yes	19.5	2.4	30.7	0.5	1.4	0	4.6	3.2	3.2	0.5	11	11.1
39	7120/2-3S	2152	Stø	0.13	15	subrounded to rounded	well to moderately -sorted	No												

## 4.1 Modal Analysis

The ternary plots are achieved after optical point counting for the rock type classification. The modal analyses show the variety of rock compositions in the Skalle well. The ternary plots are plotted for the Stø, Fuglen, Hekkingen and Lower Kolmule Formation (Fig. 4, 5, 6).

The formations are plotted based on the classification system of Dott (1964) that can be summarized by a ternary diagram showing the relative volume of quartz, feldspar, and rock fragments, with an extra dimension for matrix volume in the case of having more than 15% clay matrix (Fig. 3)

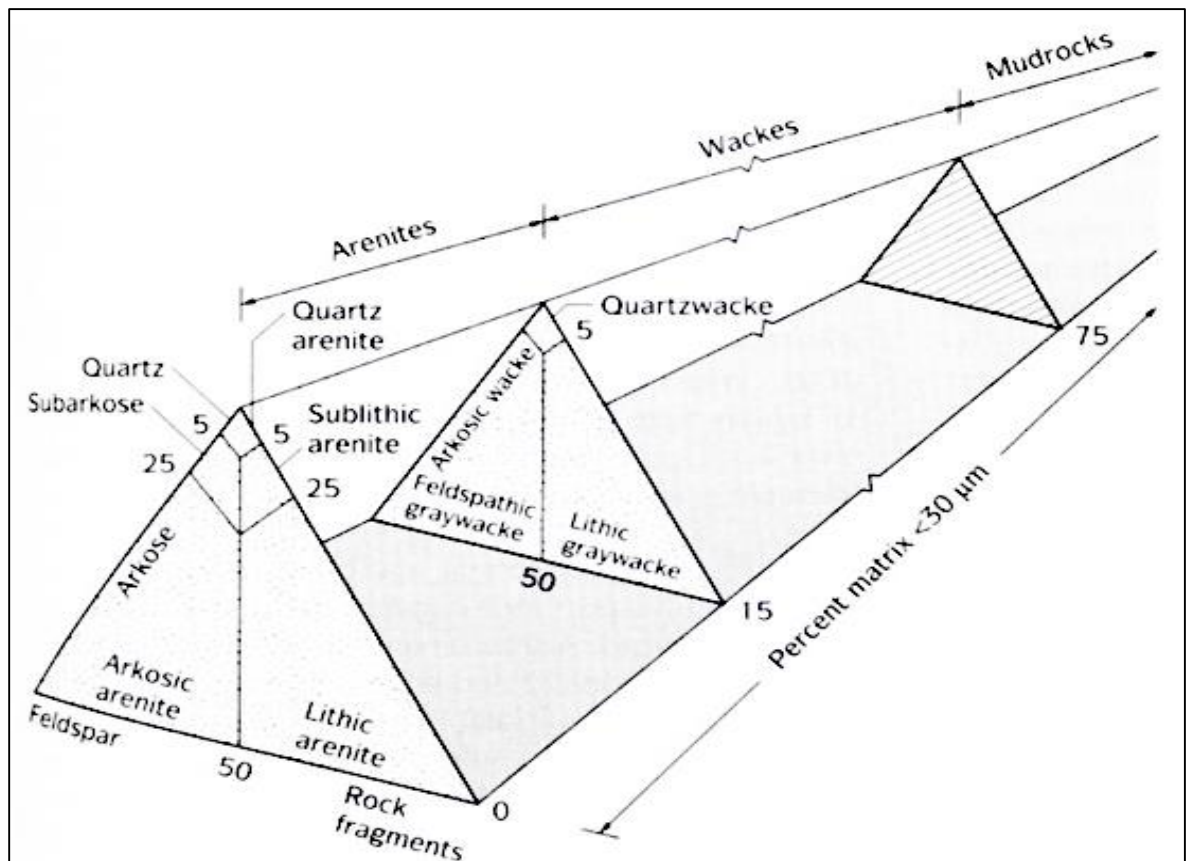


Figure 3. According to Nelson, (2013) the major framework composition, arenites are broken down into: Quartzarenite, arkosic arenite, lithic arenite and wackes, and with > 15% matrix break down into: quartzwacke, feldspathic greywacke, lithic greywacke (modified from Dott, 1964).

The Lower Kolmule Formation ternary plot is shown in Figure 4. Six samples were selected to identify the Lower Kolmule Formation composition. Samples 11 and 13 show 34.1% and 36.2% clay matrix content respectively (Table.1) and are located in the lithic greywacke position in the ternary plot.

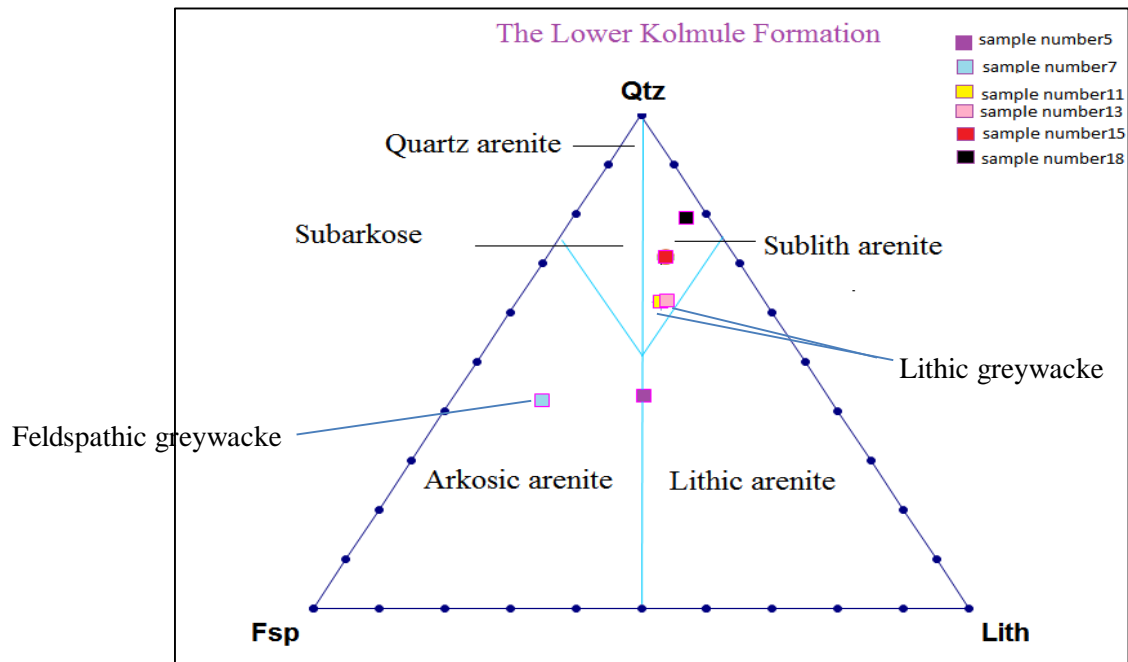


Figure 4. . Quartz-Feldspar-Lithics (QFL) plot of the sandstones of the Lower Kolmule Formation. “Lith” includes mica, heavy minerals, glauconite and the rock fragments. Two Samples (15, 18) show the sublith arenite and samples number 11 and 13 show the lithic greywacke composition due to their clay matrix composition.

Only one sample is selected for the Hekkingen Formation which is defined by the lithic greywacke composition (Fig. 5) due to 18.9% clay matrix content (Table. 1).

Seven samples with different depths (Table. 1) are point counted in the Stø Formation (Fig. 6). Samples number 31 and 35 have more than 15% clay matrix content and both of them are defined as a lithic greywacke rocks (Fig. 3). Although there is a big scatter of the composition in the ternary plot (due to the different grain-sizes in the formation), the three of samples show subarkose composition for this formation (Fig. 6) which can be considered as the main composition.

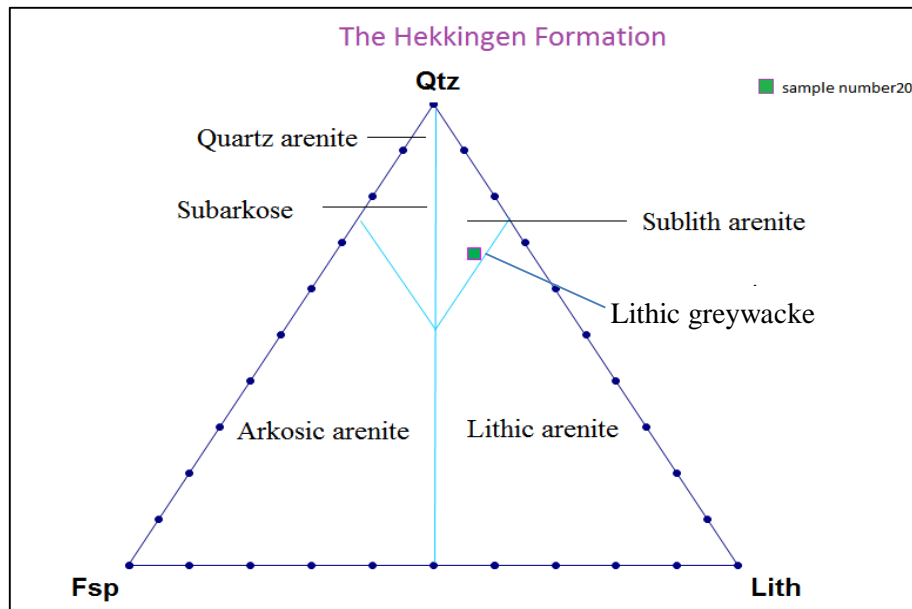


Figure 5. Quartz-Feldspar-Lithics (QFL) plot of the sandstones in the Hekkingen Formation. “Lith” includes mica, heavy minerals, Glauconite and the rock fragments. Only one sample was taken for rock types identification which shows the lithic greywacke composition due to high clay matrix content (more than 15%).

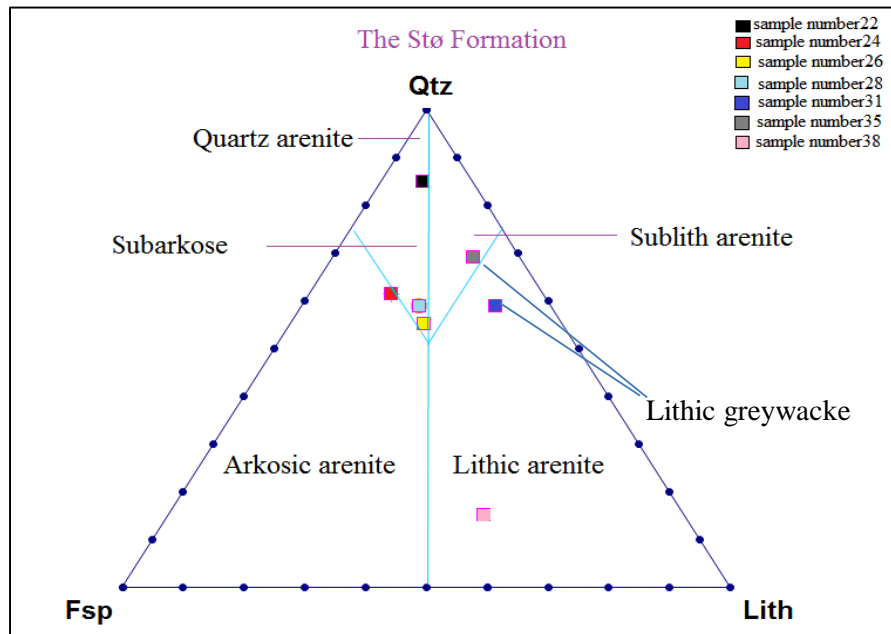


Figure 6. Quartz-Feldspar-Lithics (QFL) plot of the sandstones in the Stø Formation. “Lith” includes mica, heavy minerals, Glauconite and the rock fragments. There is a variation in the rock types but more samples are concentrated in subarkose classification. Samples 31 and 35 are defined as lithic greywacke.



## 4.2 Formations

### 4.2.1 The Lower Kolmule Formation

#### 4.2.1.1 Lithology and textures

The Lower Kolmule Formation (1583.1 m to 1636.95m) consists of fine-grained to medium-grained sandstone with the moderate to well sorting and subrounded to subangular roundness (Table. 1). Evidence of grey to green clay matrix and shale fragments in the sandstones is mostly observed at the base of this formation. The dominate minerals are quartz, feldspar, glauconite, and rock fragments are also abundant. In the middle to the base of this formation there are the records of organic matter within the clay matrix (Fig. 7). The formation has the lithic greywacke composition in the ternary plot (Fig. 4).

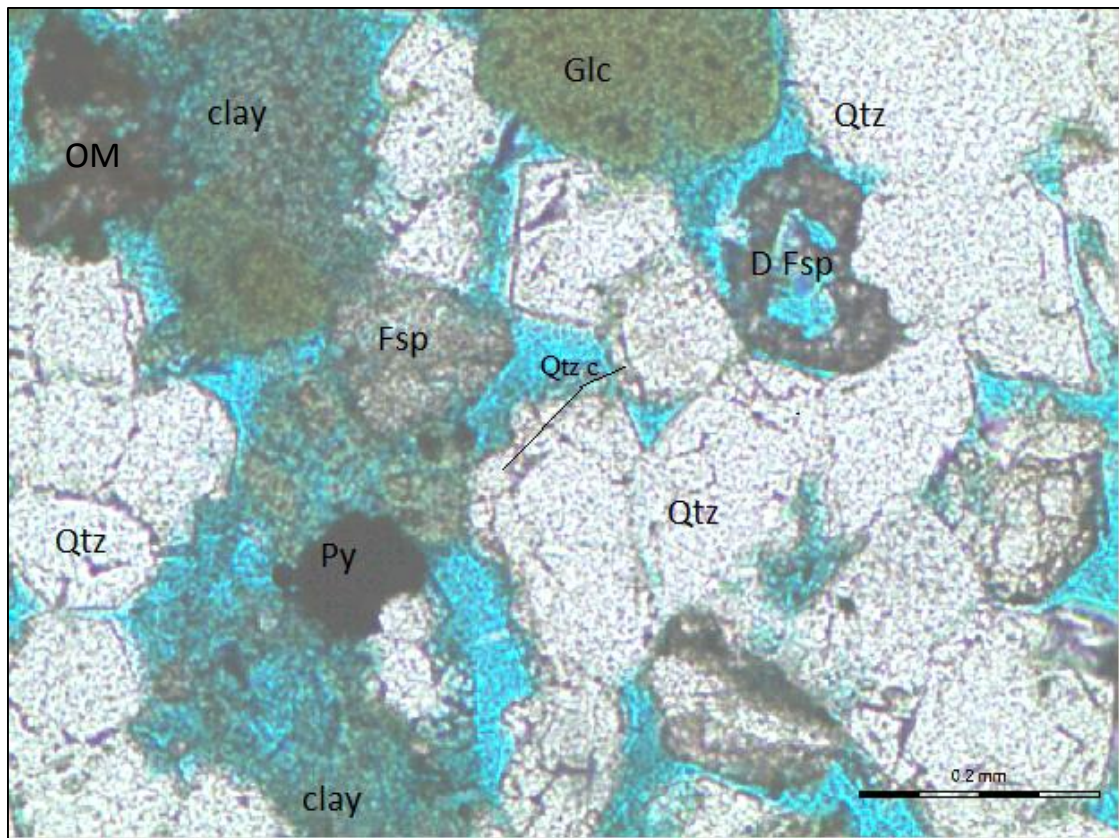


Figure 7. The Lower Kolmule Formation. Pyrite (Py) can be seen as a dark grain, detrital quartz grains (Qtz) are white in plane polarized light, Organic matter (OM) as a dark spots within the clay matrix, glauconite (Glc) as a rounded grain with a green color, Qtz C (quartz cement\ quartz overgrowth), dissolved Feldspar(D Fsp), and precipitation of clay minerals (Cly) (depth 1583.10).

#### **4.2.1.2 Detrital grains**

##### **Quartz**

Quartz is a dominant detrital mineral in all the sections and the quartz consists mostly of monocrystalline grains (Fig. 7). Diagenetic quartz overgrowth is seen in most of the intervals wherever there is no evidence of chlorite coatings. Some of the quartz overgrowths appear as rounded and irregular, indicating that they are formed in older sandstones. A very small amount of planar regular overgrowths that seem to have precipitated on quartz grains after deposition is also present. In general the quartz overgrowths are optically continuous with the substrate minerals revealing perfect crystal continuity (Fig. 7).

##### **Alkali feldspar**

Another abundant mineral after quartz is alkali feldspar. The observed alkali feldspar in this formation is microcline. It displays albite twinning and pericline twinning which in combination leads to a grid pattern. The alkali feldspars are stained in the yellow colour for distinguishing between K-rich and Na-rich feldspars. In the base of this formation evidence of alkali feldspar dissolution and precipitation of secondary minerals is observed (Fig. 7).

##### **Rock Fragments**

In this formation there are lots of rock fragments with different sizes. Mostly the rock fragments consist of chert, polycrystalline quartz (Fig. 9) or fine-grained materials like shale fragments (Fig. 8). Figure 8 illustrates big rock fragments. Due to a dissolution process on the surface of the rock fragment, the accumulation of organic matters occurred (Fig. 8). In this study all the polycrystalline quartz is included in the rock fragments category in the ternary plot (Fig. 4, 5, 6).

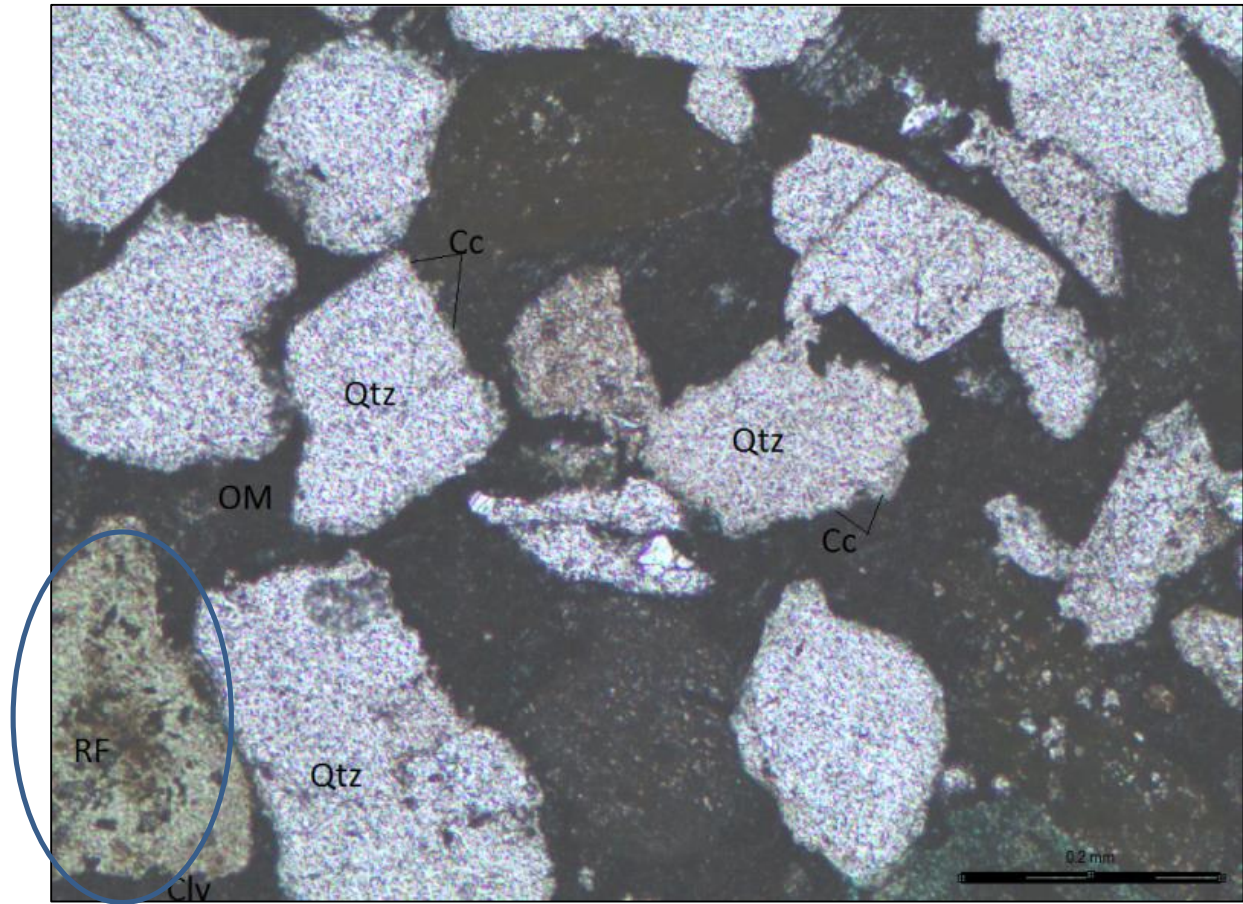


Figure 8. The coarse Rock fragment (RF) consists of organic matter and fine-grained clay in the left part of the figure (depth 1589.1).

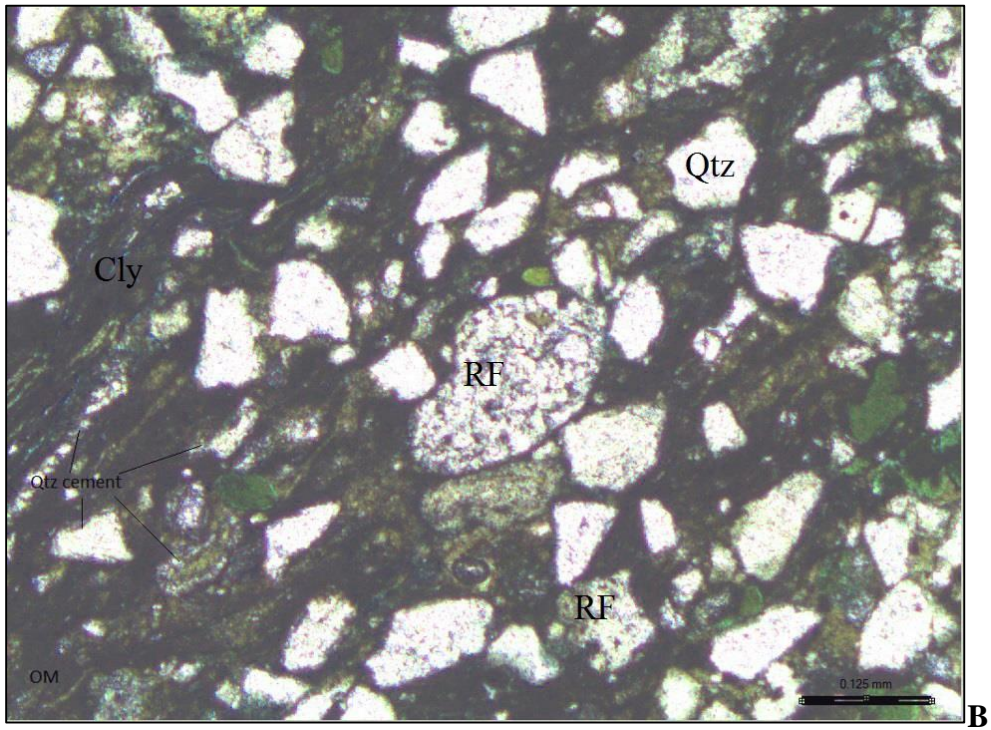
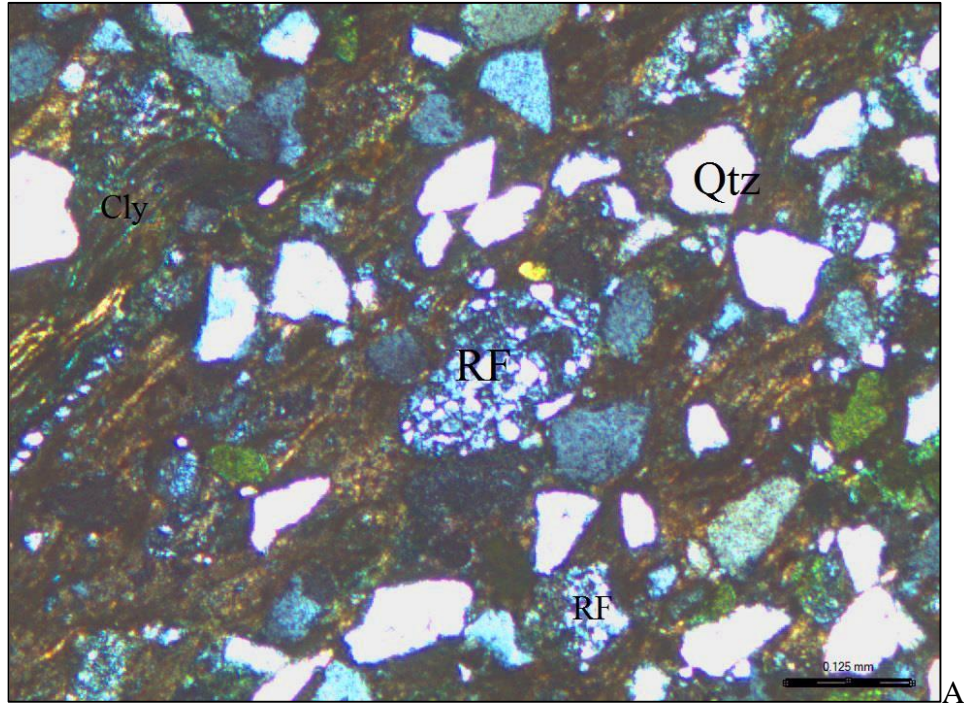


Figure 9. Polycrystalline quartz rock fragment (RF) indicator of a metamorphic source. A) In cross polars, B) In normal light (depth 1595.40).

## Heavy minerals

Heavy minerals were observed in most of the samples but in trace amount only. Yellow and green rounded tourmaline was the only heavy mineral which was observed in the Lower Kolmule formation.

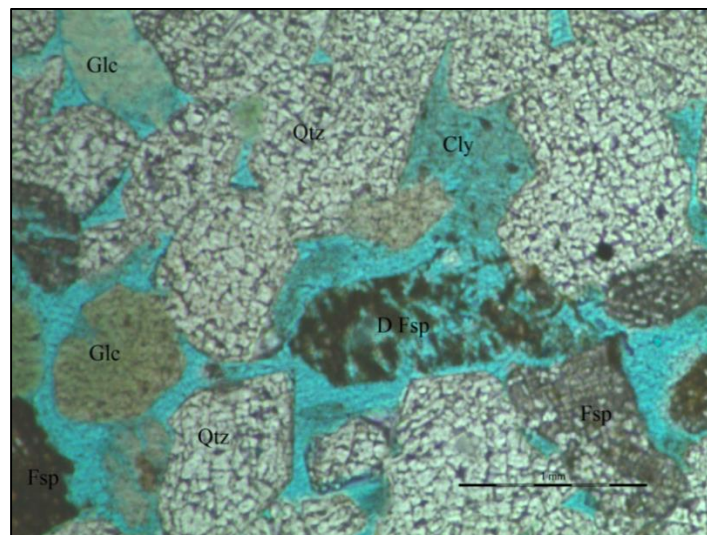
### 4.2.1.3 Diagenetic Minerals

#### Clay Minerals

In the Kolmule Formation three different clay minerals have been identified, glauconite, illite and chlorite. Smectite and kaolinite were not observed in the Kolmule Formation so it is assumed that the current illite in the formations is the product of smectite or kaolinite reactions (Bjørlykke, 2010).

#### Glauconite

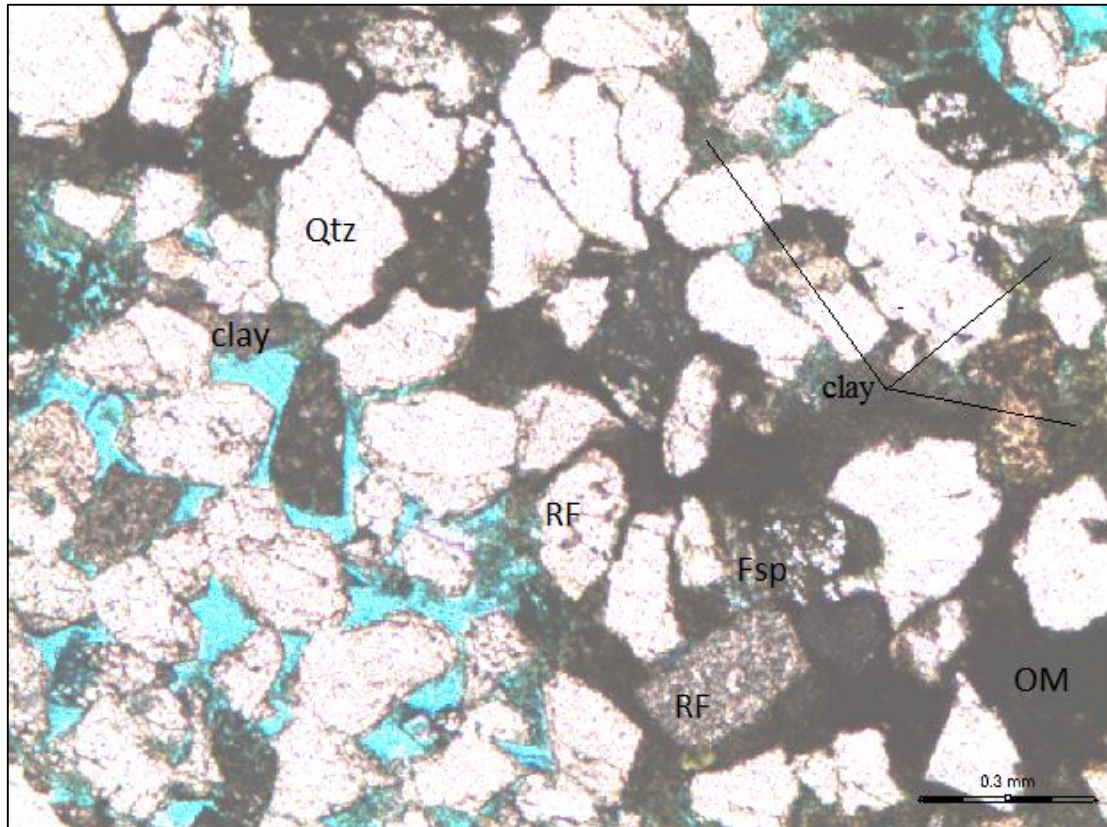
Glauconite as a third abundant mineral in this formation is observed displaying the characteristic kidney shape or sub rounded shape in some places (Fig. 10). It is seen that in most of the samples especially in shallower ones the glauconite occurs as a morphological glauconite mainly in the form of sand-sized grains (pellets). By increasing depth the number of glauconite grains were decreased and they could be identified mostly as a secondary mineral infilling cracks and hollows or replacing pre-existing minerals.



**Figure 10. Glauconite (Glc), dissolved Feldspar (D Fsp). Porosity (Po) and quartz (Qtz) are shown in this figure. Glauconite is displaying kidney shape in this sample (depth 1583.10).**

## Illite

Illite is produced by the different reactions of some other unstable clay minerals like smectite, kaolinite, and mixed-layer clay minerals or it can be formed from the feldspars.



**Figure 11. Combination of illite and chlorite clay minerals, filling the pores. Organic matter (OM) and rock fragments (RF) are illustrated in the figure (depth 1587.1).**

In this study illite was observed almost in all the samples with different quantities. Mostly it occurs along with the organic matter and pyrite (Fig. 11).

## Chlorite

The depth 1590.75 shows that chlorite is associated along with illite and causing decrease in porosity and permeability (Fig. 12).

## Pyrite

Pyrites mineral is observed along with the organic matters, mostly at the base of this formation (Fig. 13). The pyrite appears as a crystal form mineral and in some parts fills the pores as cement.

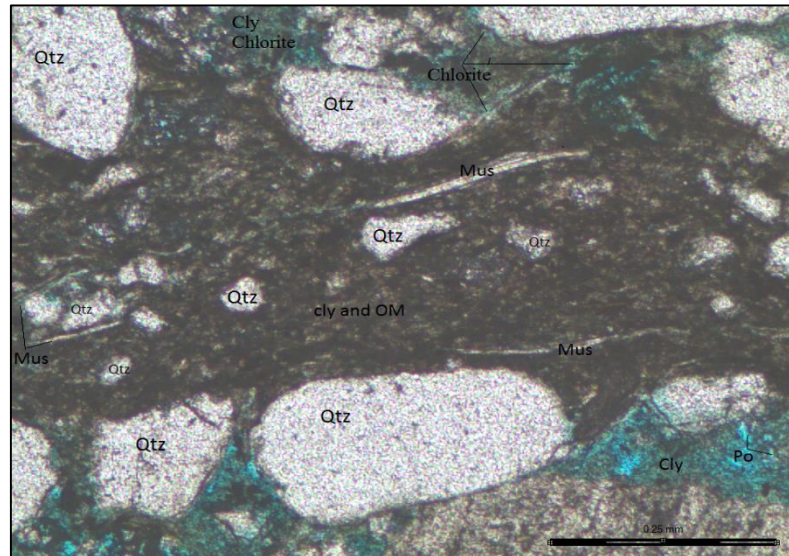


Figure 12. Chlorite (Cly) is filling the pores and reduces the porosity. Quartz (Qtz), organic matter (OM) and muscovite (Mus) are shown in this figure. Muscovite shows mechanical compaction (depth 1590.75).

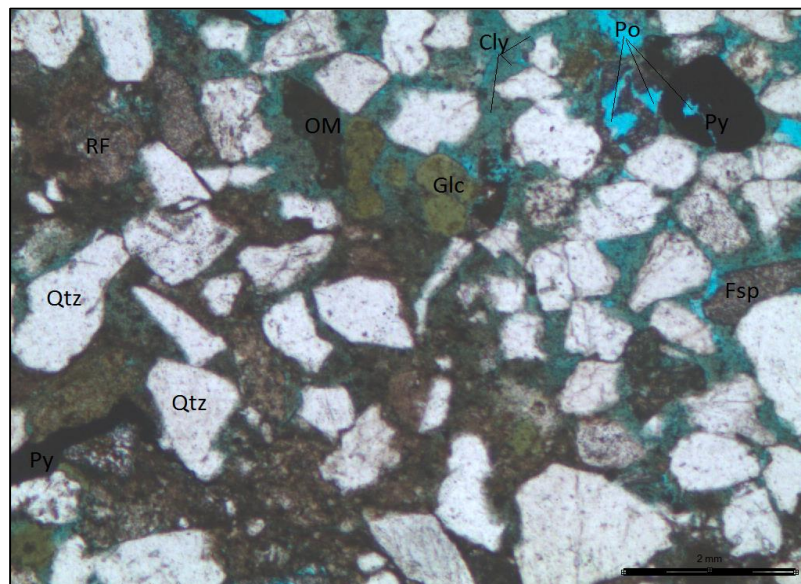
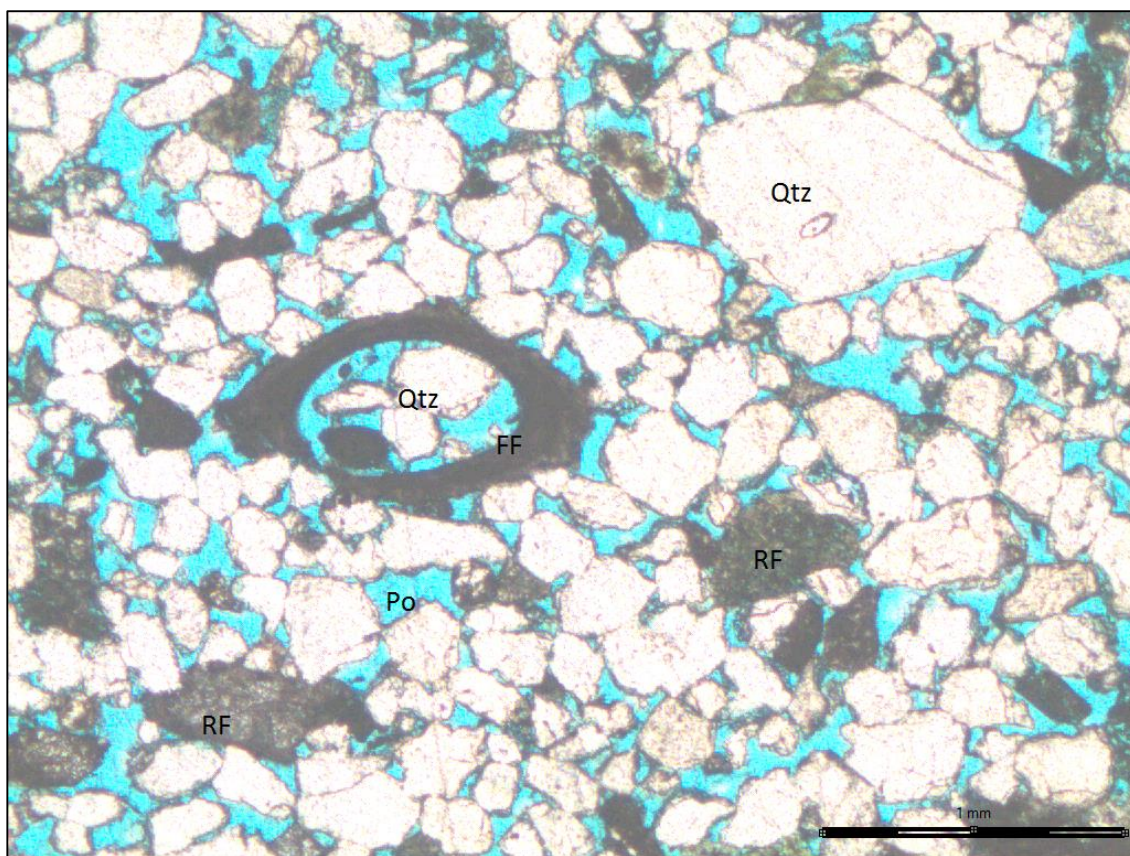


Figure 13. Pyrite (Py) is observed as a single grain in the right side of figure and also as cement in the left side of figure along with organic matter and glauconite (depth 1590.75).

#### 4.2.1.2 The observed diagenetic processes

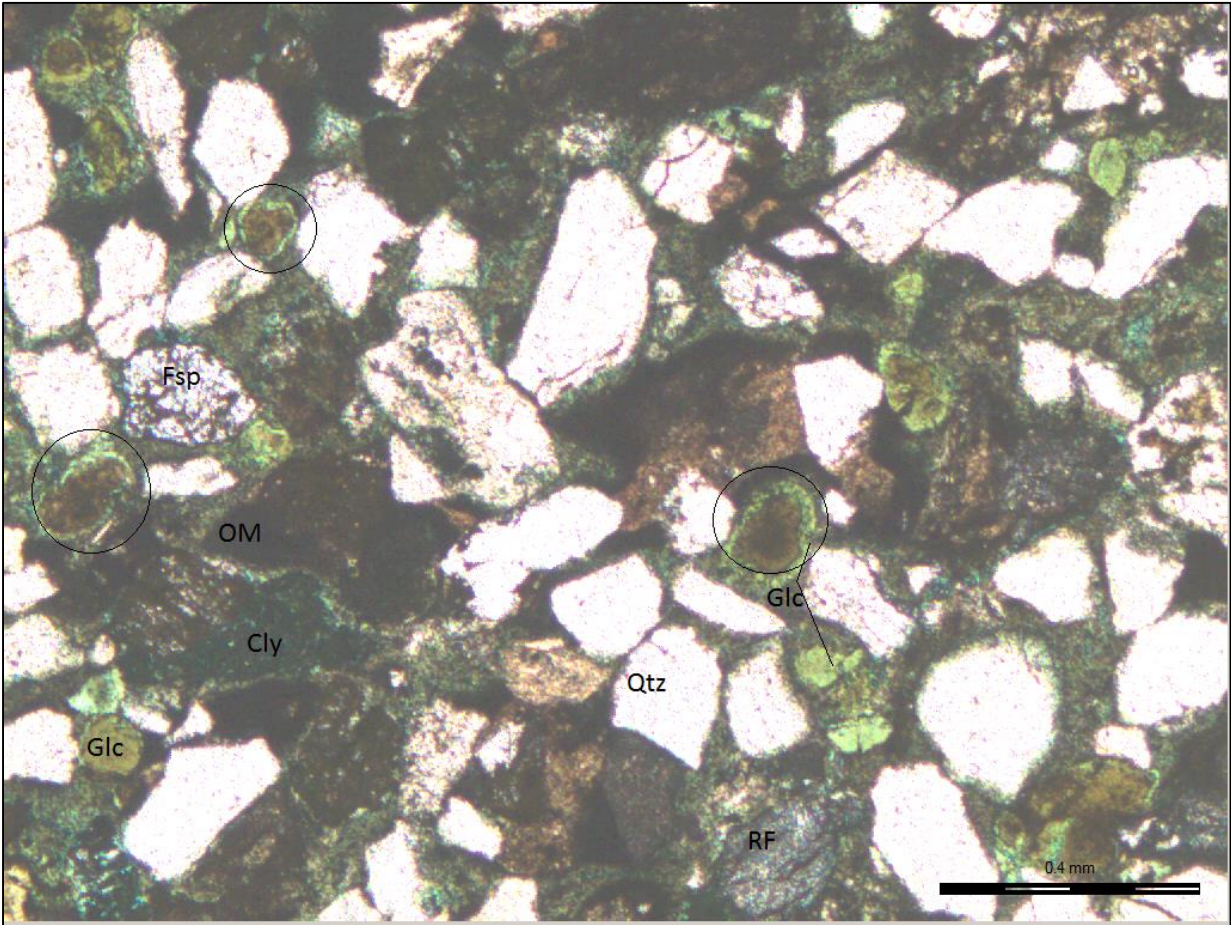
The main diagenetic processes within the Lower Kolmule Formation can be summarized as physical compaction, chemical compaction, cementation, stylolitization, glauconitization and bioturbation. Alkali feldspars are dissolved due to the chemical compaction (Fig. 7, 10). There is some evidence of dissolved fossil fragments due to this process (Fig. 14). Porosity is decreased significantly by the physical compaction, cementation and precipitation of clay minerals as a matrix that decreases the permeability as well and reduces reservoir quality. In contrast chemical dissolution has created the secondary porosity (Fig. 14) which makes higher porosity values.



**Figure 14.** The evidence of dissolved fossil fragment (FF). This sample consists of quartz as a major grain, rock fragments and minor clay matrix (depth 1635.80).

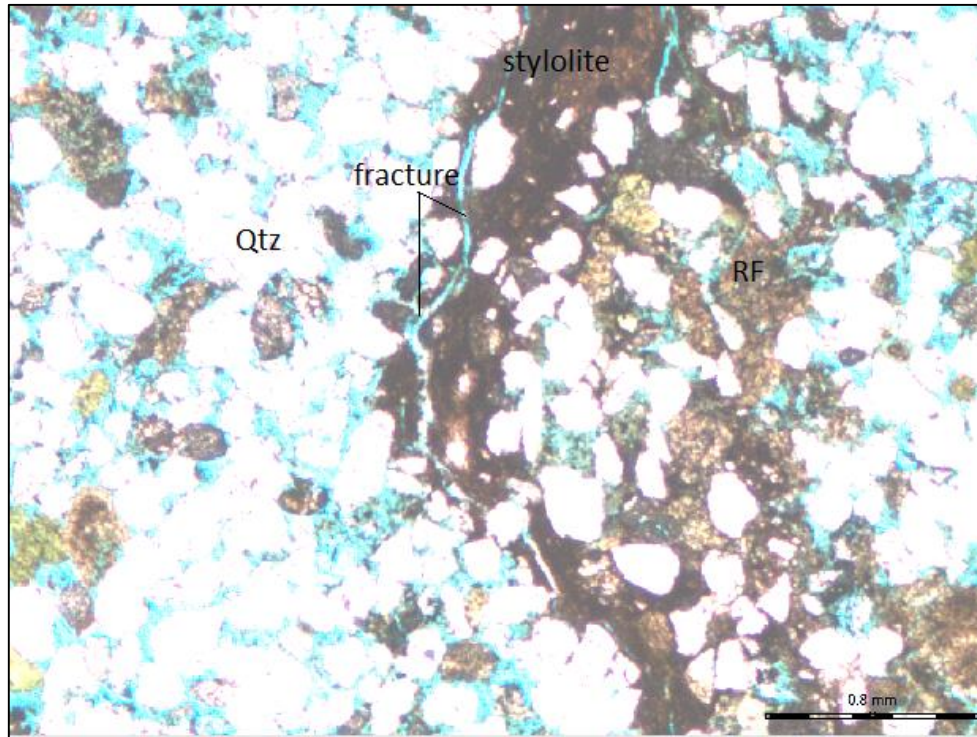
The glauconitization of cherts, pellets and quartz were observed (Fig. 15) but this process wasn't as common as other processes.





**Figure 15. The glauconitization (Glc) process is observed around the pellets. The presence of organic matter (OM), Clay minerals (cly), rock fragment (RF), feldspar (Fsp) are determined (Depth 1602.05).**

The stylolite features are also common in the Lower Kolmule Formation. These features can be formed due to the dissolution of carbonate (fossil fragments). The onset of observed Stylolitization processes is from the 1584.05m, and this process is continued to deeper formations. The accumulation of insoluble residues such as clay minerals and organic matter on the stylolite surfaces is observed in figure 16.



**Figure 16. The Stylolitization process due to the mineral dissolution and accumulation of clay minerals and organic matter on the stylolite surface (depth 1584.05m).**

#### **4.2.2 The Hekkingen Formation**

The Hekkingen Formation in the study well is represented by only two samples at 2002.05m and 2010.65m depths. In the depth interval of 2002.05 the sample shows a high porosity with well sorting (Table. 1), but the other sample which is taken from the depth interval of 2010.65 shows a significant decrease in porosity due to the extensive quartz cementation which creates the unique ribbon-like texture (Fig. 18). In this case based on the theory of Bjørkum et al., (1998) it can be assumed that the quartz dissolved at the stylolite interface due to the interaction of quartz and mica/illite clay interface and the dissolved quartz is transported into intrastylolites by diffusion process and create the quartz overgrowth or quartz cementation between the grains. In figure 17 the evidence of stylolitization are clearly observed. Quartz overgrowth is also observed in the 2002.05m (Fig. 19). The quartz grains are squeezed due to the compaction and they have gotten the suture and concave-convex contact (Fig. 19). The major components in this formation are quartz, alkali feldspar and glauconite.

The evidence of clay minerals precipitation is observed. The clay minerals mainly consist of illite and chlorite and the pores are filled with these minerals wherever there is no quartz cementation. The trace of phosphate and tourmaline (heavy mineral) is observed. According to the high amount of shale and clay matrix along with the organic matter (wood fragments) in this formation it is assumed that the Hekkingen Formation is a potential source rock for the Lower Kolmule Formation. The rock composition of this formation shows the lithic greywacke (Fig.5).



Figure 17. The evidence of stylolitization in the Hekkingen Formation is illustrated in core number 5. Only two samples are available from this core, 2002.05m and 2010.65m.

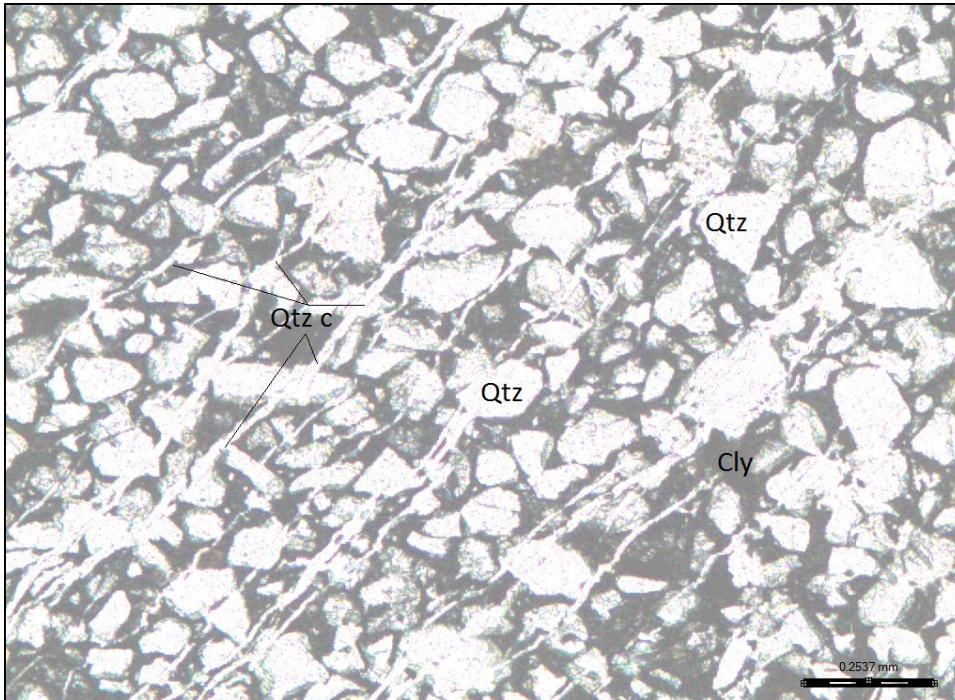


Figure 18. The depth interval of 2010.65 shows a significant decrease in porosity due to the extensive quartz cementation (Qtzc) which creates the unique ribbon-like texture. The clay matrix (Cly) occurs between the quartz (Qtz) grains.

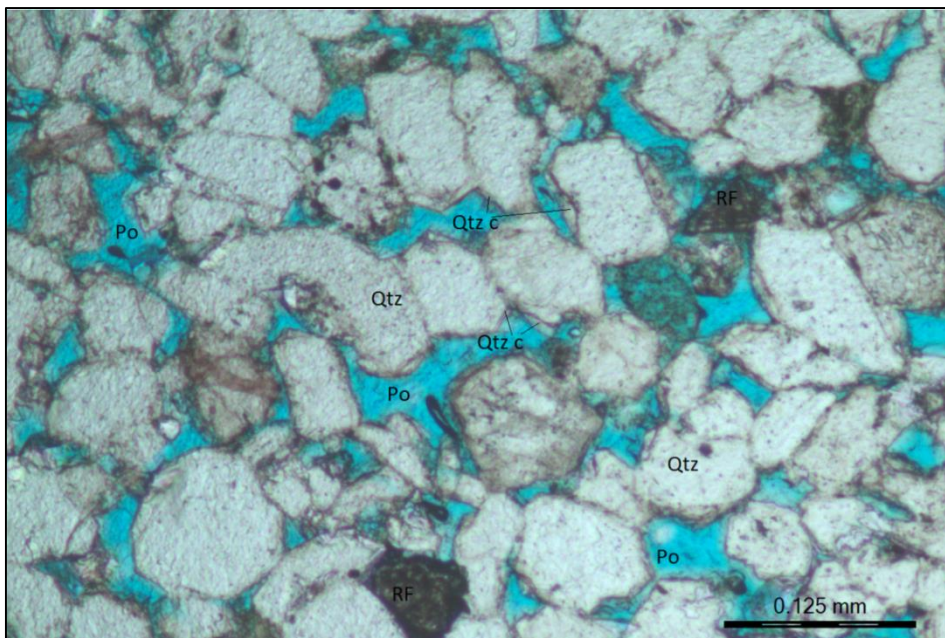


Figure 19. Quartz overgrowth is observed in the 2002.05m. The quartz contacts show the suture and concave-convex shapes due to compaction.

### 4.2.3 The Fuglen Formation

Only one sample (2019.35m) is available for the Fuglen Formation (2017.9m to 2071m) which cannot be a representative of the whole formation but according to the core images which are provided by the Lundin company it is clear that this formation consists of dark shale and pyritic mudstone with interbedded white to brownish grey limestone (according to the literature review) (Fig.20). This sample shows high clay content which decreases the porosity sharply due to the fine-grained texture.

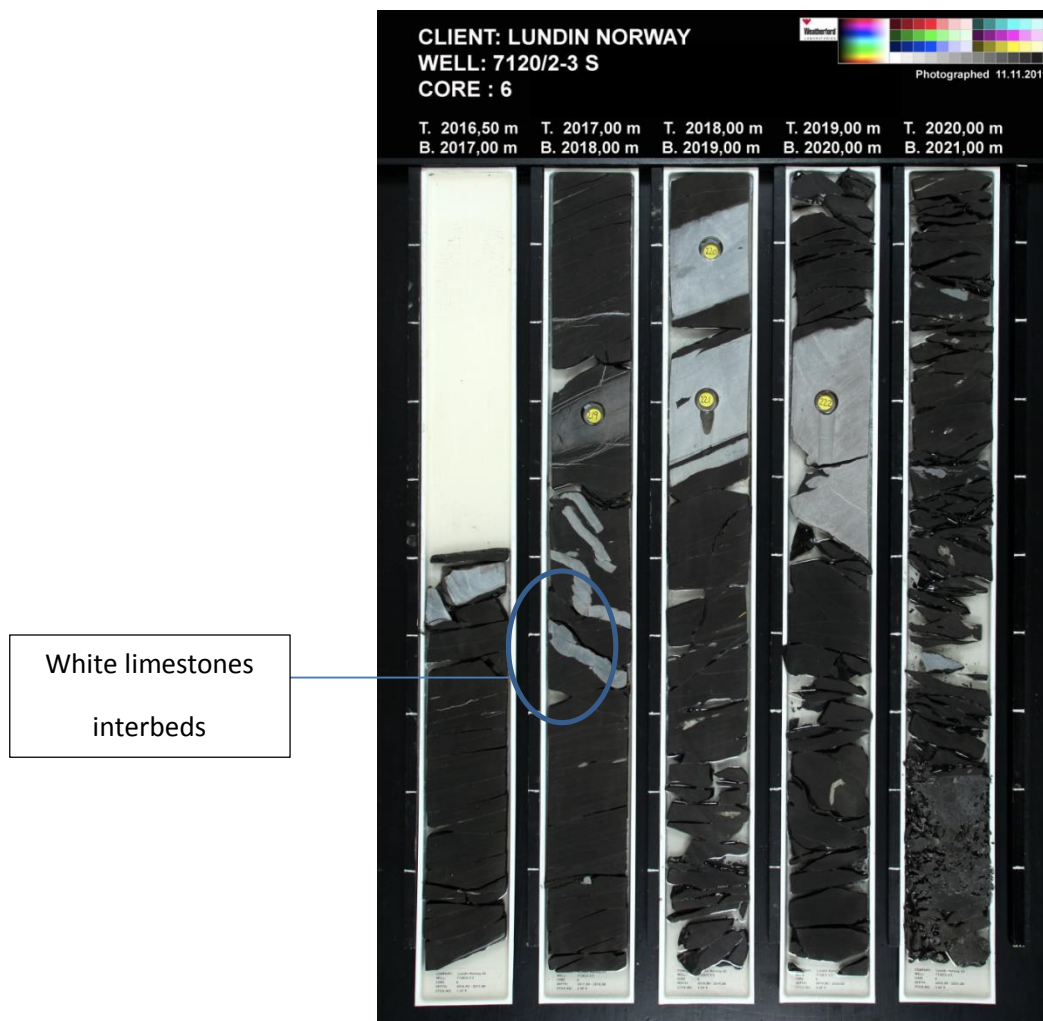


Figure 20. The Fuglen Formation consists of dark shale and pyritic mudstone with interbedded white to brownish grey limestone according to core number 6.

## **4.2.4 The Stø Formation**

### **4.2.4.1 Lithology and textures**

The Stø Formation is located from 2079.98m to 2152m in the study well. The 18 samples were picked from this formation for petrographic studies. This formation consists of medium to coarse-grained sandstone with well sorting in the most of the samples (Table. 1). The major components of this formation are quartz, alkali feldspar and the evidence of clay minerals (shale) lamina along with organic matter and the authigenic phosphate are observed.

The glauconite content is observed in distinct beds. The Stø Formation is defined as subarkosic sandstone in the ternary plot (Fig. 6). The sandstones will be referred to as fining upward sandstones due to the great variation in the grain size distributions (Table. 1).

### **4.2.4.2 Detrital grains**

Quartz is a dominant mineral in the Stø Formation and mainly consists of monocrystalline grains. The evidence of quartz overgrowths is observed at the top of this formation. Alkali feldspar is the second major mineral in this formation and commonly is observed with the microcline twins. The partial dissolution of K-feldspar is observed, but it is difficult to mention if the dissolution take place before or after deposition. Muscovite is associated as single minerals in a clay matrix, while no biotite was seen in the Stø Formation. At the depth 2094.9m the amount of muscovite is increased and some of the muscovite grains are bent due to the mechanical compaction (Fig. 21).

Heavy minerals were observed in the Stø Formation in trace amounts. Tourmaline, rutile and chrome-spinel are the main heavy minerals which were observed in this formation. Glauconites are observed at the top of this formation in small quantities, and rock fragments occur in trace amounts.

From 2152m to 2125.88m, a clean quartz arenite sandstone is observed with high intergranular porosity. Dissolution due to chemical compaction is observed, but it isn't accumulated with any organic matter or clay matrix. Fractures were observed in most of the samples at these depths. They may have been formed due to the compaction or breakage of samples during preparation (Fig. 22).

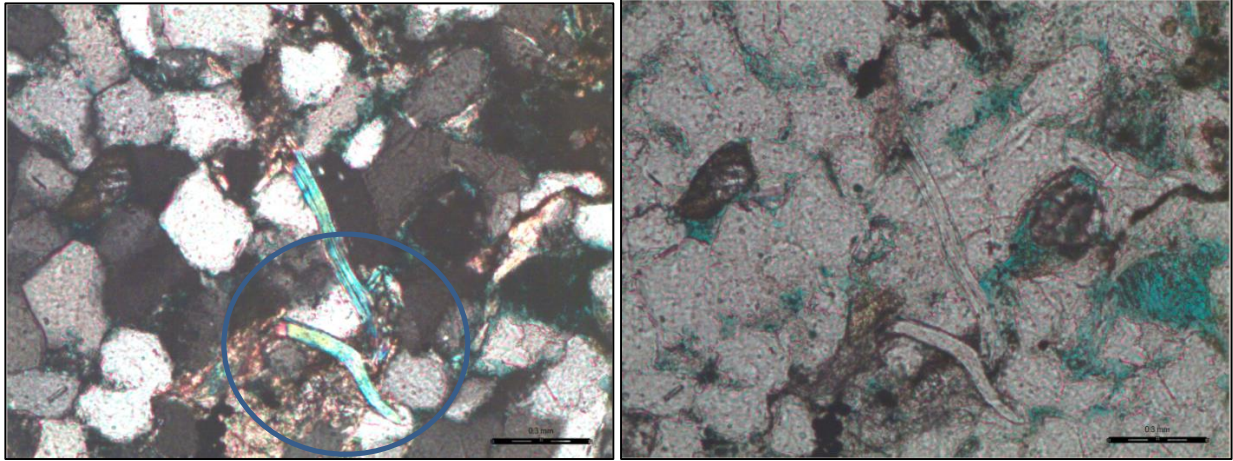


Figure 21. The muscovite is bended due to mechanical compaction in the Stø Formation (depth 2094.9m).

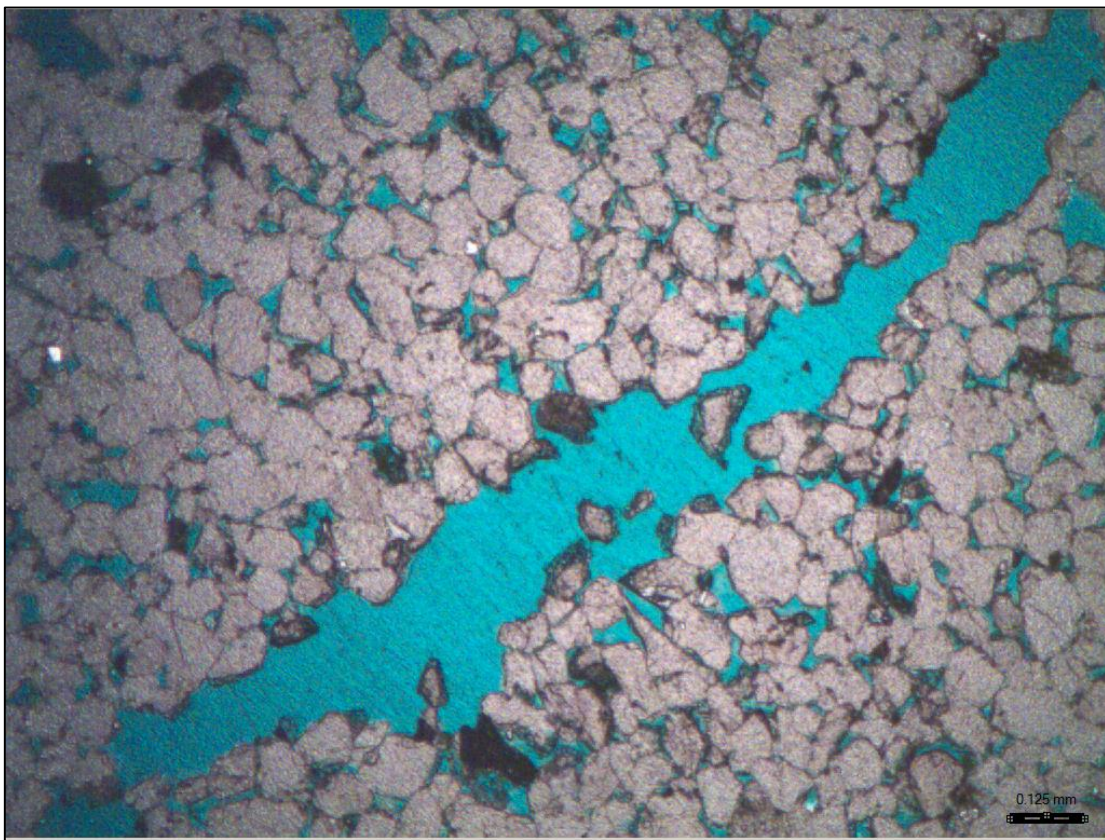


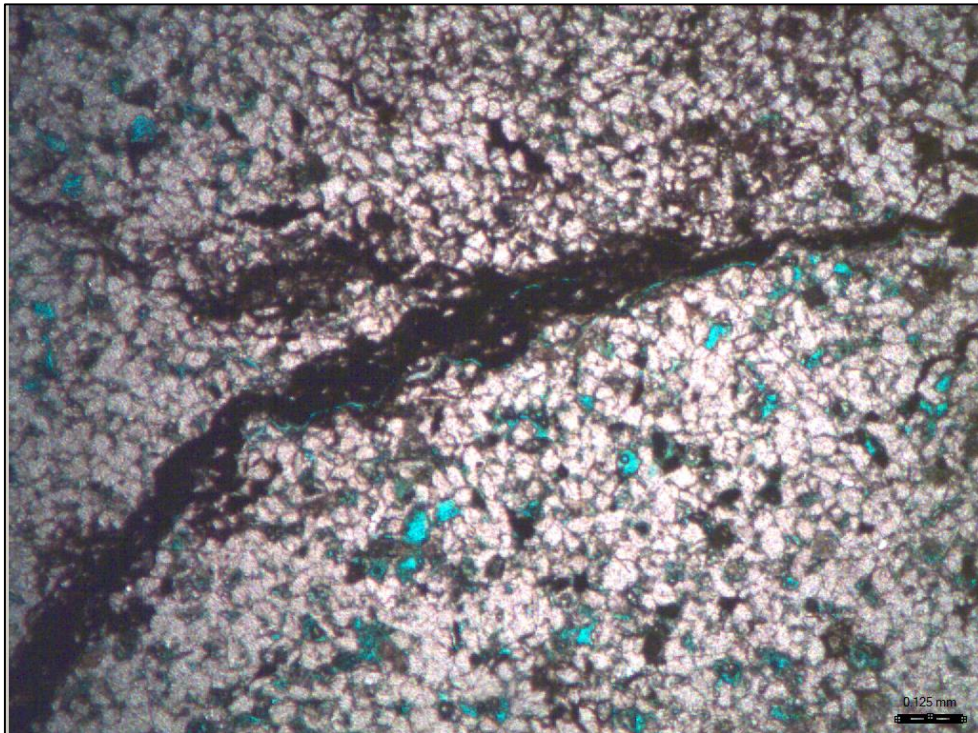
Figure 22. The fracture is observed due to the compaction and may have been enlarged by breakage of samples during preparation in the Stø Formation (depth 2133.9m).

#### 4.2.4.3 Diagenetic minerals

The main diagenetic minerals in the Stø Formation are the precipitation of clay minerals such as illite and chlorite along with moderate amounts of organic matter in the pore spaces. Pyrite occurs as isolated crystals and pore-filling cement almost in all the samples.

#### 4.2.4.4 The observed diagenetic process

Stylolitization is the main diagenetic process which is observed from 2117.86m to 2094.9m. The stylolites are occupied by the illite and chlorite clay matrix along with the organic matter (Fig. 23).



**Figure 23. The stylolitization process in the Stø Formation. The stylolites are occupied by the illite and chlorite clay matrix along with the organic matter (depth 2099.85m).**

Bioturbated laminates are observed associated with the stylolites and have affected the sediment matrix. The large amounts of organic matter and particles have been redistributed through this process (Fig. 24).



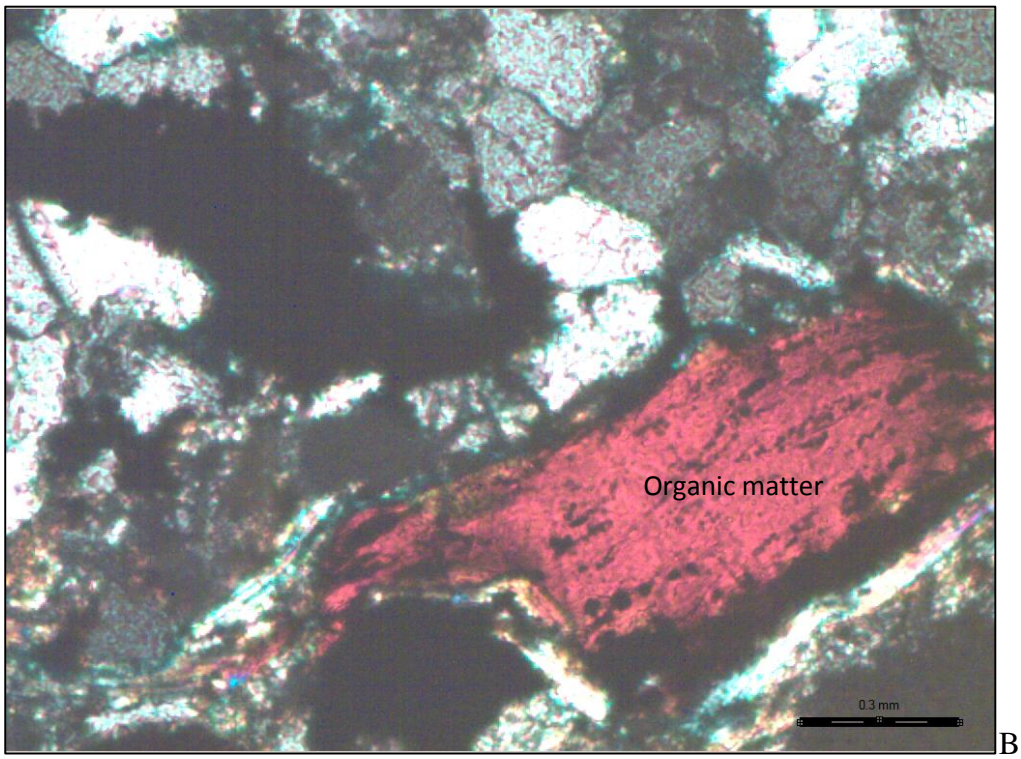
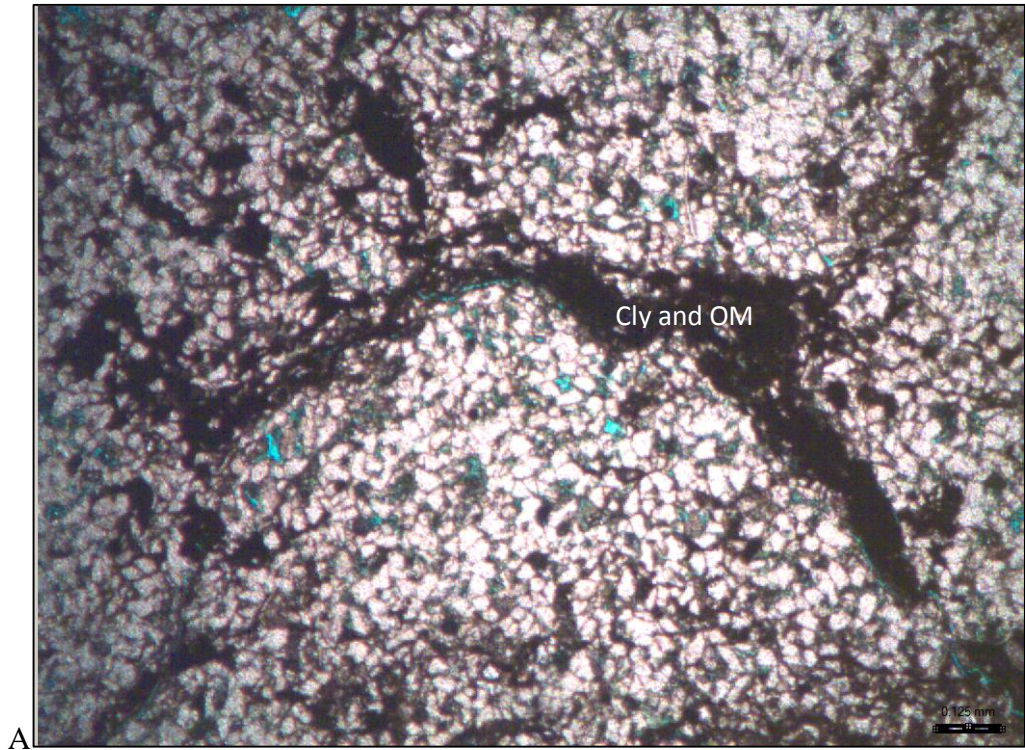


Figure 24. The bioturbation took place in the Stø Formation. Figure A shows the extensive accumulation of organic matter and redistributed particles. Figure B shows a big organic matter particle in the red color accompanied with the detrital grains (depth 2094m).

## **5. Evaluation of wire line logs**

To estimate the total amount of hydrocarbon of a given basin or prospect, source rock and the reservoir should be define. The lithology of source rock is shale or limestone with high amount of organic matter and sandstones or limestones are considered as a reservoir rocks. Because the most complete and readily available well data are wire line logs, it seemed desirable to investigate the possibility that source rocks might be recognizable from wire line logs (Meyer and Nederlof, 1984).

### **5.1 Introduction (literature review)**

Wire line logging is a conventional form of logging that employs a measurement tool suspended on a cable or wire that suspends the tool and carries the data back to the surface (Glover, 2012) and Wire line logs are created when the drill-bit is removed from the borehole.

Many information regarding porosity, permeability, formation thickness, depths, lithology, water saturation, wettability, capillary pressure and grain and pore size distributions can be obtained from the core analysis. This information from core analysis carries very detailed description from the subsurface. Visual examinations of cores are an important method to study formation features but this method has some limitations due to imprecise depth for each sample and high cost for coring process. One of the earliest goals of wire line logging was to provide a description as detailed as those obtained by coring, but more time-efficient and cheaper (Ekstrom et al., 1987). The wire line logs are providing continuous measurement of data as a function of depth, but they are used as a supplementary method to cores.

Wire line logs consist of these types of logs which are mechanical logs (e.g., calipers), electrical logs (e.g., laterologs, induction logs, SP logs), natural radiation logs (e.g., simple and spectral gamma ray logs), acoustic logs (e.g., sonic logs), pressure and temperature logs, artificial radiation logs (e.g., density and neutron logs), imaging logs (e.g., dipmeter and various other types) and special logs (e.g., NMR logs).

According to the given petrophysical data from the Skalle well 7120/2-3S, the logs that are interpreted and compared to the thin sections study are mechanical logs, natural radiation logs

electrical logs , acoustic logs and artificial radiation logs. The main focus of the log interpretation is in the depth interval 1583.1 to 2152 meters where thin sections and core photos are also available.

### 5.1.1 Mechanical log (Caliper log)

The Caliper Log is a tool for measuring the diameter and shape of a borehole. It uses a tool which has 2, 4, or more extendable arms. The arms can move in and out as the tool is withdrawn from the borehole, and the movement is converted into an electrical signal by a potentiometer (Glover, 2012). The caliper logs are plotted along with the drilling bit size, for comparison for instance, when a hole has same size as the bit-size, it is called on gauge. By this comparison it is possible to predict the probable lithology (Fig. 25).

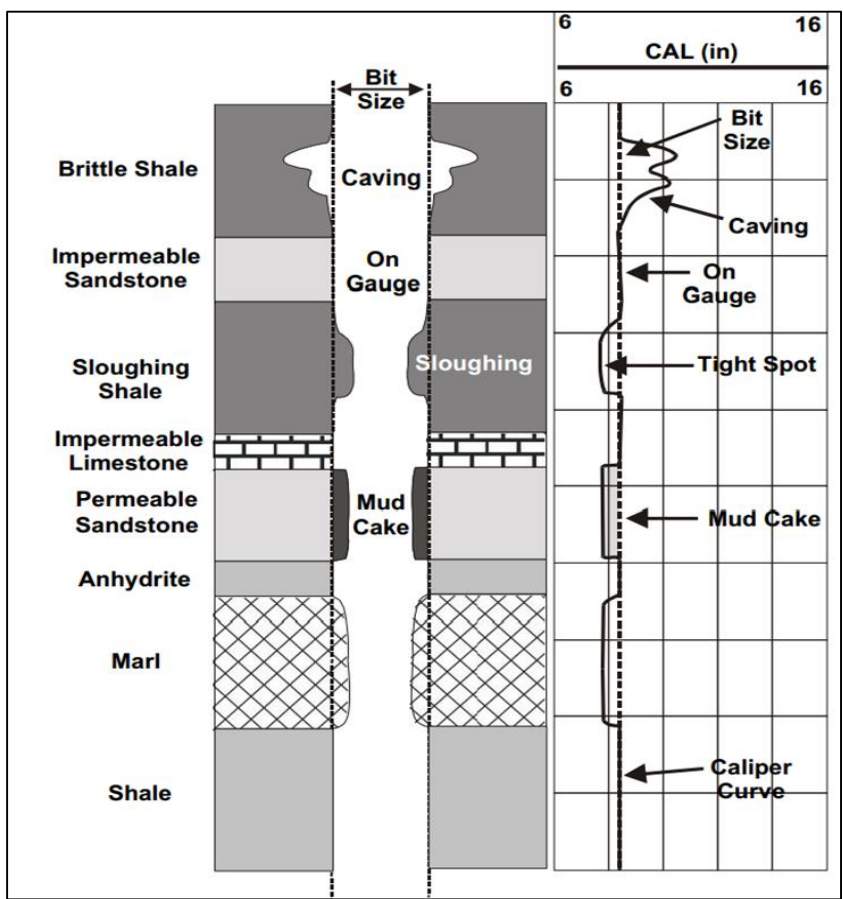


Figure 25. Typical caliper responses to various lithologies (Glover, 2012).

According to Figure 25, when the hole diameter is the same as the bit-size it shows that the formation is consolidated and non-permeable massive sandstones, calcareous shales, igneous and metamorphic rocks are possible lithologies. In the other situation, when the borehole diameter is larger than the bit-size, the formation consists of a soluble lithology such as a salt formation or brittle shale, but when the diameter is smaller than the bit-size, it is time for the development of mudcake for porous and permeable formations which indicate the permeable sandstones.

In general, caliper logs are used in connection with data which are collected by other geophysical methods for the precise determination of the geologic cross section of a borehole and for identifying the location of reservoir beds.

### **5.1.2 Natural radiation log (Gamma ray log)**

The Gamma ray is produced during the radioactivity decay of rocks. The basic detectors measure the total gamma ray activity of the formation. This tool is usually referred to as just a Gamma ray (GR).

Advanced detectors can measure the energy of incoming Gamma ray for the different radioactive elements such as potassium, uranium and thorium. These tools are called Natural Gamma ray Tool (NGT) (White, 2012).

Organic-rich rocks can be relatively highly radioactive due to their uranium content, that is, they can have a higher gamma ray reading compared to other types of lithologies like limestone or ordinary shales (Meyer and Nederlof, 1984). Uranium can be associated with clay minerals or can be dissolved in sea or river water. From solution, uranium is fixed in sediments by precipitation in reducing environments where there is a high concentration of organic matter or phosphate (Adams and Weaver, 1958). A part from uranium which can influence on gamma ray, potassium and thorium as radioactive elements can also effect on the gamma ray log and increase the reading. Potassium is an element occurring within the structure of many common detrital minerals, especially the clay minerals such as illite, mixed-layer illite/smectite, and glauconitic minerals. Other types of clays, particularly kaolinite, smectite, and chlorite, may contain negligible quantities of potassium. K-feldspar and mica

may also be important within some sandy intervals in the Pleistocene sections, but otherwise generally occurs in very small quantities (Mountain et al., 1996).

Thorium is often associated with heavy minerals, and can be identified in continental shales. In sedimentary rocks there is low concentration of radioactive minerals unless there is a complex mixture of radioactive minerals in the formation. Figure 26 shows the thorium/potassium ratio for identifying mineral type in the formation. A high Th/K ratio shows the high concentration of heavy minerals and the low proportion demonstrates the high concentration of illite.

Radioactive sandstones fall into one of six main groups (Glover, 2012): 1) clay-Bearing Sandstones, which contain clay minerals in the rock, 2) arkose sandstones, which contain feldspars and have a significant potassium, but a low thorium content. The Th/K ratio will therefore be low (<1 ppm/%), 3) micaceous sandstones, which contain mica and has a potassium content that is less than feldspars and a thorium content that is higher. The Th/K ratio is usually between 1.5 and 2.5 ppm/%, 4) greywacke, which contain both feldspars and micas, and Th/K ratios is between 1 and 2.5 ppm/%, 5) greensands, which contain glauconite and It has Th/K ratios between 1 and 1.5 ppm/%, 6) heavy mineral-bearing sandstones which contain high U or Th ( or both of them) content. The Th/K values will be above 25 ppm/%.

Total radioactivity of a formation is a sum of three elements: Th, K and U. By using the corrected concentration of K, U and Th it is possible to characterize reservoirs (Fig. 27). By this method it is possible to detect the clean reservoirs from the shale formations. Feldspathic sandstones usually have high K concentration, which can increase the gamma ray, and sandstones have low concentration of K and Th compared to shale. In general low concentration of K and Th along with high concentration of U revealed the fractured and permeable reservoir and high concentration of U and Th with low K, demonstrated the clean reservoir in association with heavy minerals (Fig. 27).

It is common method to use the maximum gamma-ray response as the shale point. However, it is known that shales composition can be changed, For example, kaolinite clays shows low gamma ray response; yet can fill the available pore space (Heslop, 2003).

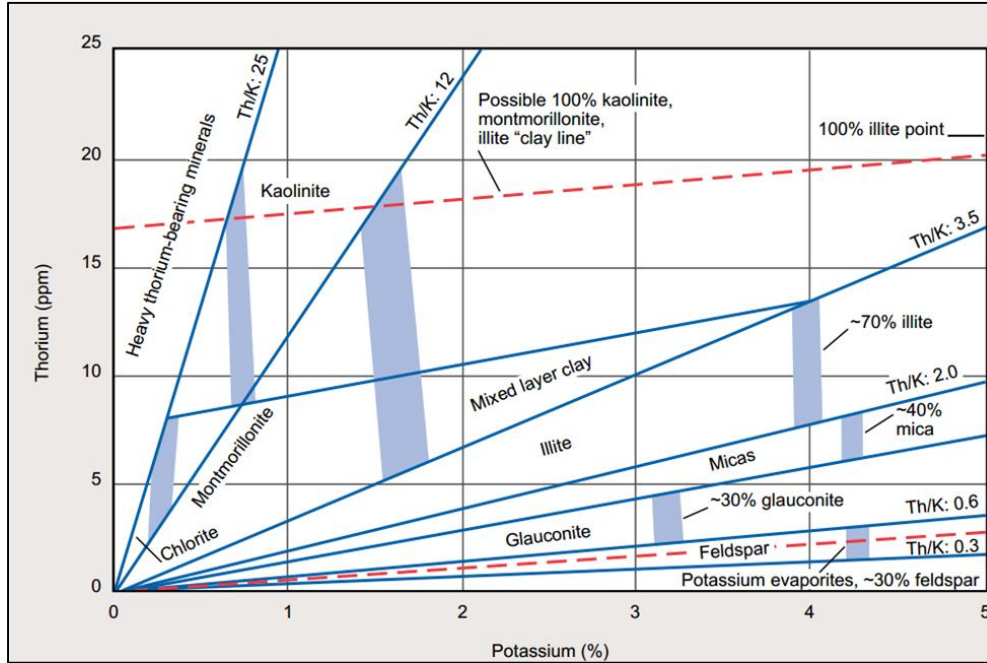


Figure 26. Mineral identification from a Thorium – Potassium plot (Schlumberger).

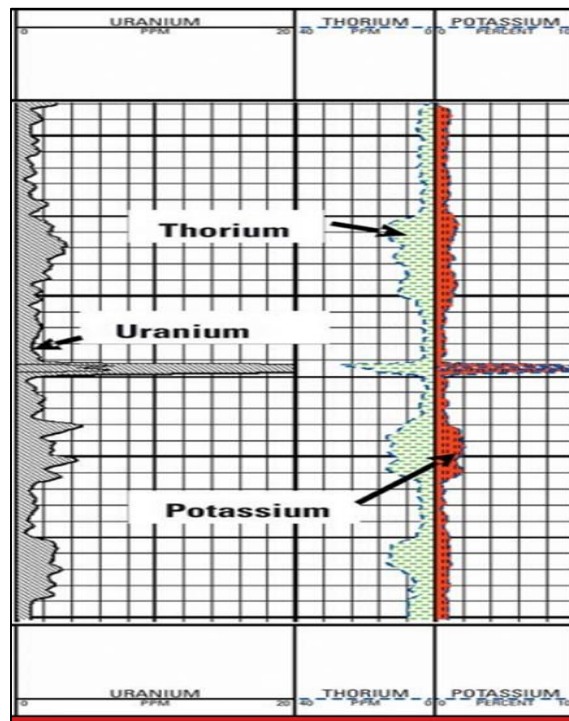


Figure 27. Corrected concentrations of K, U, and Th (Halliburton).

### 5.1.3 Electrical log (resistivity logs)

Electrical logs are perhaps the most important tools available to a petrophysicist. This is because they provide a method for calculating the water saturation, upon which calculations of STOOIP are based (Glover, 2012). Electrical logs are divided into three subcategories: laterolog, induction log and micro resistivity log. The induction log measures conductivity of the formation and can cope with highly resistive muds (oil- base mud). The modern tool for measuring the resistivity in low resistivity mud with high salinity is called laterolog. Micro resistivity is another resistivity tool which is designed to measure the resistivity of mudcake.

Since the solid components have higher resistivity than pore fluids in most rocks, resistivity is controlled by the conductivity of the pore fluids. Hydrocarbons have higher resistivity than the fresh water and fresh water has higher resistivity than the salt water. Shale formations are indicated the lower resistivity than the sandstone formations due to the presence of bound water in clays.

The correlation between deep and shallow resistivity is seen in Figure 4. The amount of separation between deep and shallow resistivity is dependent on the depth of invasion and water saturation (White, 2012). In impermeable formations all the resistivity curves overlay.

There are some general principles for working with the resistivity log as a lithology and fluid types indicator. According to Figure 28 there is no separation between the deep and shallow resistivity logs when the formation is impermeable (shale). In contrast, the separation between two resistivity logs demonstrates the permeable zone (sandstone). The high resistivity in tight sandstone formations is related to cementation or compaction, whereas porous sandstones, which are filled with water, show the low resistivity.

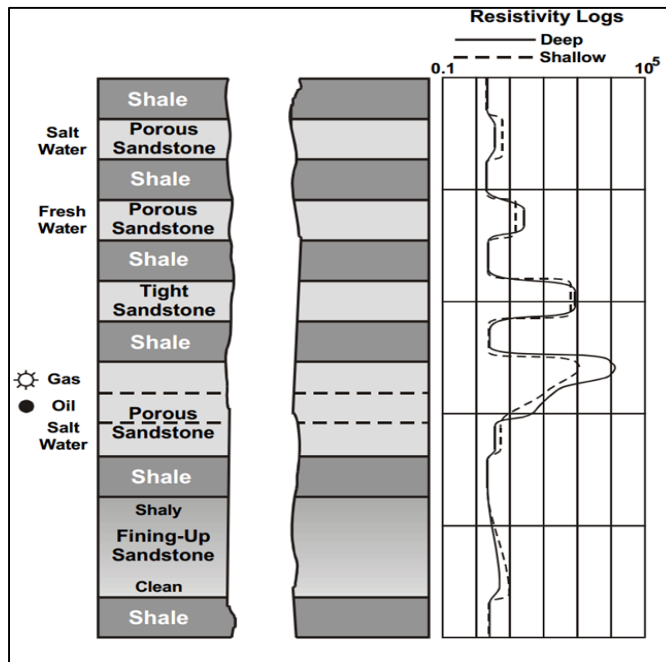


Figure 28. Typical resistivity log responses (Glover, 2012).

#### 5.1.4 Acoustic log (sonic log)

The sonic or acoustic log measures the travel time of an elastic wave through the formation. This type of log is designed to indicate porosity, lithologies, facies and stratigraphic correlation. In addition, the identification of fractures, compaction, over pressures and source rocks can be achieved.

The sonic log is sensitive only to the primary intergranular porosity. The difference between intergranular porosity measured by sonic tool and total porosity measured by density tool will give the secondary porosity.

The sonic log can identify the lithology. High velocities usually indicate carbonates; middle velocities indicate sands and low velocities, shales (Glover, 2012).

The compacted formations have high velocity of an elastic wave inside themselves. The over pressured zones which have higher pore pressure show an increase in sonic travel time.

A relative decrease in sonic transit time and an increase in resistivity indicate an organic-rich layer in impermeable sediments. Where density logs are affected by rugosity of the borehole wall or



by the presence of pyrite, sonic logs may prove more reliable than density logs (Meyer and Nederlof, 1984).

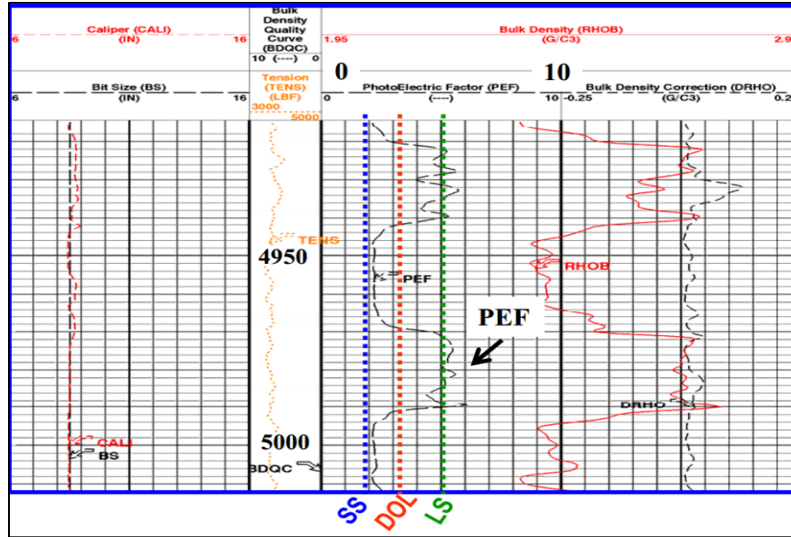
### **5.1.5 Artificial radiation logs**

#### **5.1.5.1 Neutron log**

The neutron source emits neutrons to the formation and maximum energy is lost when the neutron collides in-line with the nucleus of the same mass like hydrogen. The slowing down of the fast neutrons by hydrogen nuclei is the predominant phenomenon used, and the reading, for given hole conditions, depends mostly on the hydrogen index of the formation (Gaymard and Poupon, 1968). Shale formations contain clays that have high amount of bound water. Hence shales can contain a significant proportion of hydrogen despite being of low porosity. The porosity reading from the neutron tool in shale formations is therefore always significantly higher than the real porosity, this phenomena is called shale effect (Glover, 2012).

#### **5.1.5.2 Density log**

The density tool sends out gamma rays to the formation and the gamma rays will be scattered by an orbital electron. As a result of this interaction the gamma ray lose energy, and the electron is ejected from the orbit. This process with a medium energy is called Compton scattering and is used for density logging. The photoelectric absorption effect occurs with low energy when the incident gamma ray is completely absorbed by the electron. Pef, which is a photoelectric absorption index, is measured using gamma rays with low energy (White, 2012) and is a good lithology indicator when there are no washouts at shallow depths (Fig. 29).



**Figure 29. Pef curve shows a complex of lithologies. Sandstone (SS) shows the lowest Pef value, Dolomite (DOL) In the middle of the track and limestone (LS) with high pef value (White, 2012).**

The density log measures the bulk density of the formation which consists of the combined matrix density and the fluid density. The more fluid a formation contains; the more porous it is (Meyer and Nederlof, 1984). The density log is a good porosity indicator.

The neutron log and density log are sketched together in the same track for doing some comparison and the correlation between these two curves leads to better lithology identification. When both the density log, and neutron log show lower value it indicates the sandstone formation, and when the two types of logs overlay the lithology is limestone, and when the neutron and density value increases it indicates shale. For fluid types identification a comparison of resistivity with other logs is necessary.

## 5.2 Logs interpretation and work flow

The lithology of cores is determined by petrographic description of thin sections and the modal analysis. The petrophysical interpretation across the studied interval (1583.1 to 2152 m) can be used to check the lithology of each depth also where cores are missing, and identify the reservoir quality.

The wire line logs in this study include: caliper log, natural gamma ray log including, the Th-log, U-log and K-log, resistivity logs (shallow, medium and micro resistivity), sonic log, pef log,

density log and neutron log (Fig. 30). The petrophysical data were interpreted using the Interactive Petrophysic version 4.0. These conventional logs were used as a supplementary method for getting some information about lithology, porosity and possible diagenetic process.

Identifying the permeable beds, lithology types, fluid types and porosity are the main goal of this study. For the logs interpretation the data need to be in a good conditions. The hole conditions and mud types can effect on the quality of the logs and make some trouble in log reading or cause stationary reading of logs which is not correct and lead to misinterpretation of logs. In this study the logs have qualities without any evidence of stationary readings (Fig. 30).

The next part of log interpretation is distinguishing between the permeable and impermeable formations. The permeable zones are identified by the presence of mudcake, the separation between RDEP (deep resistivity log) and RMIC (micro resistivity) and formations with high porosity and low gamma ray and density- neutron reading similar porosity (Fig.31). The caliper log is always compared with the bit-size log. If it indicates lower value than the bit-size the formation is permeable, otherwise the formation is influenced by the wash out effects and is impermeable.

The lithology in the Skalle well is interpreted using the natural gamma ray, which is used for distinguishing between clean sands formations and shaly formations. The more impermeable zones indicate shale intervals with high concentration of clay minerals which decrease the effective porosity and permeability. Heavy minerals and organic matter or phosphate can be identified by using the Th-log and U-log respectively. High amount of K-feldspar and presence of clay minerals such as illite and glauconite can influence on the K-log. The pef log and a combination of neutron and density logs can be used for lithology identifications (see Ch5.). Permeable zones are likely to be one of the dominant mineralogies (sandstone/limestone/dolomite), but in this study sandstones are the only dominate mineralogy in permeable zones. According to the neutron and density logs (the green shaded areas) approximately most of the formations have clay contents (Fig. 30). In some conditions it is claimed that there is a shale formations according to high values for gamma ray, neutron log and density log, but resistivity logs increase, in this case the sharp increase in resistivity logs is due to a diagenetic process like compaction or cementation and there is no water content in this condition because water bearings decrease the resistivity.

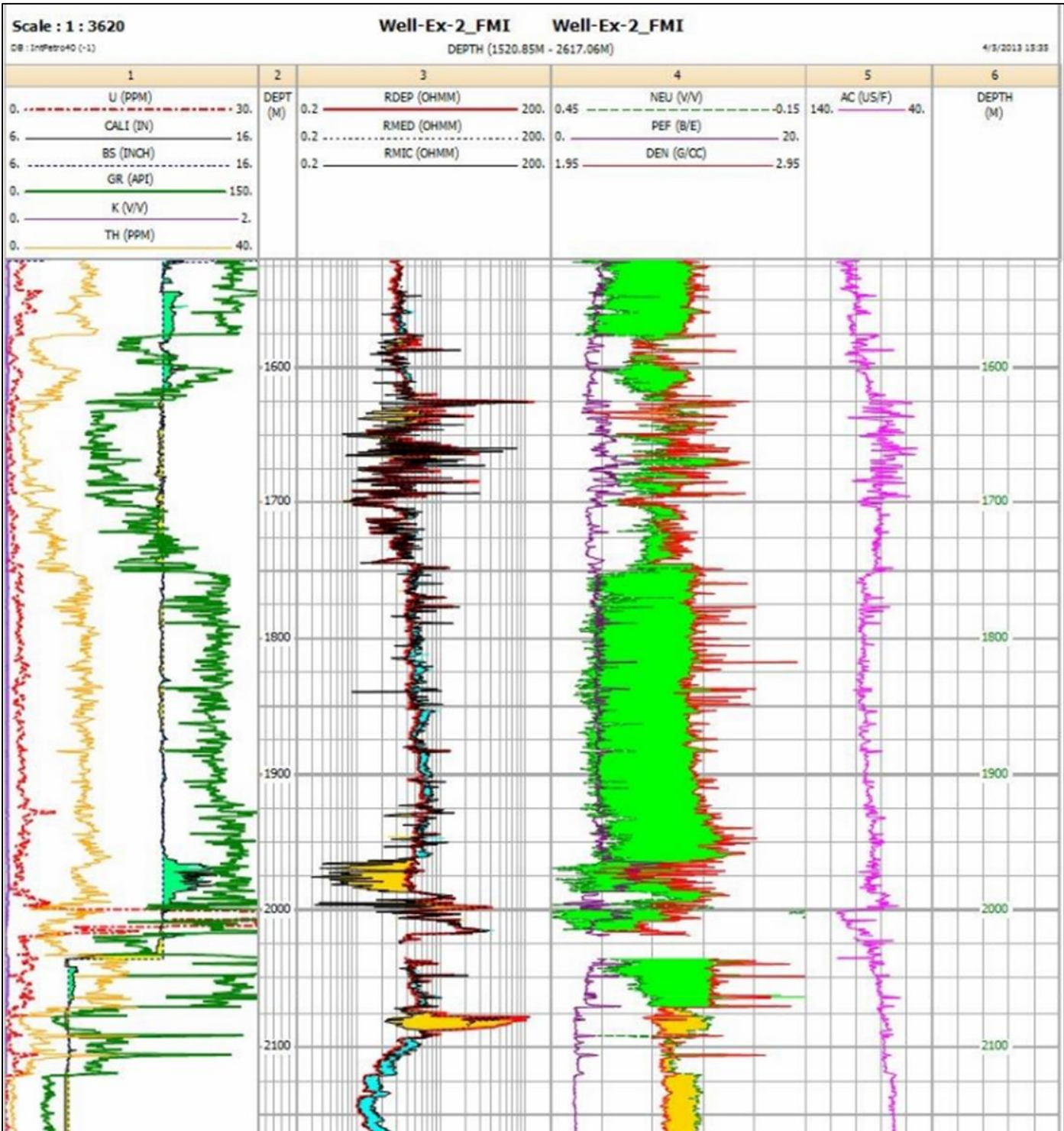


Figure 30. The conventional logs overview from the depth 1583.1m to 2152m (Skalle well 7120/2-3S). There is no evidence of stationary reading. The green shaded areas in the track 1 show the washed out effect, while the yellow shaded areas show the permeable zones. In track 2 the separation between RDEP and RMIC shows the permeable zones. Tack 4 shows the shale (the green shaded areas) and sand (the yellow shaded areas).

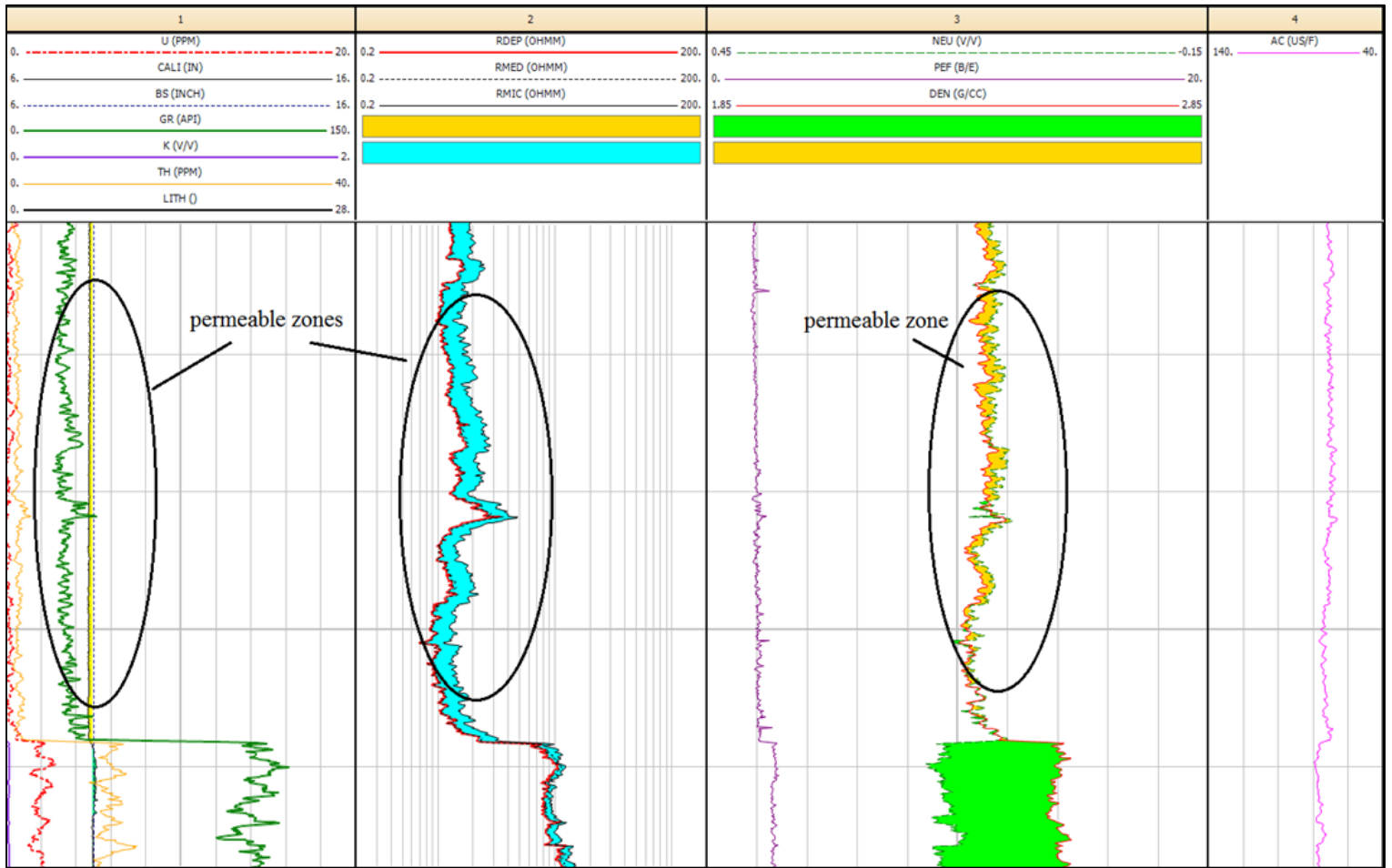


Figure 31. Permeable zones are identified from the depth 2126.9 to the depth 2242.3. Presence of mudcake (the yellow shading between caliper log and bit size log), the separation between RDEP and RMIC (the blue shading) and high porosity ( according to acoustic log with low values), low gamma ray and similar porosity reading of density-neutron are indicated the permeable zone.

### 5.3 Lithology from Sidewall Cores and wire line Logs

Interpretation of lithology of the sidewall cores is based on the petrographic description of thin sections and modal analyzing of 14-thin sections in this study. The petrophysical log interpretation across the studied interval (1576.1-2609.75m) used as a supplementary method for lithology identification especially where core material is not available.

Gamma ray, which distinguishing between the clean sandstone and clay, in combination with neutron porosity and density logs and pef-log can be used for interpretation of lithology. In the studied well, the neutron porosity and density logs are available across the studied interval, thus the lithology is interpreted easily (Fig. 32). The Figure 32 shows the log derived lithology in which the position of the formations is marked. The petrophysical log compilation from 1576.1 to 2609.75m shows 10 formations. As the side wall core are provided from 1583.1 to 2152 meters, the underlying formations such as Nordmela, Tubåen, Fruholmen and Snadd in Figure 32 are not studied. The detailed interpretations and descriptions will be done from 1576.1 to 2152 meters. The Kolje and Knurr Formations which are located at the 1750.01 to 1999.5 meters are interpreted only by the wire line logs as core material is lacking.

#### **5.4 Lithology and fluid types**

The general overview of Figure 32 shows that clay contents (shale) can be observed in all the formations along with sandstones and siltstones. The water content is observed in most of the formations (the Lower Kolmule, Kolje, Stø, Nordmela, Tubåen, Fruholmen and Snadd Formation) which show high water saturation and low deep resistivity, while gas content is only observed in the top of the lower Kolmule, Stø, Tubåen, Fruholmen and Snadd Formations that show low water saturation and high values of deep and shallow resistivity. The major reservoir in this study is the Stø Formation which consists of gas, mostly at the top of the formation (Fig. 32). The interpretations indicate no oil in this study, while gas is the only possible hydrocarbon content. The neutron-density logs responses indicate two different lithologies, shale (green shading) and sandstone (yellow shading) (Fig. 32).

The depth interval between 2018.4 and 2036.3 meters shows the bad hole conditions so that the data are not available for resistivity log, neutron-density logs, saturation and porosity. The acoustic log is not affected by this condition, so where density and neutron logs are affected by rugosity of the borehole wall the acoustic log can be reliable to use. The gray shaded areas in caliper track, show the washed out effect which can fortify the bad hole conditions (Fig. 32).

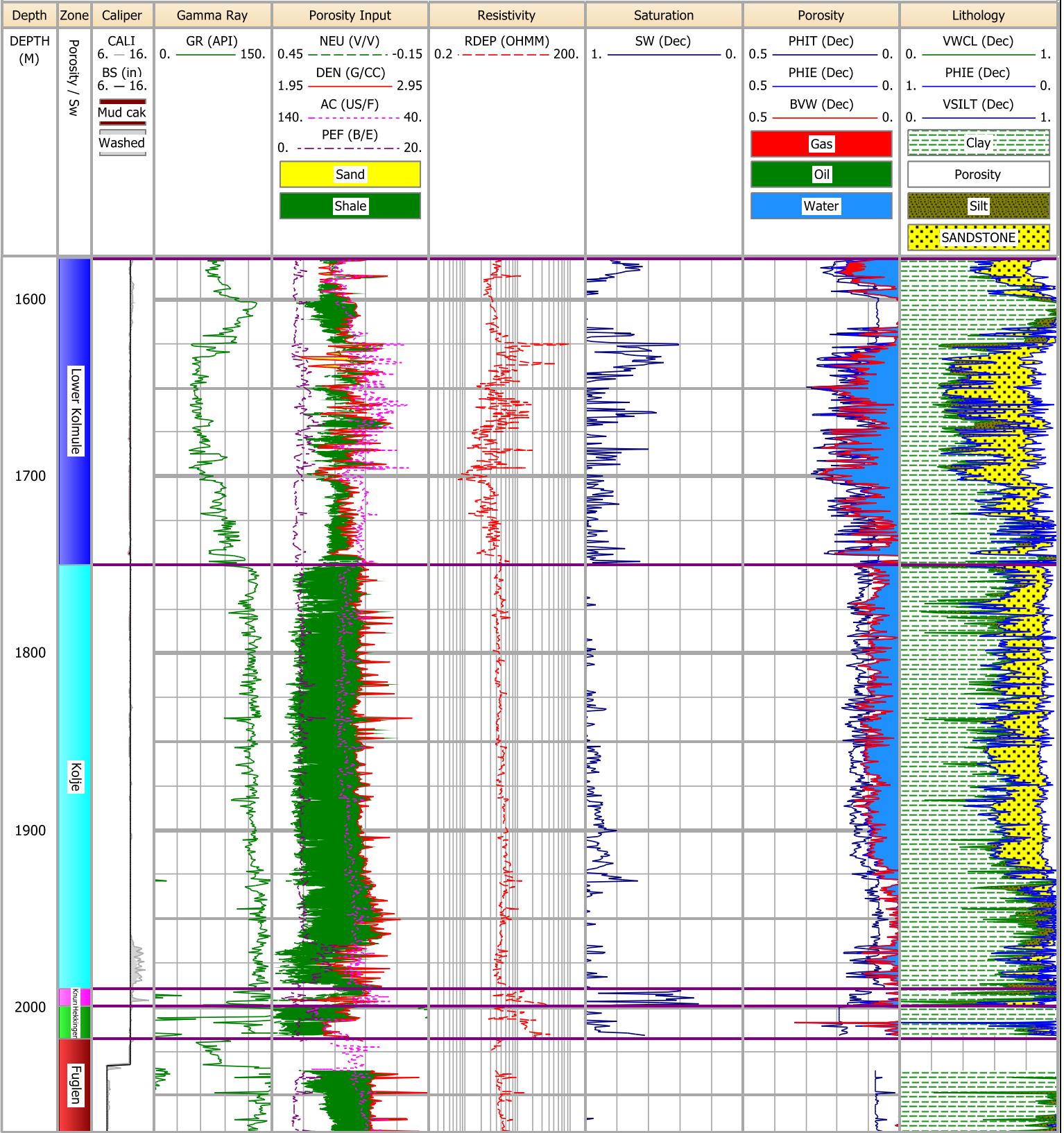
Scale : 1 : 2500

7120/2-3S

DB : IP\_Files (1)

DEPTH (1576.17M - 2070.86M)

06/13/2013 11:59



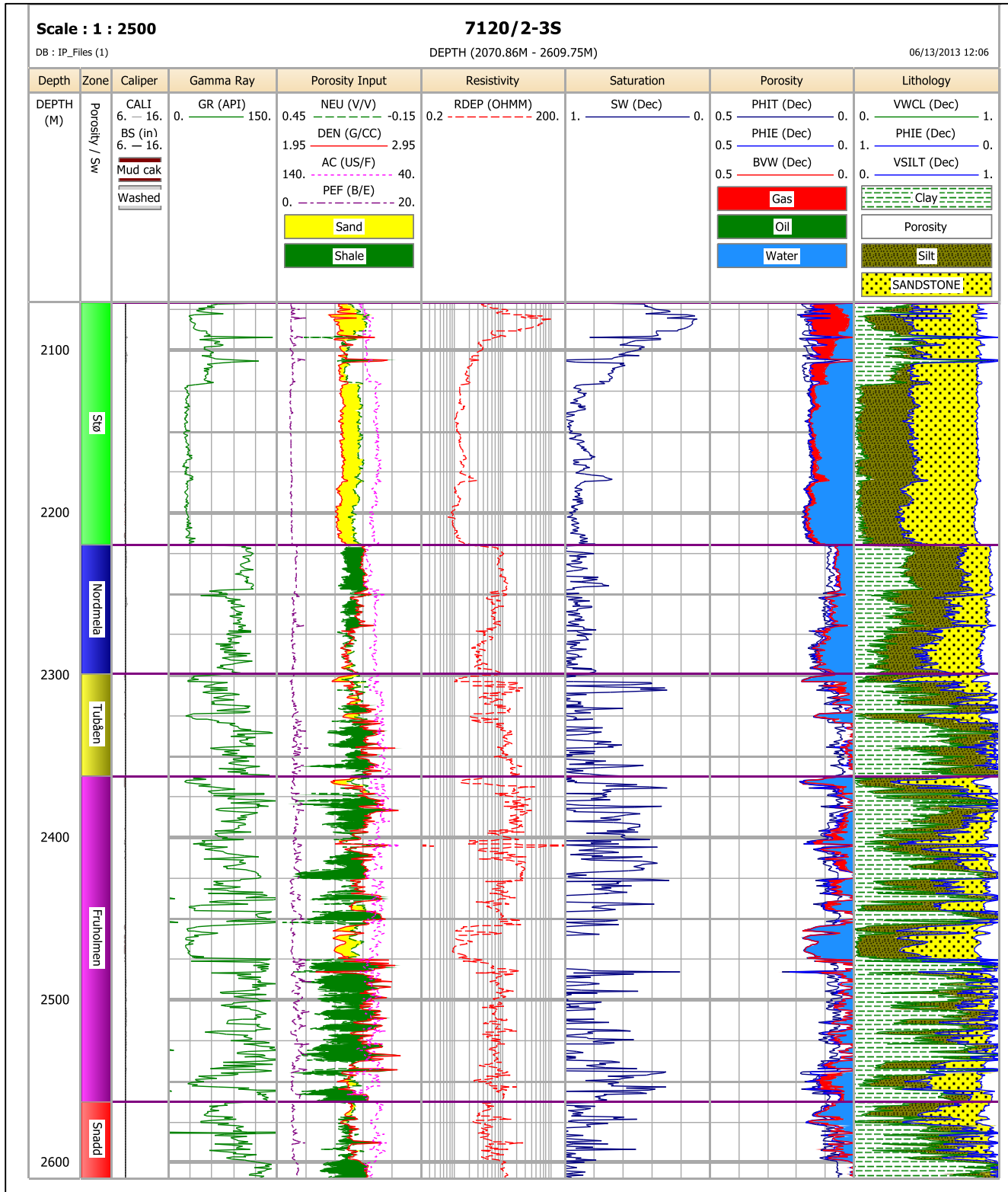


Figure 32. The overview of petrophysical logs interpretation from 1576.1 to 2609.75m show 10 formations with different lithologies, fluid types and porosity.



## **5.5 Formations**

Six formations have been interpreted based on changes in GR, neutron porosity, density log responses, pef-log and the depths and two of them (Kolje (1750.01-1989.6 m) and Knurr (1989.6-1999.5 m) are compared with petrophysical data in the section below.

### **5.5.1 The Lower Kolmule Formation interpretation**

#### **5.5.1.1 The lithology interpretation**

The Lower Kolmule Formation (1576.73-1750.01m) shows the lithic greywacke composition with the claystone interbeds according to the petrographic modal analysis (Fig. 4). The petrophysical log interpretation is indicated that this formation mainly contains clay matrix with sands and silts interbeds. The formation has a thickness of 173.28 m. According to the resistivity logs (no separation between RDEP and RMIC) the majority of this formation is impermeable wherever there is a shale content (the green shading in neutron-density log). The gamma ray log in this formation has some fluctuations and displays high gamma ray values. Strong GR log response, in the clean sand intervals, may occur by high K-feldspar and glauconite content or be affected by presence of radioactive minerals such as thorium and uranium. In this formation the Th-log signal increases gradually which indicates a high proportion of heavy minerals. At the 1624.2-1700m, the gamma ray decreases sharply and acoustic logs decreases gradually (Fig. 33). In this interval (1624.2-1700m) the separation between deep and micro resistivity logs shows the permeable zones which indicate the sand composition (Fig. 33). The low gamma ray response in the clay parts (1640-1700m) is known that the shale composition may differ, For example, kaolinite clays shows low gamma ray response (Heslop, 2003). However, it is common method to use the maximum gamma-ray response as the shale point.

#### **5.5.1.2 The fluid types and diagenetic processes interpretation**

The evidence of gas and water is observed in the lower Kolmule Formation. In the clean sand interval (Yellow shaded parts in neutron-density logs) where the resistivity logs show the high value gas is observed (Fig. 34). Water content can be found both in shale and sand intervals, where the resistivity logs show the lowest response. The acoustic log indicates low responses

(Fig. 34), and it is shown before that the Lower Kolmule Formation is affected by the chemical compaction and dissolution (K-feldspars) processes which lead to porosity increase in the middle interval (1624.2-1750m) of this formation.

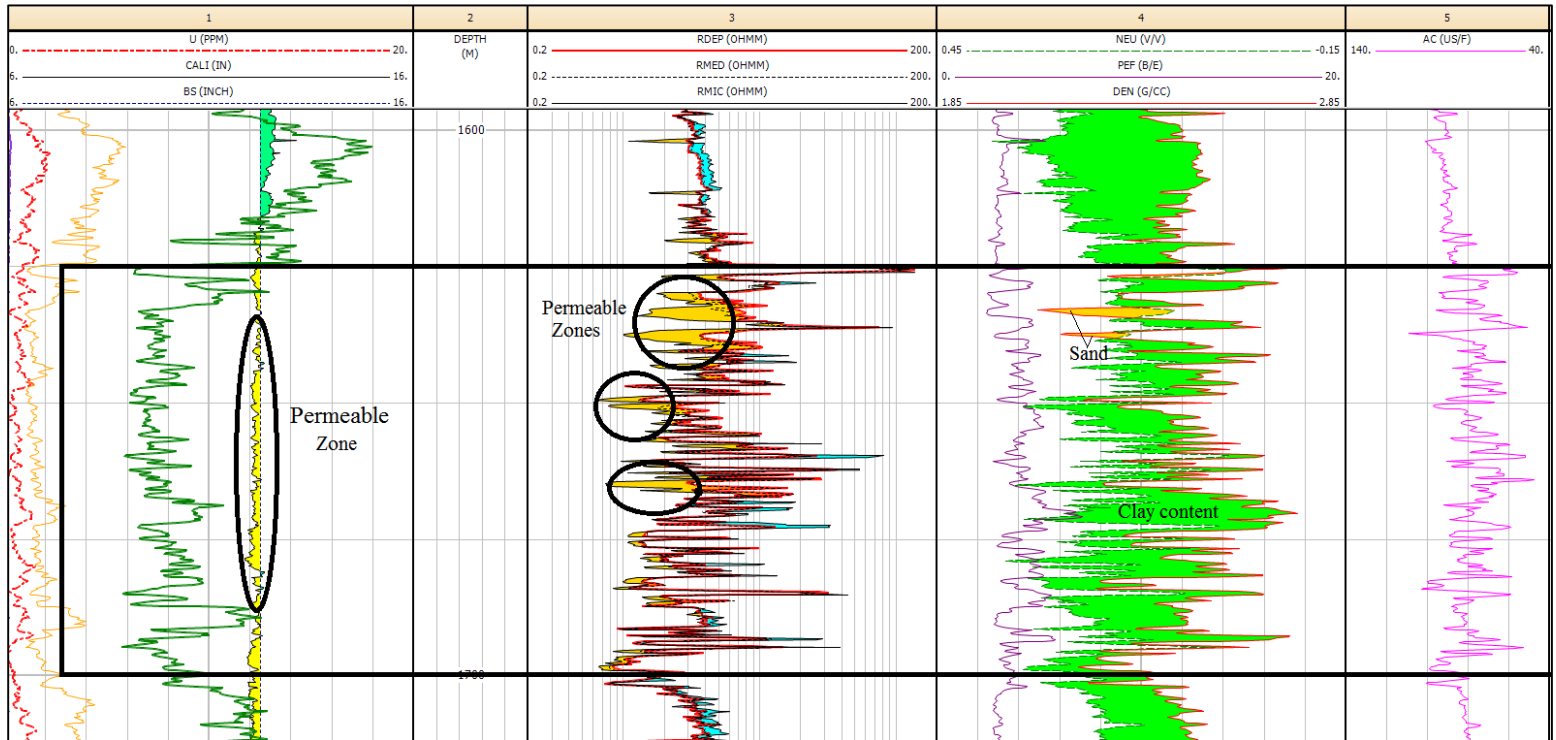


Figure 33. Scale 1:1200, Permeable zones are defined by the yellow color in track 1 (caliper log shows the lower values than the bit size) and 3 (the separation between RDEP and RMIC). In track 4 the green shaded (neutron and density show high values) shows the shale, while the yellow shaded colour (neutron and density logs show low values) shows the sand lithologies.

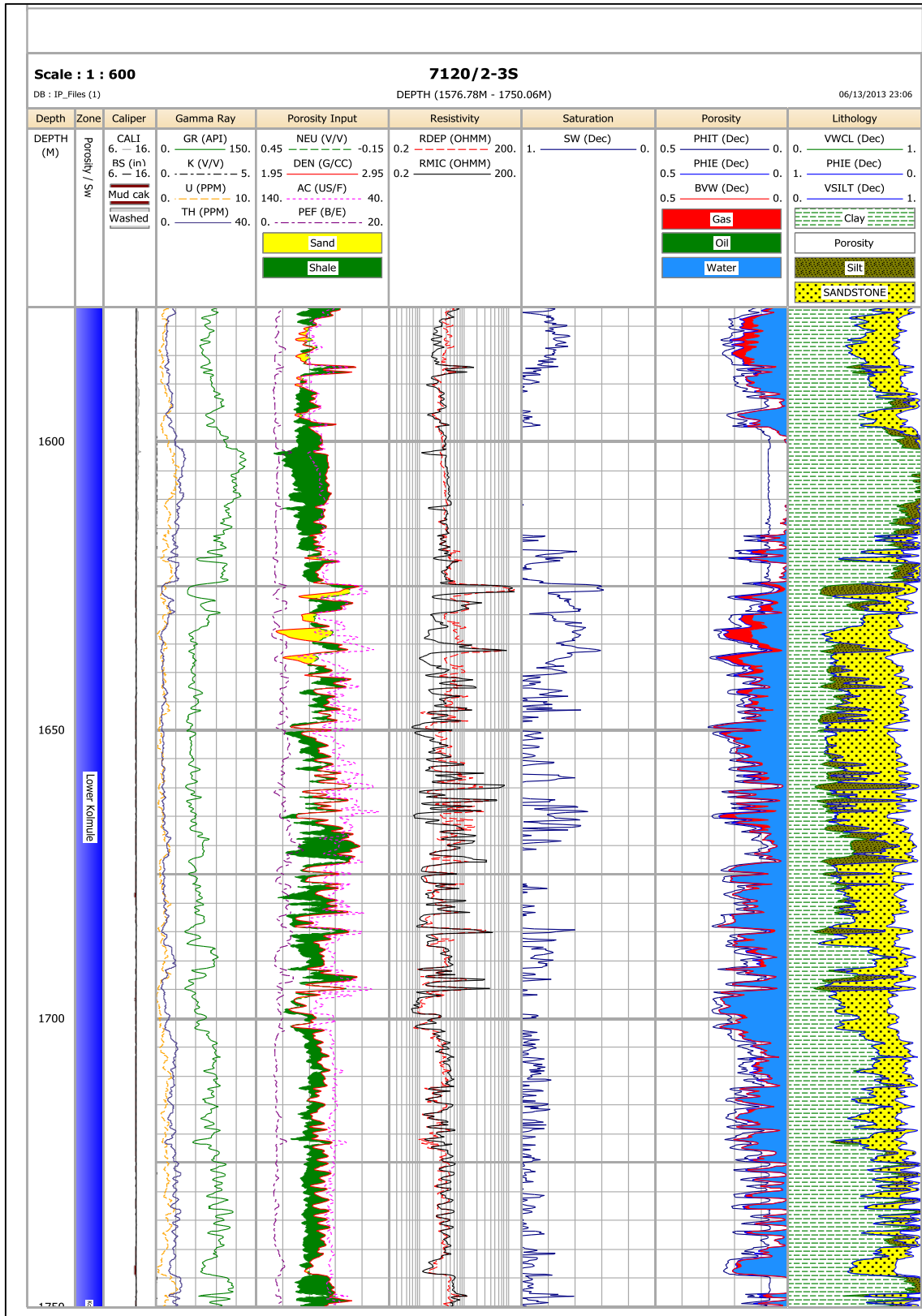


Figure 34. The petrophysical logs interpretation of the Lower Kolmule Formation (1576.73-1750.01m).

## **5.5.2 The Kolje Formation interpretation**

### **5.5.2.1 The lithology interpretation**

The Kolje (1750.01-1989.6 m) Formation has high clay contents with thin interbeds of sandstones and siltstones (Fig. 35). The formation has a thickness of 239.59 m. The gamma ray and Th-log show high values from the top of the formation to the base which indicate high amounts of clay contents and heavy minerals respectively (Fig. 35). The pef-log response at the base of this formation according to Figure 29 shows the location of limestone so the thin interbeds of limestone can be identified.

### **5.5.2.2 The fluid types and diagenetic processes interpretation**

The resistivity logs with very low values suggest the presence of water in the shaly formation (Fig. 35) and high U-log and Th-log responses show the bioturbation process within this formation. Moderate acoustic log responses indicate low compaction rate in the Kolje Formation.

## **5.5.3 The Knurr Formation interpretation**

### **5.5.3.1 The lithology interpretation**

The Knurr formation (1989.6-1999.5 m) shows a shale composition with sand and silt interbeds (Fig. 36). The shale composition, confirmed by the neutron-density log, occurs mostly at the top of the formation, whereas sandstone composition is interpreted at the base of this formation (Fig. 36). The formation has a thickness of 9.9 m. The strongest GR response occurs in the depth interval 1998.5 to 1999.5 meters, while the neutron porosity and density logs do not show high clay content this may be due to the high U, K or Th content. The high U-log response maybe caused by high organic matter volume.

### **5.5.3.2 The fluid types and diagenetic processes interpretation**

The resistivity logs decreases due to water content in the shale composition (Fig. 36). As for the Kolje Formation, the Knurr Formation is interpreted based only on the petrophysical data due to the absence of core materials.

## **5.5.4 The Hekkingen Formation interpretation**

### **5.5.4.1 The lithology interpretation**

The Hekkingen Formation (1999.5-2017.9 m) mainly consists of shale with the sandstone and siltstone interbeds (Fig. 37). According to modal analysis the sandstone is classified as lithic greywacke (Fig. 5). The formation has a thickness of 18.4 m. The acoustic log is decreasing gradually so a relative decrease in sonic transit time and an increase in resistivity indicate an organic-rich layer in impermeable sediments (Fig. 37). This observation proves the presence of organic matter in the Hekkingen Formation which was also observed in the thin section study of this formation. Furthermore the evidence of decreasing value of the acoustic log with increasing depth shows an effective porosity increase. By observing the logs and from the lithology interpretation it is clear that the Hekkingen Formation is a potential source rock for the Lower Kolmule Formation due to the presence of high organic matter within the shales.

### **5.5.4.2 The fluid types and diagenetic processes interpretation**

The gas content (Fig. 37) in the Lower Kolmule Formation may have been generated from the organic matter, mostly the wood fragments, in the Hekkingen Formation. At 2008.4 to 2014 the acoustic log increases gradually which indicates the high sonic transit time within the formation which occurs due to cementation as supported by petrography study of thin sections from this depth.

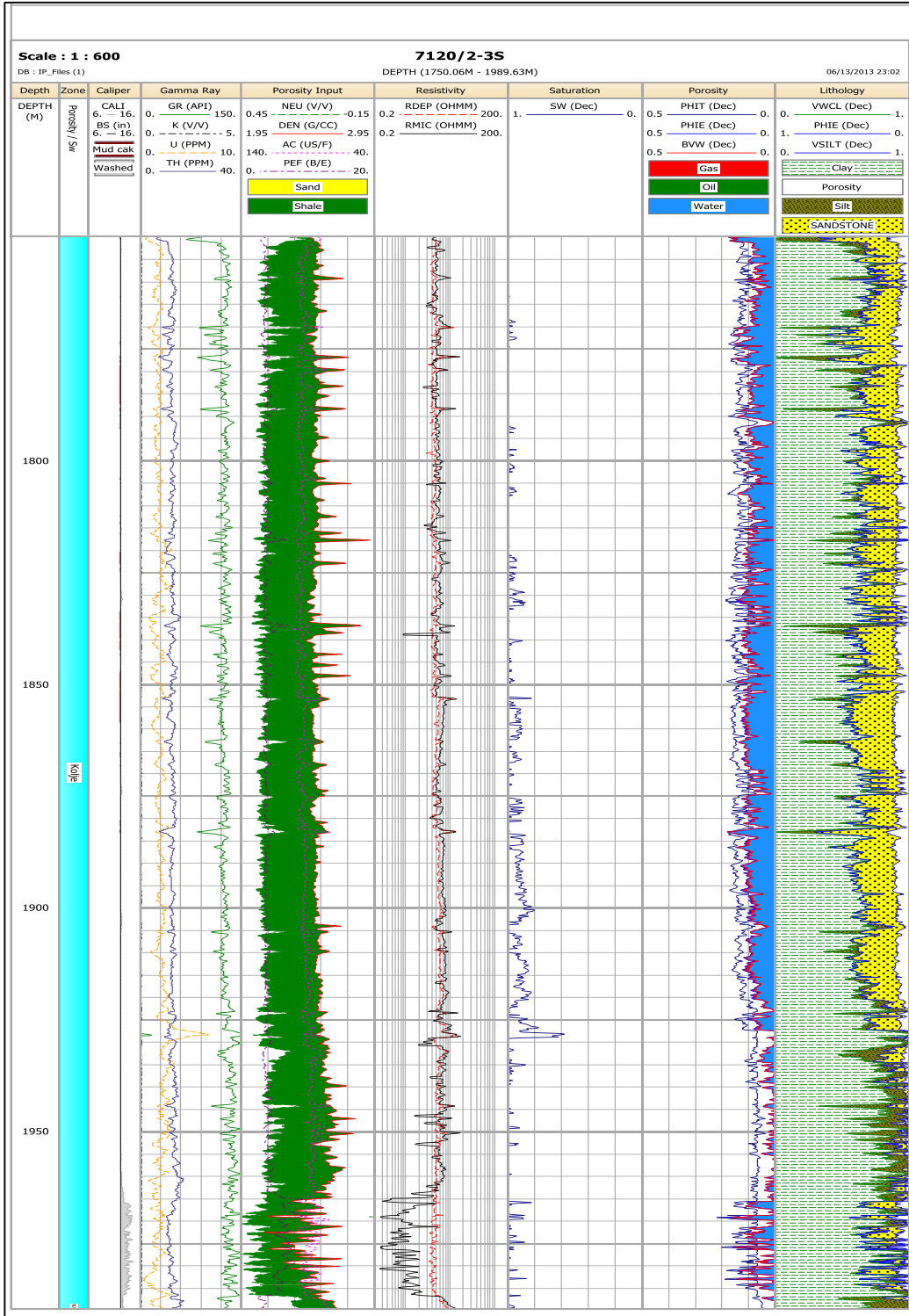


Figure 35. The petrophysical logs interpretation of Kolje Formation (1750.01-1989.6 m).

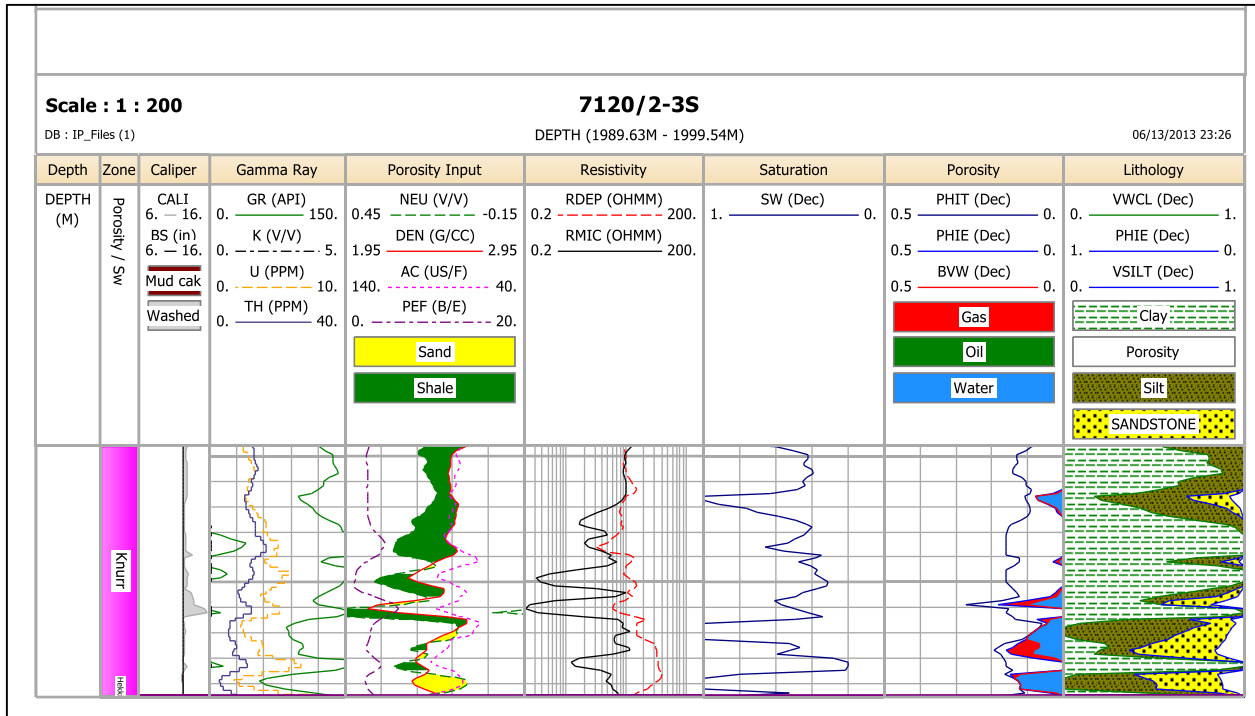


Figure 36. The petrophysical logs interpretation of Knurr Formation (1989.6-1999.5 m).

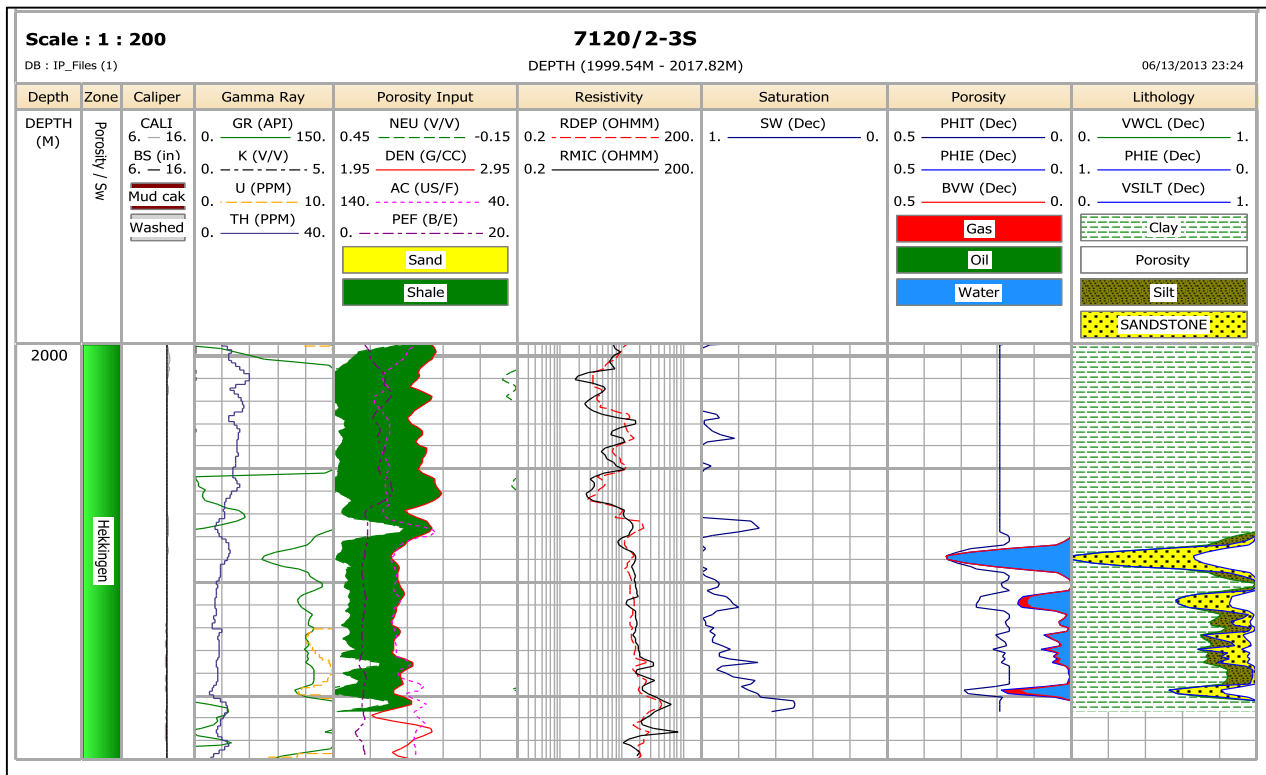


Figure 37. The petrophysical logs interpretation of Hekkingen Formation (1999.5-2017.9m).

## **5.5.5 The Fuglen Formation**

### **5.5.5.1 The lithology interpretation**

The Fuglen Formation (2017.9-2071m) according to core image (Fig.20) consists of dark shale with thin carbonate cemented interbeds. Only one sample (2019.35m) was provided for thin section study of this formation, so petrophysical log interpretation can help to improve the better interpretations. The lithology interpretation of this formation indicates high clay content with the thin interbeds of siltstones (Fig. 38). The formation has a thickness of 53.1 m. Neutron-density and gamma ray logs show high values which suggest shale compositions (Fig. 38). The depth interval between 2018.4 and 2036.3 meters shows the bad hole conditions and there is no data available for these intervals. Acoustic logs can be more reliable in this part as they have not been affected by the rugosity of the borehole (Fig. 38).

### **5.5.5.2 The Fluid types and diagenetic processes interpretation**

Hydrocarbon is not detected in this formation. The resistivity logs show high values within shale intervals, which due to carbonate cementation that increases the resistivity. In this case the porosity and permeability are decreased due to the cementation. The Fuglen Formation can be considered as a seal (cap rock) for the formation below (the Stø Formation) due to the low porosity and permeability.

## **5.5.6 The Stø Formation interpretation**

### **5.5.6.1 The lithology interpretation**

The Stø Formation (2071-2220m) is a relatively clean sandstone formation, so it can be considered as a reservoir rock with the thickness of 149 m. It is defined as subarkosic sandstone in the ternary plot (Fig.6). According to the lithology plot (Fig. 39), this formation consists mainly of sandstones and minor siltstones and shale interbeds. In the shale interbeds, a high volume of organic matter and heavy minerals is observed. The high U-log and Th-log responses and high concentration of U and Th with combined low K, demonstrate the clean reservoir in association with heavy minerals. The strong GR log response at the top of the formation in the



clean sand intervals, may result from high K-feldspar and glauconite contents, or affected by presence of radioactive minerals such as thorium and uranium.

#### **5.5.6.2 The fluid types and diagenetic processes interpretation**

At the top of this formation (2071-2091.6m) gas is evidenced where the resistivity logs show the highest value, and the density reading is gradually decreasing upward over the boundary (Fig. 39). From the 2132.6 m to the base of this formation the resistivity response changes immediately and starts to decrease downwards where gas is replaced by water. The acoustic log starts to decrease gradually at the onset of this formation which indicates the porosity increase (Fig. 39). The porosity increase can have been achieved by dissolution or chemical compaction.

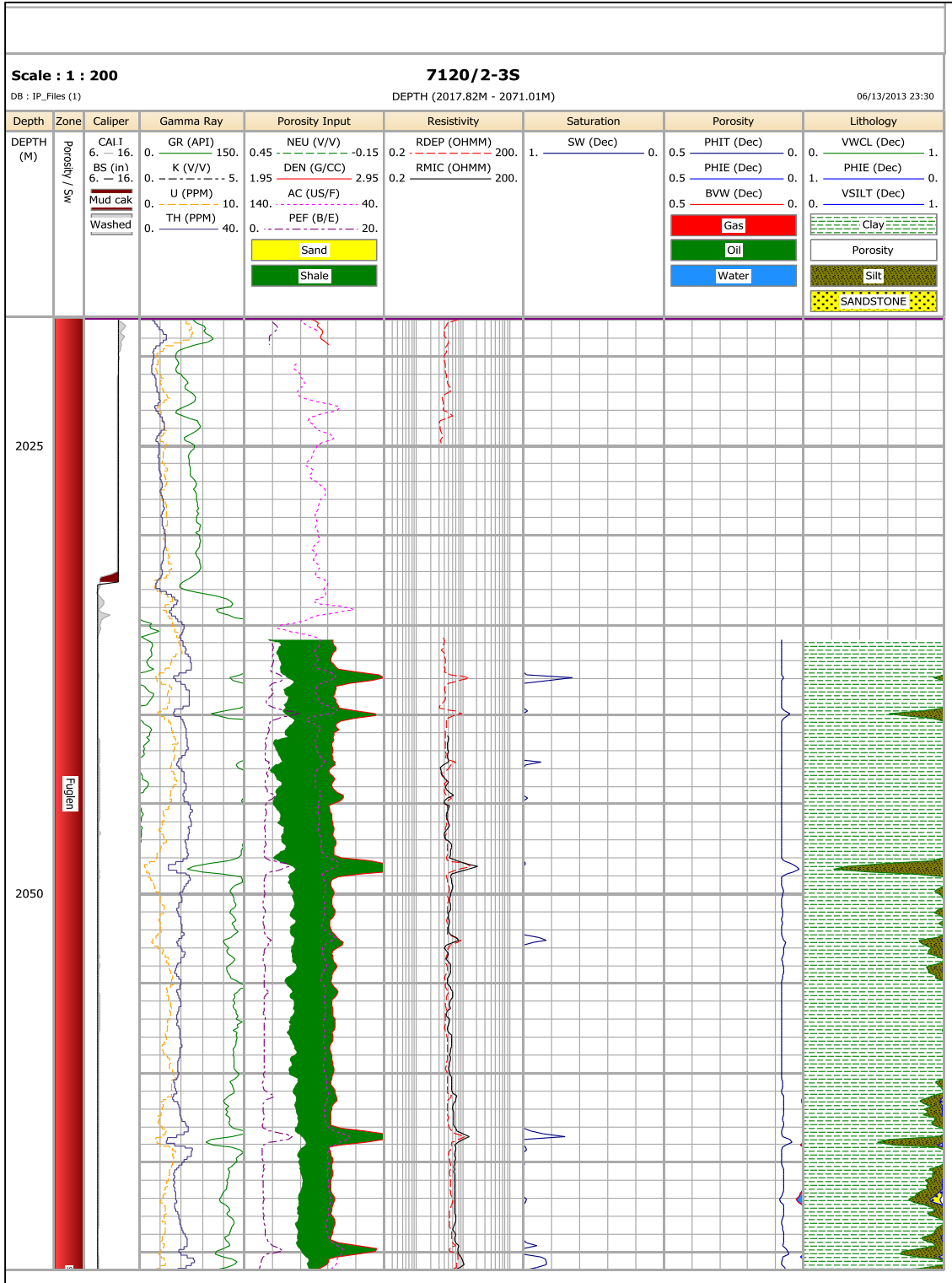


Figure 38. The petrophysical logs interpretation of Fuglen Formation (2017.9-2071m).

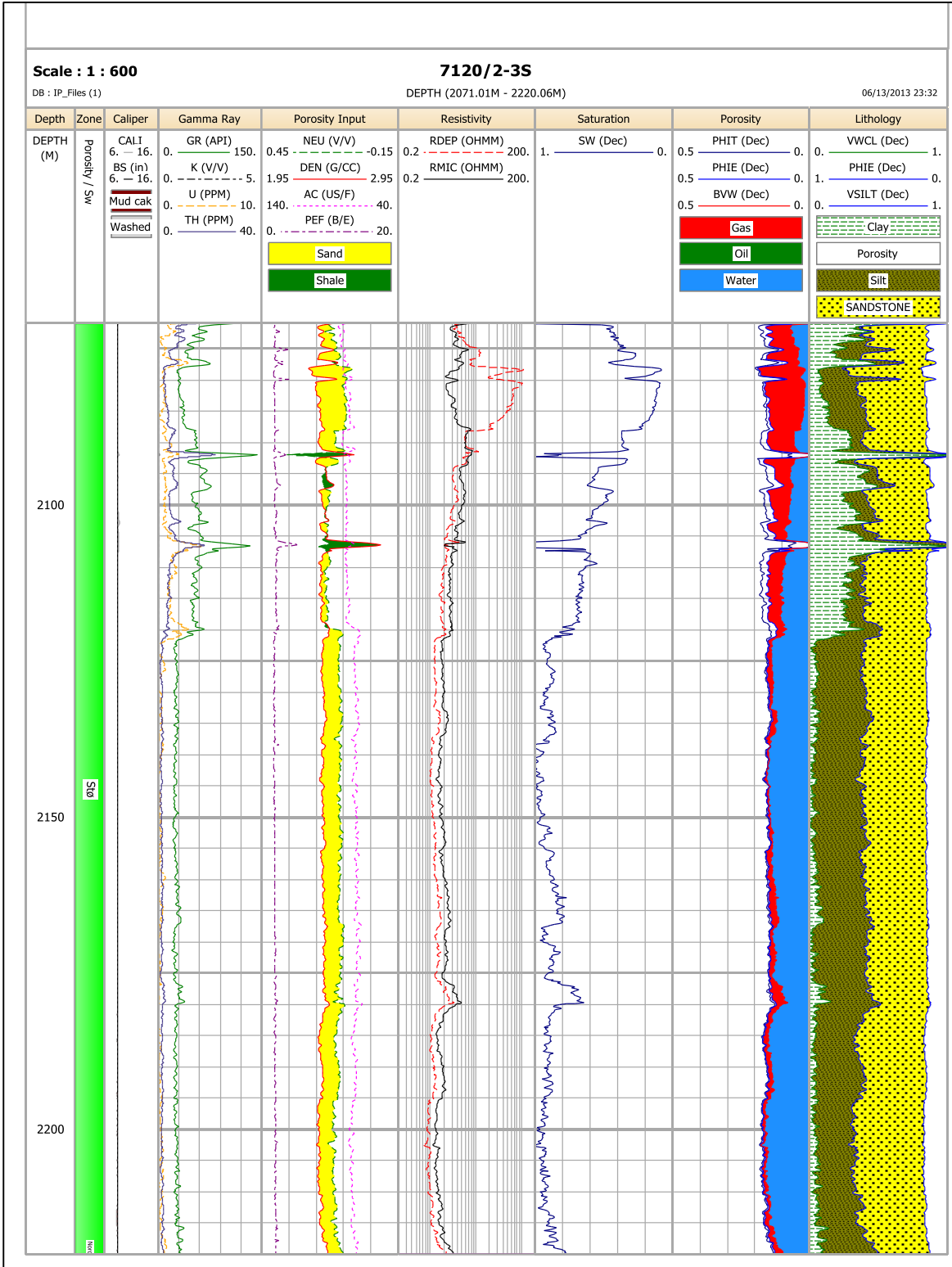


Figure 39. The petrophysical logs interpretation of Stø Formation (2071-2220m).

## 5.6 Mineral identification from a Thorium – Potassium crossplot

Clay typing from well log data is usually accomplished by using crossplots of Th/K data from the gamma ray spectral log and the photo electric effect. The Th/K ratio is a reliable method of visually identifying some rocks. According to Figure 26 the Th/K ratio list is as follows:

**Table 2. Th/K ratio in clay minerals, shows the highest value for kaolinite and the lowest value for potassium evaporate (Crain, P, 2013).**

Th/K Ratio in Clay	
High	Kaolinite
	Chlorite
	Montmorillonite
	Illite
	Mica
	Glaucanite
	Feldspar
Low	Potassium evaporite

In the thin section study, the clay minerals are observed in almost all parts of the formations, filling the pores. It was interpreted from thin section study that the clay minerals are illite, chlorite, mica and glauconite. For getting supplementary clay type identification, the Th/K ratio is a good method in the petrophysical part of study. In Table 3 the Th/K ratio is calculated for all the formations. The lower Kolmule Formation shows a variety of clay types, but the majority indicate the kaolinite composition which has the high Th/K ratio (see Fig. 26, the ratio is between 12ppm/% and 25ppm/%). The Kolje Formation shows two types, heavy minerals with thorium (see Fig. 26, the ratio is above 25ppm/%) and kaolinite. The Knurr Formation consists of heavy minerals with thorium, kaolinite and chlorite (see Fig. 26). The Hekkingen and Fuglen Formations show the high Th/K ratio which represent the heavy minerals with thorium. The Stø Formation consists of heavy minerals with thorium, chlorite, kaolinite and montmorillonite (see Fig.26). The observation through Table 3 shows that the Th-log shows higher values than the K-log due to high volume of heavy minerals, so the Th/K ratio is high (Table.2).

Table 3. Mineral identification using Th/K ratio for the Lower Kolmule, Kolje, Knurr, Hekkingen, Fuglen, and Stø Formations.

Formations	Depth (m)	Potassium (%)	Thorium (ppm)	Th/K (ppm/%)	Mineral identification
lower Kolmule	1583.1	0.34	4.36	12.82352941	Kaolinite
lower Kolmule	1584.05	0.34	4.09	12.02941176	Kaolinite
lower Kolmule	1587.1	0.34	3.65	10.73529412	Montmorillonite
lower Kolmule	1589.1	0.4	5.11	12.775	Kaolinite
lower Kolmule	1590.75	0.44	5.21	11.84090909	Montmorillonite
lower Kolmule	1592.05	0.4	6.2	15.5	Kaolinite
lower Kolmule	1593.05	0.36	4.19	11.63888889	Montmorillonite
lower Kolmule	1595.4	0.36	4.19	11.63888889	Montmorillonite
lower Kolmule	1597.1	0.38	5.33	14.02631579	Kaolinite
lower Kolmule	1599.15	0.4	8.21	20.525	Kaolinite
lower Kolmule	1600.1	0.4	7.51	18.775	Kaolinite
lower Kolmule	1602.05	0.6	11.3	18.83333333	Kaolinite
lower Kolmule	1628.9	0.2	5.51	27.55	Heavy Minerals with Thorium
lower Kolmule	1632.75	0.2	3.63	18.15	Chlorite
lower Kolmule	1634.38	0.24	2.6	10.83333333	Montmorillonite
lower Kolmule	1635.8	0.2	2.56	12.8	Chlorite
lower Kolmule	1636.6	0.2	2.19	10.95	Montmorillonite
lower Kolmule	1636.95	0.2	2.59	12.95	Chlorite
Kolje	1753.1	0.4	11.1	27.75	Heavy Minerals with Thorium
Kolje	1770.5	0.5	11.5	23	Kaolinite
Kolje	1782.2	0.54	11.8	21.85185185	Kaolinite
Kolje	1820.9	0.4	9.84	24.6	Kaolinite
Kolje	1888	0.46	12.7	27.60869565	Heavy Minerals with Thorium
Kolje	1965.6	0.54	13.5	25	Kaolinite
Knurr	1990.7	0.44	13.3	30.22727273	Heavy Minerals with Thorium
Knurr	1993.1	0.52	13.6	26.15384615	Heavy Minerals with Thorium
Knurr	1996.6	0.6	12.3	20.5	Kaolinite
Knurr	1998.2	0.48	10.7	22.29166667	Kaolinite
Knurr	1998.9	0.14	2.71	19.35714286	Chlorite
Hekkingen	2002.05	0.44	13.6	30.90909091	Heavy Minerals with Thorium
Hekkingen	2006	0.42	10.8	25.71428571	Heavy Minerals with Thorium
Hekkingen	2010.65	0.2	6.18	30.9	Heavy Minerals with Thorium
Hekkingen	2016.5	0.14	6.63	47.35714286	Heavy Minerals with Thorium
Fuglen	2024.1	0.2	9.68	48.4	Heavy Minerals with Thorium
Fuglen	2036.4	0.6	17.4	29	Heavy Minerals with Thorium
Fuglen	2063.2	0.4	18.5	46.25	Heavy Minerals with Thorium
Stø	2079.98	0.04	2.39	59.75	Heavy Minerals with Thorium
Stø	2080.83	0.04	2.12	53	Heavy Minerals with Thorium
Stø	2082.98	0.052	2.32	44.61538462	Heavy Minerals with Thorium
Stø	2083.4	0.058	2.68	46.20689655	Heavy Minerals with Thorium
Stø	2087.2	0.08	3.19	39.875	Heavy Minerals with Thorium
Stø	2094.74	0.2	5.43	27.15	Heavy Minerals with Thorium
Stø	2094.9	0.28	5.78	20.64285714	Chlorite
Stø	2095.9	0.28	6.12	21.85714286	Chlorite
Stø	2097.98	0.3	6.95	23.16666667	Kaolinite
Stø	2099.85	0.2	4.41	22.05	Chlorite
Stø	2107	0.16	7.61	47.5625	Heavy Minerals with Thorium
Stø	2108.93	0.17	5.92	34.82352941	Heavy Minerals with Thorium
Stø	2115.83	0.14	3.65	26.07142857	Heavy Minerals with Thorium
Stø	2117.86	0.152	3.89	25.59210526	Heavy Minerals with Thorium
Stø	2125.88	0.062	0.703	11.33870968	Montmorillonite
Stø	2133.9	0.06	1.23	20.5	Chlorite
Stø	2139.6	0.02	1.33	66.5	Heavy Minerals with Thorium
Stø	2152	0.048	1.52	31.66666667	Heavy Minerals with Thorium
Stø	2166	0.096	1.46	15.20833333	Chlorite
Stø	2176.8	0.068	1.39	20.44117647	Chlorite
Stø	2217	0.1	1.16	11.6	Montmorillonite

## **6. Discussion**

The study of the side-wall cores and the wire line logs included 6 formations that were penetrated in the Skalle well. Due to the core materials loss, thin sections of two formations (Kolje (1750.01-1989.6 m) and Knurr (1989.6-1999.5 m)) were not achieved. However, these two formations were identified and interpreted easily with wire line logs. The wire line log responses and lithology variations were also used to interpret the thickness of each formation.

### **6.1 The Stø Formation**

The thin section study of Stø Formation (2071-2220m) concluded with clean and mature sandstones of subarkosic arenite composition, while in the literature review this formation is classified as quartz arenite. This difference may reflect a high K-feldspar content identified due to staining in yellow colour in the studied thin sections. However, the article by Olausen et al., (1984) claims that the maturity of sandstones in general increases upward from subarkosic arenites to quartz arenites which is supported by observing more quartz near the top of the formation. The high intergranular porosity due to the dissolution of alkali feldspar makes this formation a good reservoir with high quality. According to Table 1 the petrography study of this formation indicates a fining upward sequence suggesting the transgression. In a transgressive sequence the water depth increases, while energy and sediment grain size decrease. Stylolitization is observed as a main diagenetic process in this formation which takes place from 2117.86m to 2094.9m, and also in the literature review of this formation, diagenesis of sandstone composition of this formation could be related to the distribution of stylolites, and the stylolitization is mentioned where fragment and clay laminae occur (Walderhaug et al., 2003). The stylolites are associated with clay matrix along with organic matter. High U-log and Th-log responses in this formation reflect the high concentration of organic matters and heavy minerals. The quartz overgrowths are observed, where the clay minerals (except chlorite-coating) or micaceous laminae are observed.

## **6.2 The Fuglen Formation**

The thin section study of the Fuglen Formation (2017.9-2071m) is based on only one sample (2019.35m) which cannot be representative for the whole formation, so core images and wire line logs interpretation play the main role for identifying lithology and the reservoir quality. Based on these methods this formation consists of shale with limestone interbeds. The neutron-density logs as well as the gamma ray logs show high values which indicate a shale composition. The resistivity logs responses change immediately within the shale and limestone intervals. The low resistivity logs response indicates the shale lithology and the high response are related to the limestone intervals. The depth interval between 2018.4 and 2036.3 meters shows the bad hole conditions and there is no data available for these intervals. Acoustic logs can be more reliable in this part as they are not affected by the rugosity of the borehole (Fig. 38). The lithology identification of the Fuglen Formation indicates that this formation can be considered as a seal for the Stø Formation reflecting the composition and the low porosity and permeability.

## **6.3 The Hekkingen Formation**

The thin section study of the Hekkingen Formation (1999.5-2017.9m) considers this formation as a shaly formation with thin interbeds of sandstone, while the lithology interpretations of wire lines show the thin interbeds of siltstone in this formation. The high volume of shale and organic matters which are observed by the high gamma ray and low resistivity logs responses, verify the potential of this formation for being a mature source rock. According to NPD fact page, the gas was observed in the Knurr and Lower Kolmule Formations. The Hekkingen Formation is therefore a potential Upper Jurassic source rock for the Knurr and Lower Kolmule Formations.

## **6.4 The Knurr and Kolje Formations**

The Knurr formation (1989.6-1999.5 m) and the Kolje Formation (1750.01-1989.6 m) are recognized and interpreted by the wire line logs. There were no core materials available for these

two formations, so the thin section study was not achieved. The logs interpretation show shale with sandstones and siltstones interbeds in both formations, but more clay content is observed in the Kolje Formation and more sand occurs in the Knurr Formation. The base of the Kolje Formation shows a low resistivity response due to the water in the shale, while the middle to the top of formation shows high resistivity; this may be a result of calcite cementation or over pressure conditions that cause the sudden increase. As both shale and limestone are impermeable, the Kolje Formation can be indicated as an effective seal.

### **6.5 The lower Kolmule Formation**

The thin section study of the Lower Kolmule Formation (1576.73-1750.01m) shows sandstones with large volume of clay matrix and silt interbeds, and modal analysis classify this formation as lithic greywacke. In the wire line log interpretation, there are few evidence of separation between RDEP and RMIC logs, except in sandstone intervals, which indicate the impermeable or high clay contents in the formation, but the existence of coarse-grained feldspatic sandstone as distinct intervals with high gamma ray (according to high K element) combined with high volume of clay matrix, make this formation a reservoir with poor quality. On the other hand, the low gamma ray response in clay rich parts (1640-1700m) suggests that the shale composition has changed, For example, kaolinite clays shows low gamma ray response due to the low K element. The gas is observed in the sand intervals according to the NPD fact page report. This is supported by the high resistivity log responses along with the low density and neutron values in the clean sandstone intervals.

### **6.6 Comments on diagenesis and reservoir quality**

Different diagenetic processes have occurred in the sandstones of which mineral dissolution, cementation, compaction, stylolization and clay mineral authigenesis are significant processes. The cementation occurs mostly as quartz overgrowths and occasional calcite cementations. The quartz overgrowths are observed more or less in all the formations, and are the product of quartz dissolution at stylolites interfaces. The calcite cementation occurred mostly



in the Kolje and Funglen Formations in distinct intervals where the pores have been occluded with the calcite cement. The source for the calcite can be considered as dissolution or reprecipitation of skeletal grains.

Dissolution of detrital K-feldspar is common in all the studied intervals which resulted in the creation of secondary porosity. The secondary porosity was the site for precipitation of clay minerals and in some parts calcite cementation. Feldspar dissolution may have occurred by increasing burial depth and temperature.

The evidence of mechanical and chemical compaction is observed in most of the formations. The bent muscovites between quartz grains indicate mechanical compaction which decreased the porosity. In contrast the dissolution of unstable minerals such as alkali feldspars due to chemical compaction has increased the porosity. The strong compaction of sediments is mainly a result of a high content of detrital clay, authigenic clay and mica-rich rock fragments which are mechanically weak. The large volume of stylolitization and the bent muscovites in the Lower Kolmule and Stø Formation show the high compaction rate.

Diagenetic clay minerals such as illite and chlorite are observed. Illite is the most abundant clay mineral in the study well occurring as pore-filling mineral and also as detrital matrix, while in the Th/K crossplot the majority of clay types were marked as kaolinite and heavy minerals with thorium. In the Th/K crossplot chlorite and montmorillonite were marked as well, but illite was not observed due to low K-log values; therefore, high Th/K ratio is indicated. The booklet texture of kaolinite which is the main identification for this mineral was not observed in thin section study, but the Th/K ratio marked kaolinite as a main clay mineral in this study.

As bioturbation, mass flow and soft sediments deformation are likely mechanisms for introducing detrital clay minerals in to the fabric of marine sandstones the clay minerals that occur along with organic matter and pyrite may be detrital clay minerals (Worden and Burley, 2003). Chlorite occurs as clay-coating and pore-filling in the Lower Kolmule, Hekkingen and Stø Formations. Chlorite-coated sandstones are often associated with iron-rich depositional environments like the glaucony and oolitic ironstone facies. Chlorite coating inhibits quartz cementation and increases the porosity, so where there is the evidence of quartz overgrowths, no chlorite coatings is observed. The thin chlorite coatings in the Stø Formation inhibit the quartz

cementation and increase the porosity so they have a positive effect on reservoir quality. The low resistivity and acoustic logs response at the base of Stø Formation can verify this theory.

Glaucanite, phosphate and pyrite (diagenetic minerals) are observed almost in all the formations. According to the conditions of the mineral formation, the environment is interpreted as marine with increasing reducing diagenetic conditions. The glauconitization has occurred mostly in the Lower Kolmule Formation. According to the literature review in chapter 3, the maturation of glauconite pellets will be achieved by  $K_2O$  and  $SiO_2$  increase and release of  $Al_2O_3$  from the glauconite structure. In this study it is thought that the dissolution of alkali feldspar is the main source for  $K_2O_2$  which is the main factors for glauconitization of the pellets and their maturity. Pyrite occurs as pore-filling early diagenetic cement, and also as isolated crystals. The iron supplied for pyrite formation can be achieved from dissolution of chlorite or mica.

According to the survey by Primmer et al., (1997), regarding the 5 common diagenetic styles, only two of their defined diagenetic styles can be observed in the formations; 1) quartz with lesser quantities of neoformed clay (illite) and late diagenetic ferroan carbonate, and 2) early diagenetic grain coating of chlorite that inhibits the quartz cementation during burial.

## 7. Conclusion

The thin section study of the Skalle well was used to identify the lithology and diagenesis of 4 formations, the Lower Kolmule (1576.73-1750.01m), Hekkingen (1999.5-2017.9m), Fuglen (2017.9-2071m) and Stø (2071-2220m) Formations, while the petrophysical interpretation identifies the lithology of two other formations, Kolje Formation (1750.01-1989.6 m) and Knurr Formation (1989.6-1999.5 m).

There are two gas bearing reservoirs in the Skalle well, the Stø and Lower Kolmule Formations. The Stø Formation is classified as subarkosic arenite composition consisting of clean sandstone with shale and siltstone interbeds, and the presence of gas is verified by high resistivity response in this formation. The volumes of detrital clay contents, diagenetic cements and organic matter are quite often low in this formation which, in addition, to high porosity and permeability make the Stø Formation a reservoir with high quality compared to the Lower Kolmule Formation. The partial dissolution of K-feldspar in this formation is the main factor for secondary porosity increase. The lower Kolmule Formation shows a lithic greywacke composition with considerable detrital clay, and in some cases clay matrix fills the pores. The sandstones in the shale dominated Hekkingen Formation show lithic greywacke composition. The shales are indicated as a potential source rock for the Lower Kolmule Formation and as a seal for the Stø Formation. The fine grain-size of the Hekkingen and Fuglen Formation sandstones in general has had a negative effect on permeability, so they are very poor reservoirs.

The evidence of glauconite, phosphate, and pyrite in subarkosic arenite (the Stø Formation) and lithic greywacke (the Lower Kolmule and Hekkingen Formations) compositions support a shallow marine environment with low rate of sedimentation and increasing reducing diagenetic conditions.

Different diagenetic processes such as compaction (mechanical and chemical), cementation (quartz overgrowths and calcite cementation), and dissolution (K-feldspar), and stylolitization, glauconitization and clay matrix infiltration have affected the primary composition.

The wire line logs in this study provides continuous measurement of data as a function of depth and helps to achieve more detailed information regarding lithology and fluid types, so this method is a useful supplementary method to cores for reaching precise results.

For achieving more reliable results the author would like to suggest for further works to use more than one well for the area in order to recognize any changes due to the lithology and diagenetic effects laterally which can be more representative of the whole formations. Having more core data and petrophysical data can help to approach to more reliable results and also using more methods other than the thin section study for clay type identification. SEM, X-ray diffraction and Th/K ratio are good methods to achieve this goal.

## References

Adams, A.E, Mackenzie, W.S, Guilford, C., 1984: Atlas of sedimentary rock under the microscope, pp.104.

Adams, J.A.S., and Weaver, C.E., 1958: Thorium-to-uranium ratios as indicators of sedimentary processes: example of concept of geochemical facies. AAPG Bull, p.42-387.

Almon, W.R., and Davies, D.K., 1981: Formation damage and crystal chemistry of clays, pp.116.

Arduini, M., Golfetto, F. and Ortenzi, A., 2009: The Chlorite-Bearing Reservoirs: Effects of the Main Petrographic Parameters on Reservoir Quality, p.1-23.

Barrère, C., Ebbing, J. and Gernigon, L., 2009: Offshore prolongation of Caledonian structures and basement characterization in the western Barents Sea from geophysical modeling, Geological Survey of Norway, Tectonophysics 470, p.71-88.

Banerjee, S., Chattoraj, S.L, Saraswati, P.K, Dasgupta, S., Sarkar, U., 2012: Substrate control on formation and maturation of glauconite in the Middle Eocene Harudi formation, western Kutch, India Marine and Petroleum Geology, p.144-160.

Bjørkum, P.A, Oelkers, E.H, Nadeau, P.H, Walderhaug, O., and Murphy, W.M, 1998: Porosity prediction in quartzose sandstones as a function of time, temperature, depth, stylolite, frequency and hydrocarbon saturation, p. 637-648.

Bjørlykke, K., 2010: Sedimentary geochemistry: How Sediments are Produced, pp.96.

Boggs, S. Jr., 1992: Petrology of sedimentary rocks: New York, Macmillan Publishing Co., pp.355.

Brekke, H., Sjulstad, H.I., Magnus, C. and William, R.W., 2001: Sedimentary environments offshore Norway – an overview. In Martinsen, O.J. and Dreyer, T. (eds.): Sedimentary environments offshore Norway – Paleozoic to Recent. Norwegian Petroleum Society (NPF), Special Publication 10. Elsevier, Amsterdam, p. 7-37.

Bugge, T., Elvebakk, G., Fanavoll, S., Mangerud, G., Smelror, M., Weiss, H.M., Gjelberg, J., Kristensen, S.E. and Nilsen, K., 2002: Shallow Stratigraphic drilling applied in Hydrocarbon Exploration of the Nordkapp Basin, Barents Sea. *Marine and Petroleum Geology* 19, p.13-37.

Burley S. D., 1997: *Petroleum Geology of Northwest Europe*, pp.1295.

Bøe, R., Fossen, H. and Smelror, M., 2010: Mesozoic sediments and structures onshore Norway and in the coastal zone. *Norges geologiske undersøkelse Bulletin*, p.15-32.

Dalland, A., Worsley, D., Ofstad, K., 1988: NPD-BULLETIN NO 4: The lithostratigraphic scheme for the Mesozoic and Cenozoic succession offshore mid and northern Norway, p.51-57.

Dott, R.H., 1964: Wacke greywacke and matrix-what approach to immature sandstone classification, p. 625-632.

Ekstrom, M. P., Dahan, C. A., Chen, M., Lloyd, P. and Rossi, D., 1987: Formation imaging with microelectrical scanning arrays. *Log Analyst*, 28, p.294-306.

Gaymard, R. and Poupon, A., 1968: Response of neutron and formation density logs IN hydrocarbon, bearing formation, p.3-12.

Glover, P., 2012, *Petrophysics MSc Course Notes: Wire line logging*, p.55-246.

Houseknecht, D.W., 1987: Assessing the Relative Importance of Compaction Processes and Cementation to Reduction of Porosity in Sandstones, p. 633-642.

Kristensen, E., Lopes, G.P., Delefosse, M., Valdemarsen, T., Quintana, C.O., Banta, G.T., 2012: What is bioturbation? The need for a precise definition for fauna in aquatic sciences, p.285-302.

Larsen, G.B., Elvebakk, G., Henriksen, L.B., Kristensen, S.E., Nilsson L., Samuelsberg, T.J., Svånå, T.A., Stemmerik, L. and D,worsley, 2002: Upper Paleozoic Lithostratigraphy of the Southern Norwegian Barents Sea, pp.69.

Leith, T.L., Weiss, H.M., Mørk, A., Århus, N., Elvebakk, G., Embry, A.F., Brooks, P.W., Stewart, K.R., Pchelina, T.M., Bro, E.G., Verba, M.L., Danyushevskaya, A., Borisov, A.V., 1993: Mesozoic hydrocarbon source-rocks of the Arctic region. In: Vorren, T.O., Bergsager, E.,

Dahl-Stammers, O.A., Holter, E., Johansen, B., Lie, E., Lund, T.B. (Eds.), Arctic Geology and Petroleum Potential. NPF Special Publication, vol. 2. Elsevier, p.1 –25.

Mackenzie, F.T., 2004: Sediments, diagenesis, and sedimentary rocks, pp.446.

McRae, S.G., 1972: Glauconite. Earth-Science Reviews, pp.397.

Meyer, B.L., and Nederlof, M. H., 1984: Identification of Source Rocks on Wire line Logs by Density/Resistivity and Sonic Transit Time/Resistivity Crossplots, pp.121.

Mountain, G.S., Miller, K.G., Blum, P., Poag, C.W., and Twichell, D.C. (Eds.), 1996: Proceedings of the Ocean Drilling Program, Scientific Results: Spectral gamma-ray logs in relation to clay mineralogy and sequence stratigraphy, Cenozoic of the atlantics margin, offshore, New Jersey, pp.411.

Mørk, M. B. E., 1999: Compositional variations and provenance of Triassic sandstones from the Barents Shelf. Journal of Sedimentary Research 69, p.690-710.

Nnucu, J. O and Dsrr, C. I, 1974: Diagenetic Formation of iron Phosphates in Recent Lake Sediments, Department of the Environment, pp.934.

Olaussen, S., Dalland, A., Gloppen, T.G. and Johannesen, E., 1984: Depositional environment and diagenesis of Jurassic reservoir sandstones in the eastern part of Troms I area. In Spencer, A.M., Holter, E., Johnsen, S.O., Mørk, A., Nysaether, E., Songstad, P. and Spinnangr, Å. (Eds.), Petroleum geology of the North European Margin. Norwegian Petroleum Society (NPF), Graham and Trotman, p.61-79.

Ryseth, A., Augustson, J.H., Charnock, M., Haugerud, O., Knutsen, S.M., Midbøe, P.S., Opsal, J.G. and Sundsbø, G., 2003: Cenozoic stratigraphy and evolution of the Sørvestsnaget Basin, southwestern Barents Sea. Norwegian Journal of Geology, vol. 83, Bergen. ISSN 029-196X, p.107-130

Rønnevik, H. and Jacobsen, H. P., 1984: Structural highs and basins in the western Barents Sea. In: Spencer, A.M. et al. (Eds): Petroleum Geology of the North European margin. Norwegian Petroleum Society (Graham and Trotman), p. 98-107.

Storvoll, V., Bjørlykke, N., Karlsena, D., Saigal, G., 2002: Porosity preservation in reservoir sandstones due to grain-coating illite: a study of the Jurassic Garn Formation from the Kristin and Lavrans fields, offshore Mid-Norway, p.779-781.

Sujkowski, Z.b.L., 1958: Diagenesis, Bulletin of the American Association of Petroleum Geologists, p.1323-1344.

Suslova, A.A., Stoupakova, A.V., Burlin, Y.K., Kirykhina, N.M., Golinchik, P.O., 2007: Jurassic reservoirs of the Barents Sea shelf. Environments of sedimentation, p.4-56.

Syed, A.A., Clark, w.j., Moore, W.R., Dribus, J.R., 2010: Diagenesis and Reservoir quality, p.14-27.

Walderhaug, O. and Bjørkum, P.A., 2003: The effect of stylolite spacing on quartz cementation in the Lower Jurassic Stø Formation, southern Barents Sea. Journal of Sedimentary Research 73, p.146-156.

Waldschmidt, W.A., 1941: Cementing materials in sandstones and their probable influence on migration and accumulation of oil and gas: American Association of Petroleum Geologists, vol.25, p.1839-1879.

White, J., 2012, Schlumberger: Gamma ray, pp.293.

Worden R.H., Burley S.D., 2003: Sandstone diagenesis; the evaluation of sand to stone, p.3-44.

### **Web references**

Bennington, J.B., 1999, Geol 135 Sedimentation,  
[http://people.hofstra.edu/j\\_b\\_bennington/135notes/clastics.html](http://people.hofstra.edu/j_b_bennington/135notes/clastics.html), visited: 13.05.2013.

Crain, P., 2013 <http://www.spec2000.net/13-lithkut.htm>, visited: 22.06.2013

Halliburton, 2013, [http://www.halliburton.com/public/lp/contents/data\\_sheets/web/h/h03574.pdf](http://www.halliburton.com/public/lp/contents/data_sheets/web/h/h03574.pdf)),  
visited: 05.05.2013.



Kenneth Heslop (LogX Inc.) and Alan Heslop (Anadarko Canada Corp.), 2003: Interpretation of Shaly Sands, [http://www.lps.org.uk/docs/heslop\\_shaly\\_sands.pdf](http://www.lps.org.uk/docs/heslop_shaly_sands.pdf), visited: 02.06.2013.

Nelson, S.A., <http://www.tulane.edu/~sanelson/eens212/sandst&cong.htm>, visited: 30.04.2013.

Norwegian Petroleum Directorate factpages: <http://factpages.npd.no/factpages>, visited: 12.05.2013.

Pedersen, J.H., Karlsen, D.A., Brunstad, H., and Jan Lie, E.: Department of Geosciences, University of Oslo:

<http://oilandgasgeology.com/Source%20Rocks%20of%20the%20Norwegian%20Barents%20Sea.pdf>, visited: 22.06.2013.

Primary Industries and Regions South Australia (PIRSA), 2013

[http://www.pir.sa.gov.au/minerals/geological\\_survey\\_of\\_sa/commodities/heavy\\_minerals](http://www.pir.sa.gov.au/minerals/geological_survey_of_sa/commodities/heavy_minerals), visited: 01.05.2011.

Schlumberger, 2013,

[http://www1.uis.no/Fag/Learningspace\\_kurs/PetBachelor/webpage/tech%5CSchlumberger%20charts%5C07\\_cp\\_4-20\\_4-33.p11.pdf](http://www1.uis.no/Fag/Learningspace_kurs/PetBachelor/webpage/tech%5CSchlumberger%20charts%5C07_cp_4-20_4-33.p11.pdf), visited: 05.05.2013.

Spring Energy Norway AS, <http://www.springenergy.no/en/news2/2011/discovery-on-the-skalle-prospect-in-pl-438-8-july>, visited: 10.04.2013.